

# NAVAL POSTGRADUATE SCHOOL

Monterey, California

AD-A205 935



## THESIS

THREE-DIMENSIONAL ANALYSIS OF  
OPTICAL TRANSITION RADIATION

by

Wilmer Gregg Longstaff

December 1988

Thesis Advisor:

Xavier K. Maruyama

Approved for public release; distribution unlimited

DTIC  
ELECTE  
MAR 28 1989  
S a D  
H

89 3 27 079



REPORT DOCUMENTATION PAGE

1a. REPORT SECURITY CLASSIFICATION <b>UNCLASSIFIED</b>			1b. RESTRICTIVE MARKINGS		
2a. SECURITY CLASSIFICATION AUTHORITY			3. DISTRIBUTION/AVAILABILITY OF REPORT Approved for public release; distribution unlimited.		
2b. DECLASSIFICATION/DOWNGRADING SCHEDULE					
4. PERFORMING ORGANIZATION REPORT NUMBER(S)			5. MONITORING ORGANIZATION REPORT NUMBER(S)		
6a. NAME OF PERFORMING ORGANIZATION Naval Postgraduate School		6b. OFFICE SYMBOL (If applicable) 33	7a. NAME OF MONITORING ORGANIZATION Naval Postgraduate School		
6c. ADDRESS (City, State, and ZIP Code) Monterey, CA 93943--5000			7b. ADDRESS (City, State, and ZIP Code) Monterey, CA 93943-5000		
8a. NAME OF FUNDING/SPONSORING ORGANIZATION		8b. OFFICE SYMBOL (If applicable)	9. PROCUREMENT INSTRUMENT IDENTIFICATION NUMBER		
8c. ADDRESS (City, State, and ZIP Code)			10. SOURCE OF FUNDING NUMBERS		
PROGRAM ELEMENT NO.		PROJECT NO.	TASK NO.	WORK UNIT ACCESSION NO.	
11. TITLE (Include Security Classification) <b>THREE--DIMENSIONAL ANALYSIS OF OPTICAL TRANSITION RADIATION</b>					
12. PERSONAL AUTHOR(S) Longstaff, Wilmer G.					
13a. TYPE OF REPORT Master's Thesis		13b. TIME COVERED FROM _____ TO _____		14. DATE OF REPORT (Year, Month, Day) December 1988	15. PAGE COUNT 145
16. SUPPLEMENTARY NOTATION The views expressed in this thesis are those of the author and do not reflect the official policy or position of the Department of Defense or the U.S. Government.					
17. COSATI CODES			18. SUBJECT TERMS (Continue on reverse if necessary and identify by block number)		
FIELD	GROUP	SUB-GROUP	Transition radiation; particle beams; coherent transition radiation; two foil interferometer; beam diagnostics. (jgd)		
19. ABSTRACT (Continue on reverse if necessary and identify by block number) A three-dimensional analysis of the intensity distribution of backward optical transition radiation has been performed. The effects of variations in electron energy and beam divergence and on material properties such as dielectric permittivities and the resultant coherence length upon the angular distribution and polarization of optical transition radiation has been investigated. A surprising observation important to the use of optical transition radiation as a diagnostic tool for high energy electron beams is the behavior of the perpendicular component of the intensity. In contrast to low energies where the parallel component dominates, at electron energies above 200 MeV, the perpendicular component dominates. This requires the use of a polarization filter to diagnose particle beam properties at high energies. <i>Keywords: Theses.</i>					
20. DISTRIBUTION/AVAILABILITY OF ABSTRACT <input checked="" type="checkbox"/> UNCLASSIFIED/UNLIMITED <input type="checkbox"/> SAME AS RPT <input type="checkbox"/> DTIC USERS			21. ABSTRACT SECURITY CLASSIFICATION Unclassified		
22a. NAME OF RESPONSIBLE INDIVIDUAL Xavier K. Mariyama			22b. TELEPHONE (Include Area Code) (408) 646-2431	22c. OFFICE SYMBOL 61Mp	

Approved for public release; distribution is unlimited

Three-Dimensional Analysis  
of Optical Transition Radiation

by

Wilmer Gregg Longstaff  
Lieutenant, United States Navy  
B.S., Miami University of Ohio, 1981

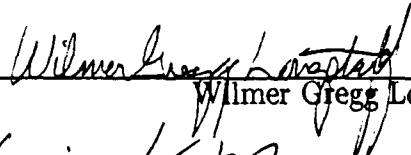
Submitted in partial fulfillment of the  
requirements for the degree of

MASTER OF SCIENCE IN PHYSICS

from the

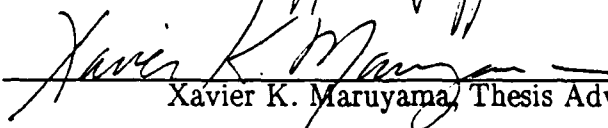
NAVAL POSTGRADUATE SCHOOL  
December 1988

Author:

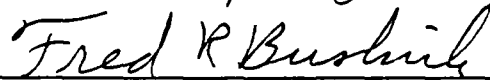


Wilmer Gregg Longstaff

Approved By:



Xavier K. Maruyama, Thesis Advisor



Fred R. Buskirk, Second Reader



Karlheinz E. Woehler, Department of Physics



Gordon E. Schacher, Dean of Science and Engineering

## ABSTRACT

A three-dimensional analysis of the intensity distribution of backward optical transition radiation has been performed. The effects of variations in electron energy and beam divergence and on material properties such as dielectric permittivities and the resultant coherence length upon the angular distribution and polarization of optical transition radiation has been investigated. A surprising observation important to the use of optical transition radiation as a diagnostic tool for high energy electron beams is the behavior of the perpendicular component of the intensity. In contrast to low energies where the parallel component dominates, at electron energies above 200 MeV, the perpendicular component dominates. This requires the use of a polarization filter to diagnose particle beam properties at high energies.

Accession For	
NTIS GRA&I	<input checked="" type="checkbox"/>
DTIC TAB	<input type="checkbox"/>
Unannounced	<input type="checkbox"/>
Justification	
By	
Distribution/	
Availability Codes	
Dist	Avail and/or Special
A-1	

## TABLE OF CONTENTS

I.	INTRODUCTION	1
II.	CALCULATIONAL APPROACH	10
	A. SINGLE FOIL	10
	B. INTERFEROMETER	14
	C. THE GRAPHICS PROGRAM	17
III.	SINGLE FOIL TRANSITION RADIATION	18
	A. ENERGY	18
	B. BEAM DIVERGENCE	42
	C. DIELECTRIC CONSTANT	57
IV.	COHERENT TRANSITION RADIATION	64
	A. COHERENCE LENGTH	64
	B. ENERGY	68
	C. BEAM DIVERGENCE	74
	D. DIELECTRIC CONSTANTS	81
	E. FINITE BANDWIDTH	85
V.	RECOMMENDATIONS AND CONCLUSIONS	93
	REFERENCES	95
	APPENDIX A—USER'S MANUAL	96
	APPENDIX B—PROGRAM LISTINGS	113
	INITIAL DISTRIBUTION LIST	137

## ACKNOWLEDGEMENTS

The author is deeply indebted to the inspiration and assistance of Dr. D. W. Rule and Dr. R. B. Fioritio. The sincerest appreciation is due to his thesis advisor, Dr. X. K. Maruyama, for his patient guidance, instruction, and support throughout this work. The author is especially grateful to many of the physics staff at the Naval Postgraduate School for their dedication and assistance. Finally, a sincere work of thanks to my wife, Laurie, and daughters, Nikki and Rachel, for their patience, understanding, and support.

## I. INTRODUCTION

Transition radiation is produced whenever a uniformly moving charged particle passes from one medium into another. In introducing the concept in 1944, Frank and Ginsburg [Ref. 1] noted that the intensity, polarization and angular distribution of transition radiation are dependent upon the dielectric constants of the two media and that transition radiation is not connected with changes in velocity of the charged particle. This behavior of transition radiation, particularly the angular distribution and polarization dependence on energy makes it a promising technology for use as a diagnostic for charged particle beams at low energy.

Since its introduction, many investigations of the nature of transition radiation in such diverse environments as the boundary between two media, electromagnetic fields, plasmas, inhomogeneous media, and media in which the properties vary with time have been published, providing an exhaustive bibliography. Ginzburg and Tsytovich [Ref. 2], Ter-Mikaelian [Ref. 3], and Garibian [Ref. 4] provide brief overviews of some of the established concepts resulting from those investigations. Unfortunately, the calculations on the subject were always awkward in nature, since the formulas developed were very complicated. Many formulas developed independently of each other differed considerably from one publication to the next. The situation was exacerbated by the lack of specifics or standardization with respect to definitions of key concepts and adoption of universal conventions. Wartski [Ref. 5] attempted to rectify the

problem by returning to fundamental theories, building upon basic hypotheses, and emphasizing the conventions adopted by early pioneers in this field. Rule and Fiorito et al. [Ref. 6–8] refined and extended Wartski's work to develop analytical solutions concerning the components of radiation intensity. Much of the analysis in this thesis is based upon those analytical solutions.

It is necessary to first discuss the physical processes involved in which transition radiation occurs. The simplest case to consider is that of a charged particle moving at a uniform velocity which encounters a boundary between two media. The media are characterized by their respective dielectric permittivities,  $\epsilon_1$  and  $\epsilon_2$ . The dielectric permittivities are complex functions of the refractive index  $n$  and the absorption coefficient  $\kappa$  of the medium. The motion of the charged particle creates, by definition, an electrical current which in turn generates associated electric and magnetic fields. Since the particle is assumed to travel in a uniform motion in which it does not experience acceleration, it does not emit radiation until encountering the boundary between the media.

At least three types of radiation are emitted as the particle transits through the interface between the media. These are Cherenkov, bremsstrahlung, and transition radiation. Transition radiation is closely related to Cherenkov radiation but exhibits different properties. Bremsstrahlung radiation is an entirely separate mechanism involving particle acceleration. The form of transition radiation may be found by examining the fields involved. The electric and magnetic field in each medium are described by the solutions to the Maxwell equations for a point charge moving at constant velocity. However, the electric and magnetic field components in each media fail to satisfy the continuity requirements across the interface.

The solutions of homogeneous Maxwell equations must be added to those of the electric and magnetic fields in each medium to meet the boundary conditions. The required radiation fields described by these solutions meeting the boundary conditions are the transition radiation. [Ref. 4,9]

Obviously, finding the solution for the transition radiation fields is quite complicated. Ter-Mikaelian [Ref. 3] and Wartski [Ref. 5] provide an excellent account of the full derivation. The results of those derivations will be presented and analyzed in this thesis so as to promote a better understanding of transition radiation and its potential applications for beam diagnostics.

As stated earlier, the simplest case is that of a charged particle moving at uniform velocity encountering a boundary between media. For purposes of this study, a vacuum to medium transition was assumed in which  $\epsilon_1 = 1$  and  $\epsilon_2$  can be written simply as  $\epsilon$ . The medium encountered is a thin metallic foil. Transition radiation may be observed from the front face of the foil and is called backward transition radiation since it is reflected back from the foil. Transition radiation is also emitted in the forward direction from the back side of the foil and is thus termed forward transition radiation. Observation of forward transition radiation is difficult because of its proximity to the beam of charged particles. The backward transition radiation, however, may be diverted from the beam by reflecting it at an angle. For this reason, the beam of charged particles may be made to encounter the metallic foil at an oblique angle of 45 degrees. This has historically been the preferred angle of incidence because, since the angle of reflection equals the angle of incidence, it allows the observation equipment to be set up 90 degrees from the

beam axis along the axis of reflection. This configuration permits the study of backward transition radiation apart from the beam while keeping calculations relatively simple.

The mean angle at which optical transition radiation appears is the angle of specular reflection. If the beam has an angular divergence then the charged particles have different angles of incidence upon the transition radiation foil. If the angle of a particular particle is  $\alpha$  with respect to the beam axis, then the optical transition radiation will appear at an angle  $\alpha$  to the axis of specular reflection. Figure 1 demonstrates the definition of the particle angle  $\alpha$  with respect to the beam axis, angle of specular reflection  $\Psi$ , and angle of observation  $\theta$ .

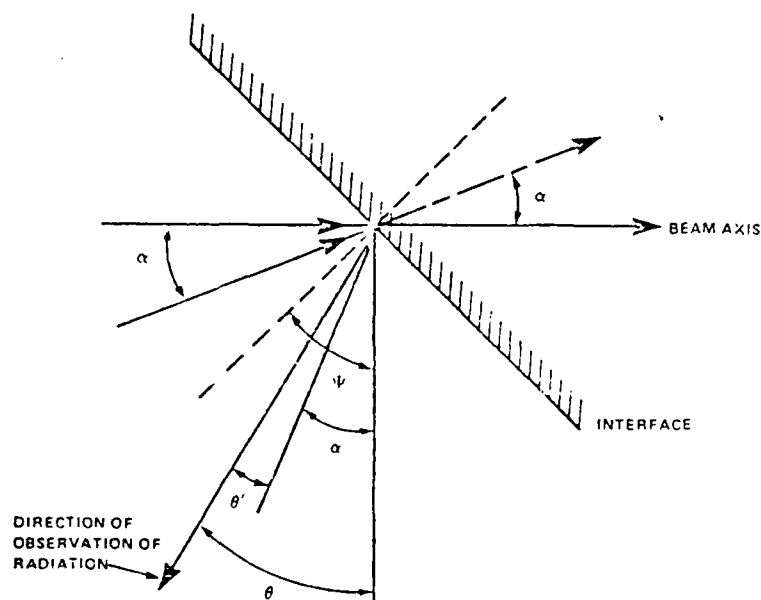


Figure 1. Definition of the particle angle  $\alpha$  with respect to the beam axis, angle of specular reflection  $\Psi$ , and the observation angle  $\theta$  with respect to the angle of specular reflection for a particle encountering a boundary at an oblique angle. [Ref. 5,9].

The interest here is the intensity of the radiation at any point in the plane of observation as a function of the observation angle  $\theta$ . The angular information of transition radiation obtained from this is valuable as a potential diagnostic for charged particle beams. The TR3 program used in this study was based upon the analytical solution of this single foil case developed by Rule and Fiorito [Ref. 6-8] for this purpose. This program extends Rule and Fiorito's solution into three dimensions, thus using the advantage of three-dimensional graphics to aid in interpreting the results.

Recall that the motion of the charged particle induces electromagnetic fields in the medium and that radiation is emitted when the particle encounters a boundary between two media of dissimilar dielectric constants. When that transition from one medium to another occurs, the electromagnetic fields induced by the particle motion as well as the fields induced by the transition must adjust to the change in dielectric permittivity. The distance over which this adjustment occurs is known as the coherence length. (It is also sometimes referred to as the formation length). The definition of this length is a bit arbitrary, but is usually chosen so that the radiation emitted at the interface adds coherently with the fields generated by the particle. It has been found that a phase difference of one radian is the condition for the rays to become coherent. The fields at much greater distances may be considered to be pure radiation fields.

Coherence length is related to both the particle velocity and to the phase difference between the particle's fields and the radiation fields from the transition. The coherence length in the medium can be expressed [Ref. 5] as

$$L_m = \frac{\beta c}{\omega} \left| \frac{1}{1 - \beta \sqrt{\epsilon} \cos \theta} \right| = \frac{\beta \lambda}{2\pi} \left| \frac{1}{1 - \beta \sqrt{\epsilon} \cos \theta} \right|, \quad (1.1)$$

where  $\beta$  is the ratio of the particle velocity to the speed of light,  $\omega$  is the angular frequency ( $=2\pi c/\lambda$ ),  $\theta$  is the angle of observation, and  $\lambda$  is the wavelength of the radiation in the medium. The coherence length in a vacuum may be found by setting  $\sqrt{\epsilon}=1$ .

Coherence length takes on a special significance when considering a particle encountering more than one boundary as with the two-foil interferometer developed by Wartski [Ref. 5]. This interferometer consists of two parallel foils set at an angle of 45 degrees to the trajectory of the charged particle beam. Particles traversing the foils emit radiation from the back of the first foil that is reflected off the front surface of the second foil. Transition radiation is also produced by the transit through the second foil. The radiation emitted from the front of the second foil forms an interference pattern with the radiation from the back of the first foil (Figure 2). The interference pattern is centered around the axis of specular reflection. The phase difference between the transition radiation emitted from the first and second foils is

$$\phi = (2\pi L/\lambda\beta)(1-\beta\cos\theta) = L/L_v, \quad (1.2)$$

where  $L$  is the separation between the foils and  $L_v$  is the formation length in a vacuum. This phase difference should be an integer multiple of one radian for the transition radiation from the two foils to add coherently. That is, the separation between the foils should be an integer multiple of the coherence length in a vacuum.

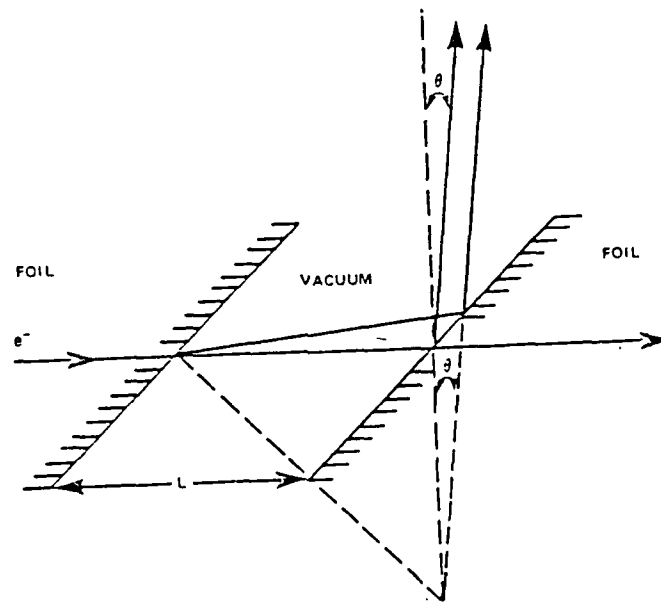


Figure 2. Diagram of the Wartski's two-foil interferometer. [Ref. 5,9]

Rule and Fiorito [Ref 6-8] developed an analytical solution to the transition radiation emitted from Wartski's two-foil interferometer [Ref. 5]. The COHER3 program used in this study extended that solution into three dimensions for use with three-dimensional graphics to aid the analysis.

Most current theories on transition radiation were built on the simplification of assuming a point value for both energy and frequency in order to evaluate complex integrals. In reality, however, energy and frequency extend over a finite range of values. The assumption may be responsible for some slight differences between theoretical and actual data. The capability of examining the effects of a

finite bandwidth of wavelength (and thus frequency) was built into the COHER3 program. This thesis provides one of the few investigations on finite frequency bandwidth effects.

The TR3 and COHER3 programs created an output compatible with the Three-dimensional graphics program, SON OF SURF3D. This graphics program was written by Don Gilbert of Dogstar Software as an extension of SON OF SURF. At the time of this writing, SON OF SURF3D was still under development and not yet ready for public release. This thesis was one of the first thorough testings of the SON OF SURF3D graphics program. As such, it may play a key role in determining whether the SON OF SURF3D program will be fully developed for commercial use. Use or discussion in this thesis of any commercially available product does not constitute endorsement.

The purpose of this thesis was to promote a better understanding of transition radiation based upon the theoretical developments presented in references 1-9. It provides an investigation of the effects of finite bandwidth on radiation intensity distribution. The programs and graphics package used in this thesis could become powerful research tools in the development of TR as a diagnostic for charged particle beams. The behavior of the polarization and angular distribution of transition intensity in response to changes in specific parameters demonstrated in this thesis should provide a guide for further development of transition radiation *theory for this purpose. By building upon basic concepts and examining the nature of the complex formulas involved, with the aid of three-dimensional graphics, this thesis proposes to clarify the concepts of transition radiation so that even the laymen could obtain a basic understanding.*

Chapter II describes the analytical solutions of Rule and Fiorito for transition radiation from the single foil and two-foil interferometer cases [Ref. 6-9] and the TR3 and COHER3 programs used in this study which extended those solutions to three dimensions. The chapter closes with a brief description of the three dimensional graphics program, SON OF SURF3D, used in conjunction with these programs.

Chapter III contains the analysis of the effects of energy, beam divergence, and dielectric properties on the distribution of transition radiation intensity for the single foil case. An investigation into the effects of coherence length and optical frequency bandwidth as well as energy, beam divergence, and dielectric properties for the two-foil interferometer case forms the content of Chapter IV.

The conclusions resulting from the analysis as well as recommendations for further study, hardware, and software are discussed in Chapter V. For convenience, a users manual for the single foil and two-foil interferometer programs and for the three-dimensional graphics program was developed and included as Appendix A. Appendix B contains the listing for the single foil program TR3 and the two-foil interferometer program COHER3.

## II. CALCULATIONAL APPROACH

The core of the analysis of this study are analytical solutions developed by D. W. Rule et al. of the Naval Surface Warfare Center [Ref 6-9] for single foil and for two-foil interferometer transition radiation. A series of programs developed by D. W. Rule et al. around those analytical solutions were used in the study of transition radiation characteristics to produce theoretical two-dimensional profiles of relative intensity [Ref. 7-9].

Rule's programs were modified to extend the analysis to three dimensions and to add flexibility in setting data parameters during run time. The resulting program for the single foil case is called TR3 and an interferometer program which took into account coherence length and frequency bandwidth is called COHER3. Both programs were tailored specifically to be compatible with the three-dimensional graphics program, SON OF SURF3D, written by Don Gilbert of Dogstar Software [Ref. 10]. SON OF SURF3D was in the developmental stage, not yet ready for public release as an improved version of SON OF SURF, extending the capabilities of that program to plot three-dimensional surfaces from data files. A description of SON OF SURF3D follows the discussion of the theoretical basis of the TR3 and COHER3 programs.

### A. SINGLE FOIL

The program TR3 was a modification of TRADS1, which was one of a series of single-foil transition radiation programs written by D. W. Rule [Ref. 8]. The TRADS1 program calculated a two-dimensional intensity distribution as a function

of angle measured from the angle of specular reflection. The angle of specular reflection was chosen to be forty-five degrees as measured from the target plane and ninety degrees from the beam axis (Figure 1) for the reasons discussed in chapter one. The program assumes a Gaussian distribution of beam divergence angle and a vacuum to medium transition. The medium is characterized by a dielectric constant which is in general complex. All calculations were based on energy and the incremental values of the observation angle ( $\theta$ ), measured from the angle of specular reflection. The TR3 program extended the analysis of the TRADS1 series of programs to three-dimensions in conjunction with the three-dimensional graphics program SON OF SURF3D.

The values of the parallel and perpendicular components of intensity as well as the total intensity were based on an analytical approach developed by D. W. Rule and associates [Ref. 7,8] in accordance with the theoretical treatment of transition radiation by Wartski [Ref. 5]. Using the small angle approximation of  $\cos \theta$  and  $\sin \theta$ , Rule [Ref. 7] showed that, for small angles, the intensity per unit frequency and solid angle could be expressed

$$I_{\parallel} \approx \frac{e^2 \beta^2}{c \pi^2} \left[ \frac{|r_{\parallel}|^2 \theta^2}{(\gamma^{-2} + \theta^2)^2} + \frac{\text{Re } r_{\parallel} \theta}{(\gamma^{-2} + \theta^2)} \right], \quad (2.1)$$

and

$$I_{\perp} \approx \frac{e^2 \beta_{\perp}^2}{c \pi^2} \left[ \frac{|r_{\perp}|^2}{(\gamma^{-2} + \theta^2)^2} + \frac{\text{Re } r_{\perp}}{(\gamma^{-2} + \theta^2)} \right], \quad (2.2)$$

where  $\beta$  is the velocity of the particle in units of the speed of light,  $\beta_{\perp}$  is the component of the velocity that is perpendicular to the observation plane,  $\gamma$  is the

dimensionless Lorentz factor for energy, and  $r_{\parallel}$  and  $r_{\perp}$  are respectively the parallel and perpendicular Fresnel reflection coefficients. The Lorentz factor  $\gamma$  and the velocity  $\beta$  are defined

$$\gamma = \frac{E}{m_0 c^2} = 1 + \frac{KE}{m_0 c^2}, \quad (2.3)$$

and

$$\beta = \sqrt{1 - \frac{1}{\gamma^2}} = \frac{v}{c}. \quad (2.4)$$

The parallel and perpendicular reflection coefficients  $r_{\parallel}$  and  $r_{\perp}$  are calculated in terms of the observation angle  $\theta$  and dielectric constants of the media. As discussed earlier, a vacuum to medium transition was assumed in which the dielectric constant  $\epsilon_1$  of the vacuum is equal to one, and the dielectric constant of the medium may be written as  $\epsilon$ . Then  $r_{\parallel}$  and  $r_{\perp}$  are given by

$$r_{\parallel} = \frac{\epsilon \cos \theta - \sqrt{\epsilon - \sin^2 \theta}}{\epsilon \cos \theta + \sqrt{\epsilon - \sin^2 \theta}}, \quad (2.5)$$

$$r_{\perp} = \frac{\cos \theta - \sqrt{\epsilon - \sin^2 \theta}}{\cos \theta + \sqrt{\epsilon - \sin^2 \theta}}. \quad (2.6)$$

Equations (2.1) and (2.2) contain only the two highest terms in the Lorentz factor  $\gamma$  [Ref. 8]. Note that the odd-powered factor of  $\theta$  in  $I_{\parallel}$  gives rise to an

asymmetric pattern as the angle changes sign. The TR3 program preserves this asymmetric behavior by reversing the sign of the angles represented in the first 32 columns in the 64 by 64 array used to calculate and organize the data.

Rule's analytical calculations took into account the effect of beam divergence on the transition radiation intensity pattern. This was done by folding Gaussian distributions for the projected angles into equations (2.1) and (2.2), resulting in

$$I_{\parallel} = \frac{e^2}{c} \beta^2 (2\pi)^{-3/2} \sigma_x^{-1} \{ |r_{\parallel}|^2 \operatorname{Re}[(\gamma + \sqrt{2}Z\sigma_x) \times W(Z) - \left[ \frac{2}{\pi\sigma_x^2} \right]^{1/2} - 2\operatorname{Re}(r_{\parallel}) \operatorname{Im} W(Z)] \}, \quad (2.7)$$

and

$$I_{\perp} = \frac{e^2}{c} \beta^2 (2\pi)^{-3/2} \sigma_x^{-1} \sigma_y^2 \gamma^2 |r_{\perp}|^2 \times \operatorname{Re}[(\gamma - \sqrt{2}Z/\sigma_x)W(Z) + \sigma_x^{-1} (2/\pi)^{1/2}], \quad (2.8)$$

where  $Z$  is defined as  $(\gamma^{-1} + i\theta)/\sqrt{2}\sigma_x$ ,  $\sigma_x$  as the rms beam angle of divergence projected into the observation plane, and  $\sigma_y$  as the rms angle of beam divergence perpendicular to this plane and containing the beam axis. Rule ignored the second term of equation (2.2) for equation (2.8) and it was also assumed that the rms beam divergence was small, i.e.  $\sigma \ll \gamma^{-1}$ . The function  $W(Z)$  is given in terms of the error function  $\phi(Z)$  in the non-standard form

$$W(Z) = [1 - \phi(Z)] \exp(Z^2). \quad (2.9)$$

The whole of the single foil program, TR3, was built around the analytic solutions embodied by equations (2.7–2.9). Total intensity was defined simply as

the sum of the perpendicular and parallel components. All intensities were calculated in terms of charge squared divided by the speed of light per unit frequency and solid angle and were normalized for plotting purposes. Actual values of intensities as defined here were stored in a file labelled RADOUT.DAT. Note that if the beam divergence is symmetric such that  $\sigma_x = \sigma_y$  then the total divergence angle is  $\sqrt{2}\sigma$ . This case was built into the single foil program.

Rule's analytic solutions were extended into three dimensions by calculating the parallel and perpendicular components of radiation intensity and the total radiation intensity over an angular distribution centered around the angle of specular reflection. This angular range was broken down into a 64 by 64 array in which the intensities were calculated for each point in the array. The parallel component, perpendicular component, or total intensity for each point may be stored in the graphics output file for plotting. Each point in the array represents an angle and position measured from the axis of specular reflection. The axis was set at the center of the array in the thirty-second column of the thirty-second row of the array. In terms of data storage, the rows of the array correspond to records and the columns correspond to field elements. Each of the 64 records contain 64 field elements. Since the program takes several minutes to calculate the data, progress is indicated by a record number.

## B. INTERFEROMETER

The interferometer program, COHER3, was based on the TEM series of transition radiation programs developed by D.W. Rule et al. that culminated in the two-dimensional program COHER1. The COHER1 program was developed around Rule's analytical solutions for transition radiation in the case of Wartski's two-foil

interferometer. A finite optical frequency bandwidth was also built in, allowing for a study of the affects of finite bandwidth on transition radiation intensity distribution. The COHER3 program simply extended COHER1 to three dimensions, modifying it so as to allow flexibility in altering data parameters during run time, and tailoring the output to be compatible with the three-dimensional graphics program, SON OF SURF3D

At the time of this writing, Rule and Fiorito had not published a full discussion of their analytical solution for the two-foil interferometer case. However, a discussion of the development of the analytical code for parallel component of intensity was published [Ref. 7] and formed the basis of the presentation here. The perpendicular component follows a similar argument in development.

Rule and Fiorito's analysis began with Wartski's [Ref. 5] development of the two-foil interferometer. Wartski showed that the parallel component of TR intensity per unit frequency and solid angle in this case could be written

$$I_{\parallel} = F(\psi, \theta, \omega) \frac{e^2 \beta^2 \sin^2 \theta}{4 \pi^2 c (1 - \beta \cos \theta)^2} |1 - e^{-i\phi}|^2, \quad (2.10)$$

where  $\omega$  represents frequency,  $\Omega$  represents a solid angle,  $\psi$  represents the angle of specular reflection,  $\theta$  represents the observation angle as measured from  $\psi$ , and  $F(\psi, \theta, \omega)$  represents a Fresnel coefficient which for a vacuum to medium transition is defined

$$F(\psi, \theta, \omega) = \left| \frac{[\epsilon - \sin^2(\psi + \theta)]^{1/2} - \epsilon \cos(\psi + \theta)}{[\epsilon - \sin^2(\psi + \theta)]^{1/2} + \epsilon \cos(\psi + \theta)} \right|. \quad (2.11)$$

The exponential term is the interference term for the transition radiation patterns differing in phase by  $\phi$ . This phase difference is defined in equation (1.2) as the ratio of the interfoil spacing to the coherence length. For relativistic particles, with a Gaussian distribution of beam angles folded in and averaged over particle angles with respect to the beam  $\alpha$ , the intensity per unit frequency and solid angle may be written

$$I_{\parallel} = 4F(\psi, \omega) \frac{e^2}{\pi^2 c} \int_{-\infty}^{\infty} \frac{(\theta - \alpha)^2}{[\gamma^{-2} + (\theta - \alpha)^2]^2} \times \\ \times \sin^2 \left[ \frac{\pi L}{2\lambda} [\gamma^{-2} + (\theta - \alpha)^2] [2\pi\sigma_x^2]^{-1/2} e^{-\alpha^2/2\sigma_x^2} d\alpha \right. \\ (2.12)$$

The basis of the COHER3 program is the analytical code developed by Rule and Fiorito to solve both equation (2.12) and the integral for the perpendicular component of intensity as well. The result for each component may be written

$$I_{\parallel} = \frac{e^2}{c} \beta^2 (2\pi)^{-3/2} \sigma_x^{-1} \left[ |r_{\parallel}|^2 \operatorname{Re} \left[ \gamma + \frac{(1/\gamma - i\theta)W(z)}{\sigma_x^2} \right] \right. \\ \left. - \frac{1}{2\pi^2 \sigma_x^2} \right] + \frac{\beta^2 \operatorname{Re} |r_{\parallel}| \operatorname{Im} W(z)}{\pi \sqrt{2\pi} \sigma_x}, \quad (2.13)$$

$$I_{\perp} = \frac{e^2}{c} \beta^2 (2\pi)^{-3/2} \sigma_y^2 \sigma_x^{-1} \gamma^2 \left[ |r_{\perp}|^2 \operatorname{Re} \left[ \gamma - \frac{(1/\gamma - i\theta)W(z)}{\sigma_x^2} \right] \right. \\ \left. + \frac{1}{2\pi^2 \sigma_x^2} \right]. \quad (2.14)$$

### C. THE GRAPHICS PROGRAM

The three-dimensional graphics program used in conjunction with the TR3 and COHER3 programs for the analytical study of transition radiation was SON OF SURF3D [Ref. 10]. This program was a derivative of a program written by Don Gilmore of Dogstar Software to explore the graphics capabilities of TurboHalo 3.0 [Ref. 11]. SON OF SURF3D is able to plot three-dimensional surfaces from data files containing three-dimensional point information of up to 100 by 100 arrays.

The data points stored in the output file for the graphics program SON OF SURF3D are automatically standardized relative to the axes according to the following formula [Ref. 10]

$$Z' = \frac{(Z - Z_{\min} - Z_{\text{cen}})}{(Z_{\max} - Z_{\min})}. \quad (2.15)$$

The TR3 and COHER3 programs store normalized real values of the parallel component, perpendicular component, or total intensity in an output file named by the user. For purposes of the analysis, the z-maximum value was set at 1.0 and both the z-minimum and z-center values were set at 0.0. Doing so sets the axis markers at the bottom of the data set in the three-dimensional plots and shows the intensities relative to a maximum intensity. An option was provided to normalize all intensities to the maximum intensity at 100 MeV.

### III SINGLE FOIL TRANSITION RADIATION

The TR3 program was run many times while changing one parameter each time in order to study the effect of that parameter on the distribution of transition radiation intensity. The effects of energy, beam divergence, scattering foil, and dielectric constant foil were studied in this manner.

#### A. ENERGY

The single foil case for transition radiation was calculated for energies of 1 GeV, 500 MeV, and for 10 MeV to 100 MeV in increments of 10 MeV. The total intensity distribution as a function of angle was calculated over an angular range of  $-.05$  to  $+.05$  radians with respect to the angle of specular reflection. Several observations were made from the resulting data (Tables I,II) and associated three-dimensional plots (Figures 3-7). The data for Figures 3-7 were normalized to the maximum value of intensity for the energy plotted. Therefore the maximum relative value is one (1.0), which is represented by the top of the z-axis. The units on the z-axis are thus the dimensionless ratio of intensity to maximum intensity. The angular distribution was over 0.05 radians as measured from the z-axis in either direction along the x and y axes. The endpoints on the x and y axes coincide with .0625 radians.

The most obvious observation was that the shape of the plots varied greatly from one energy to the next when using the fixed parameters described above. However, the plots appear nearly identical when plotting the data over a relative scale such as a multiple of the predicted angle of maximum intensity.

Such is the case for Figures 8–10 in which the data was calculated over an angular distribution of five times the predicted angle of maximum intensity for the energy plotted, i.e.  $|\theta| \leq 5/\gamma$ .

At low energy the plot was a gently curved cone shape centered around the z-axis with the opening extending almost the full angular width of the plot. The angular separation measured from the angle of specular reflection (z-axis) was defined as theta (Figure 1 of chapter I). The angle between the z-axis and the sides of the cone form a particular value of theta. As the energy was increased, the cone became more sharply defined and the angle steadily decreased. Wartski [Ref. 5] showed this phenomenon was predicted in theory from the equation for transition radiation intensity per unit frequency and solid angle in this case for a vacuum to medium transition.

$$I = \frac{q^2 \beta^2}{4\pi^2 c} \sin^2 \theta \left| \frac{1}{1-\beta \cos \theta} + \frac{r_{\parallel}}{1+\beta \cos \theta} - \frac{f_{\parallel}}{\epsilon} \frac{1}{1-\beta \sqrt{\epsilon} \sin^2 \theta} \right|^2 \quad (3.1)$$

where  $q$  is the charge on the particle,  $\epsilon$  is the dielectric constant of the medium, and the fresnel coefficients  $r_{\parallel}$  and  $f_{\parallel}$  are defined as

$$r_{\parallel} = \frac{\epsilon \cos \theta - \sqrt{\epsilon - \sin^2 \theta}}{\epsilon \cos \theta + \sqrt{\epsilon - \sin^2 \theta}} \quad (3.2)$$

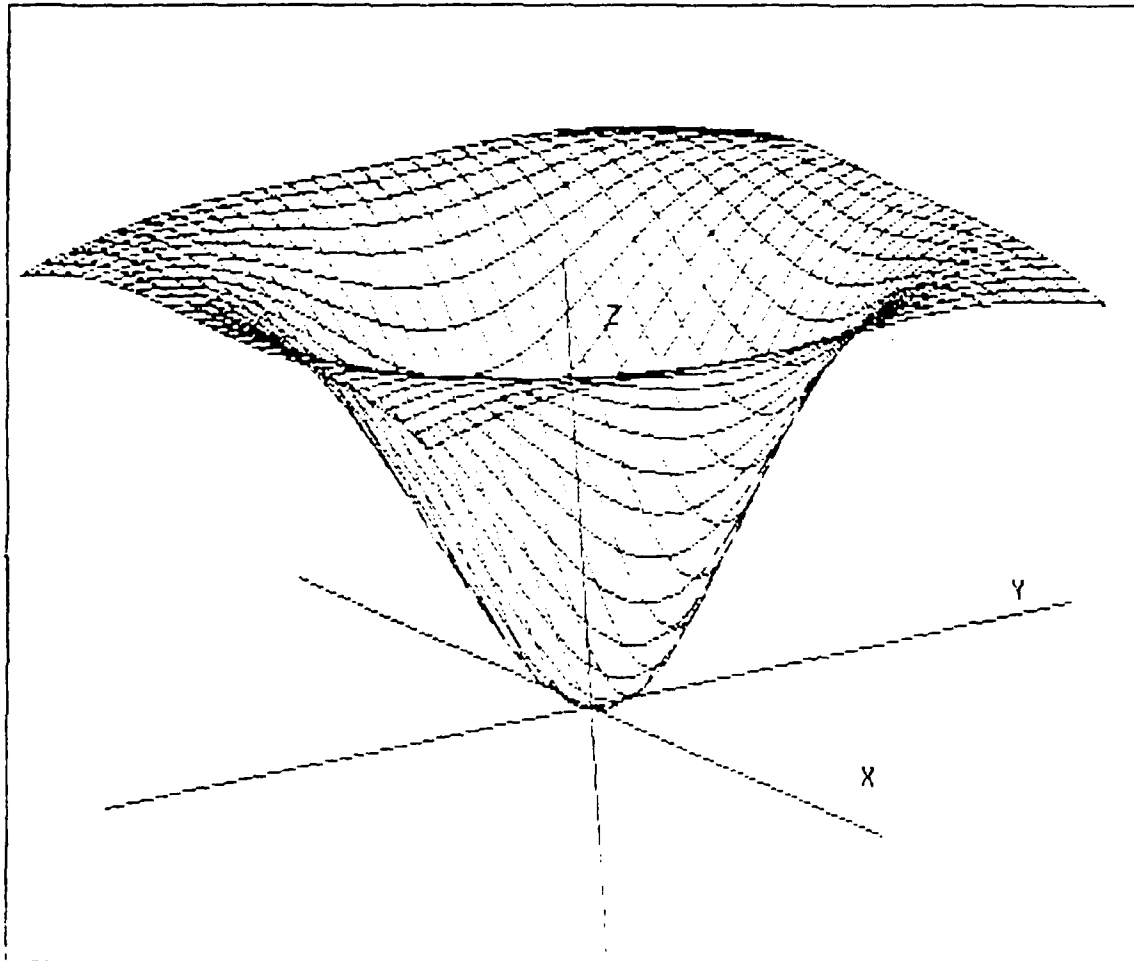


Figure 3. Single foil transition radiation at 10 Mev. Note the overall cone shape of the plot. The sides of the cone describe the angle at which the maximum intensity occurs relative to the axis of specular reflection (Z-axis). The X-Y plane depicts the angular distribution in radians. The data extends to from  $-0.05$  to  $+0.05$  radians on each axis. The endpoints on the X and Y axes correspond to  $\pm 0.0625$  radians. The units measured along the Z-axis are the dimensionless ratio of intensity to maximum intensity. The top of the Z-axis corresponds to the maximum value of the data.

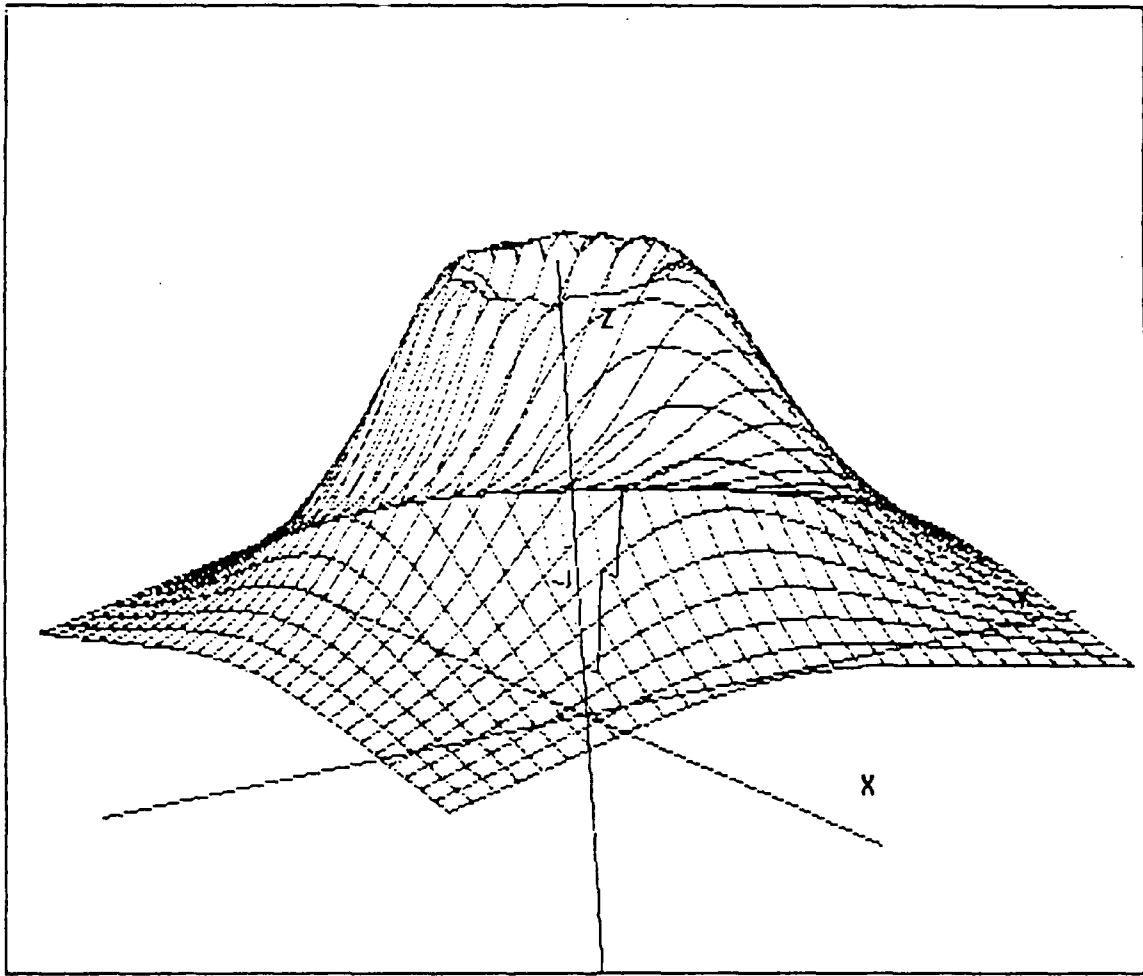


Figure 4. Single foil transition radiation at 40 Mev. The cone shape still exists in the center of the plot, but the angle describing the position of maximum intensity is considerably smaller. The X-Y plane depicts the angular distribution in radians. The data extends to from  $-.05$  to  $+.05$  radians on each axis. The endpoints on the X and Y axes correspond to  $\pm.0625$  radians. The units measured along the Z-axis are the dimensionless ratio of intensity to maximum intensity. The top of the Z-axis corresponds to the maximum value of the data.

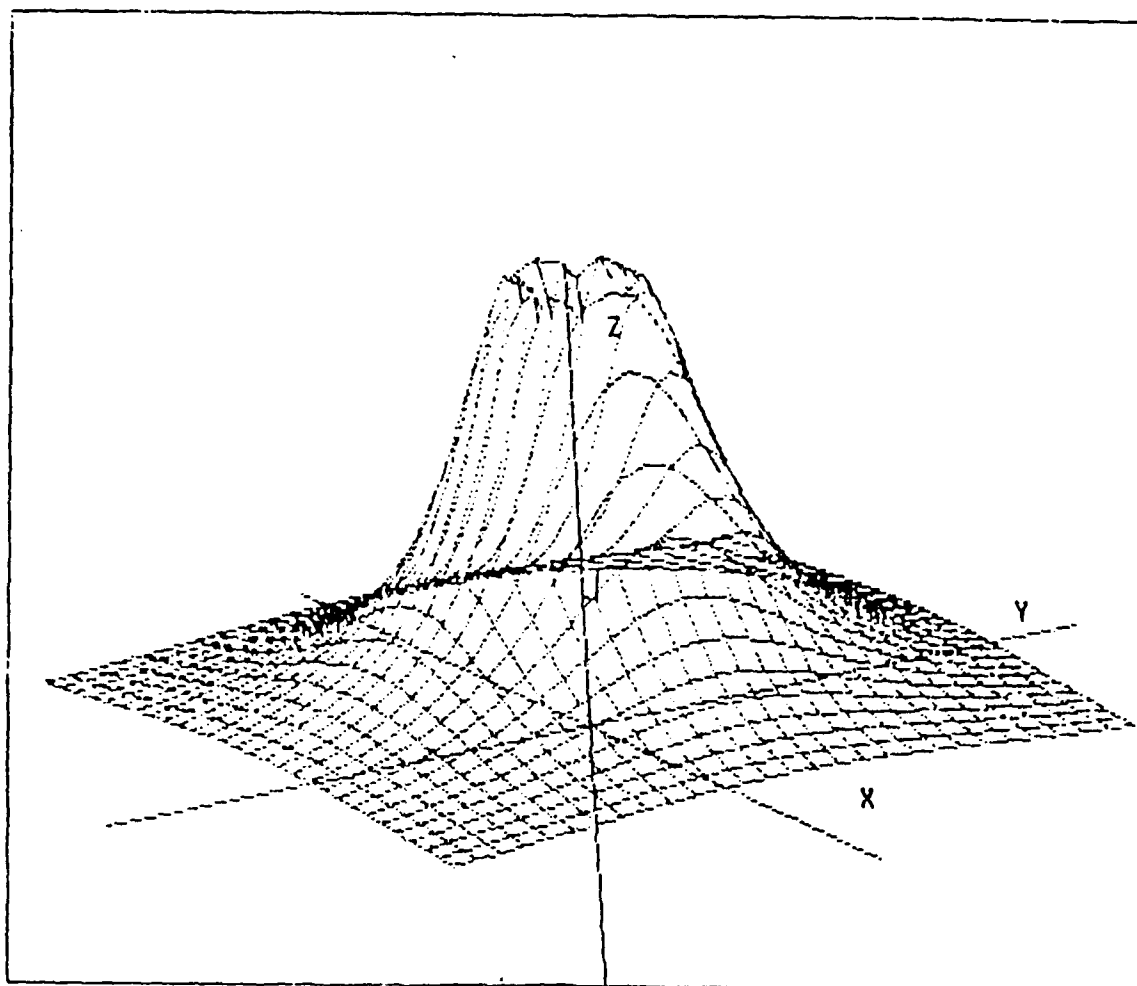


Figure 5. Single foil transition radiation at 70 Mev. The original shape of a cone is nearly lost in the center of the plot. The angle describing the position of maximum intensity is again much smaller. The X-Y plane depicts the angular distribution in radians. The data extends to from  $-0.05$  to  $+0.05$  radians on each axis. The endpoints on the X and Y axes correspond to  $\pm 0.0625$  radians. The units measured along the Z-axis are the dimensionless ratio of intensity to maximum intensity. The top of the Z-axis corresponds to the maximum value of the data.

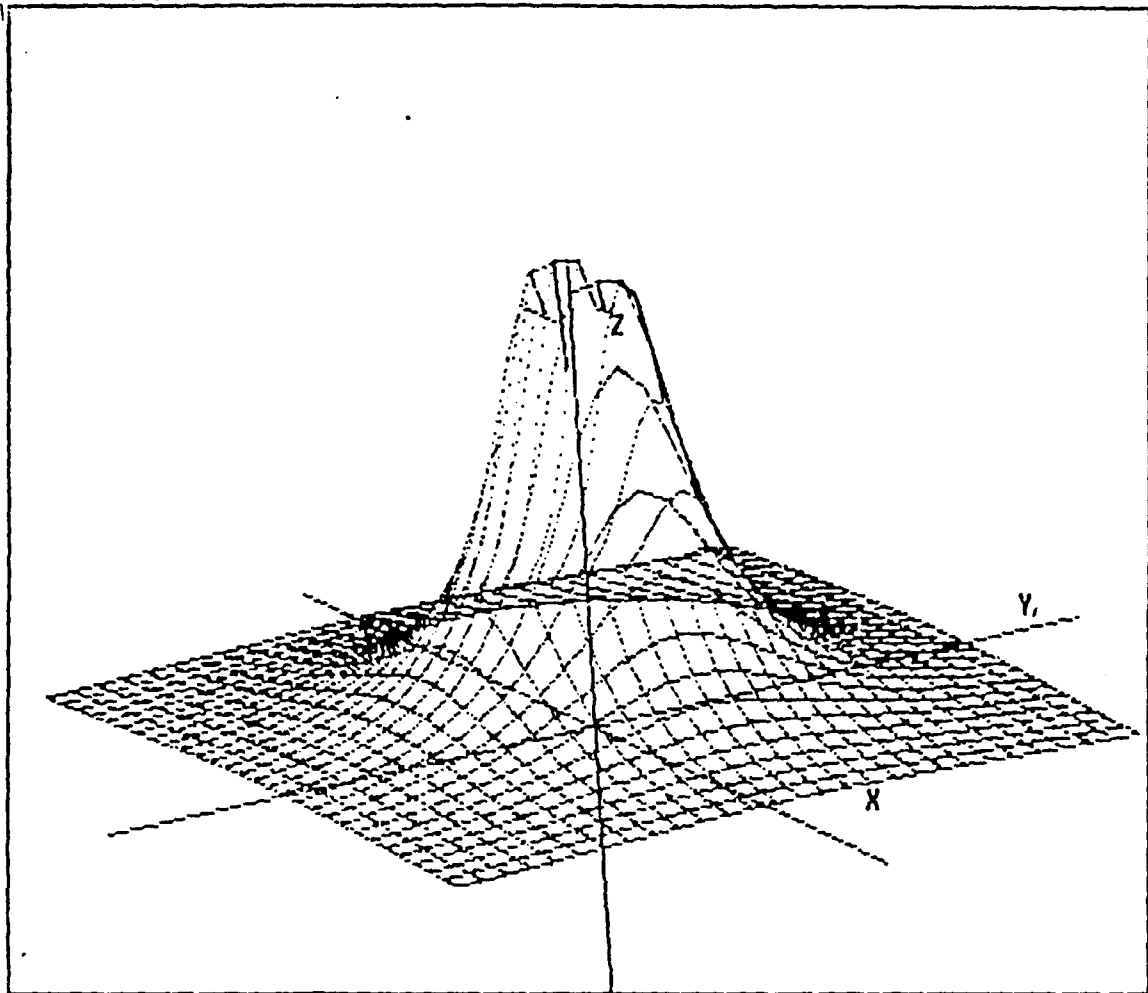


Figure 6. Single foil transition radiation at 100 MeV. The only remaining evidence of the original cone appears to be the rim occurring at the top of the plot around the Z-axis. The apparent asymmetry of the rim is due to the plotting algorithm and is not a physical reality. The X-Y plane depicts the angular distribution in radians. The data extends to from  $-0.05$  to  $+0.05$  radians on each axis. The endpoints on the X and Y axes correspond to  $\pm 0.0625$  radians. The units measured along the Z-axis are the dimensionless ratio of intensity to maximum intensity. The top of the Z-axis corresponds to the maximum value of the data.

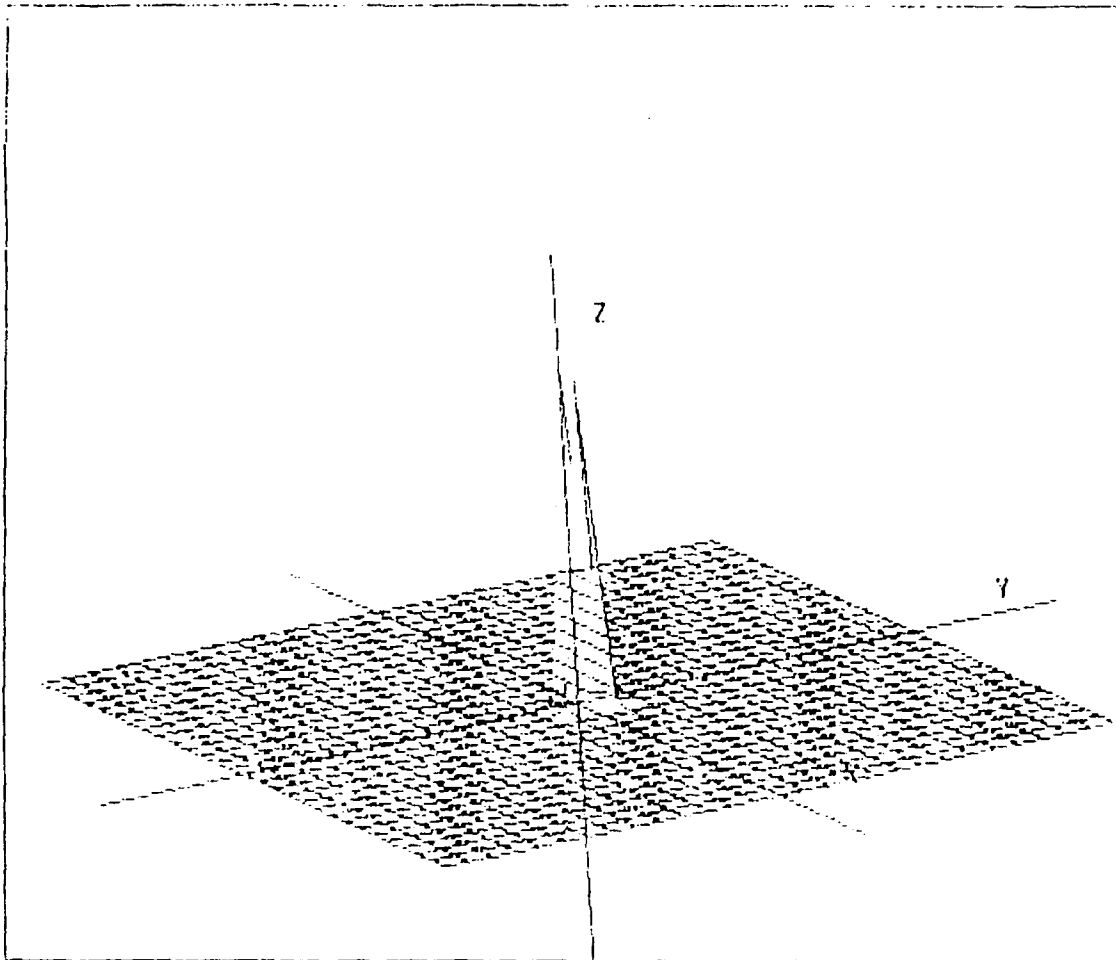


Figure 7. Single foil transition radiation at 1 GeV. The data appears to converge to a point below the top of the Z-axis which should represent the maximum value of the data. In fact, the maximum value occurred on the axis of specular reflection represented by the Z-axis. Furthermore, maximum value of the data occurred as a point which is at the top of the Z-axis. The X-Y plane depicts the angular distribution in radians. The data extends to from  $-0.05$  to  $+0.05$  radians on each axis. The endpoints on the X and Y axes correspond to  $\pm 0.0625$  radians. The units measured along the Z-axis are the dimensionless ratio of intensity to maximum intensity. The top of the Z-axis corresponds to the maximum value of the data.

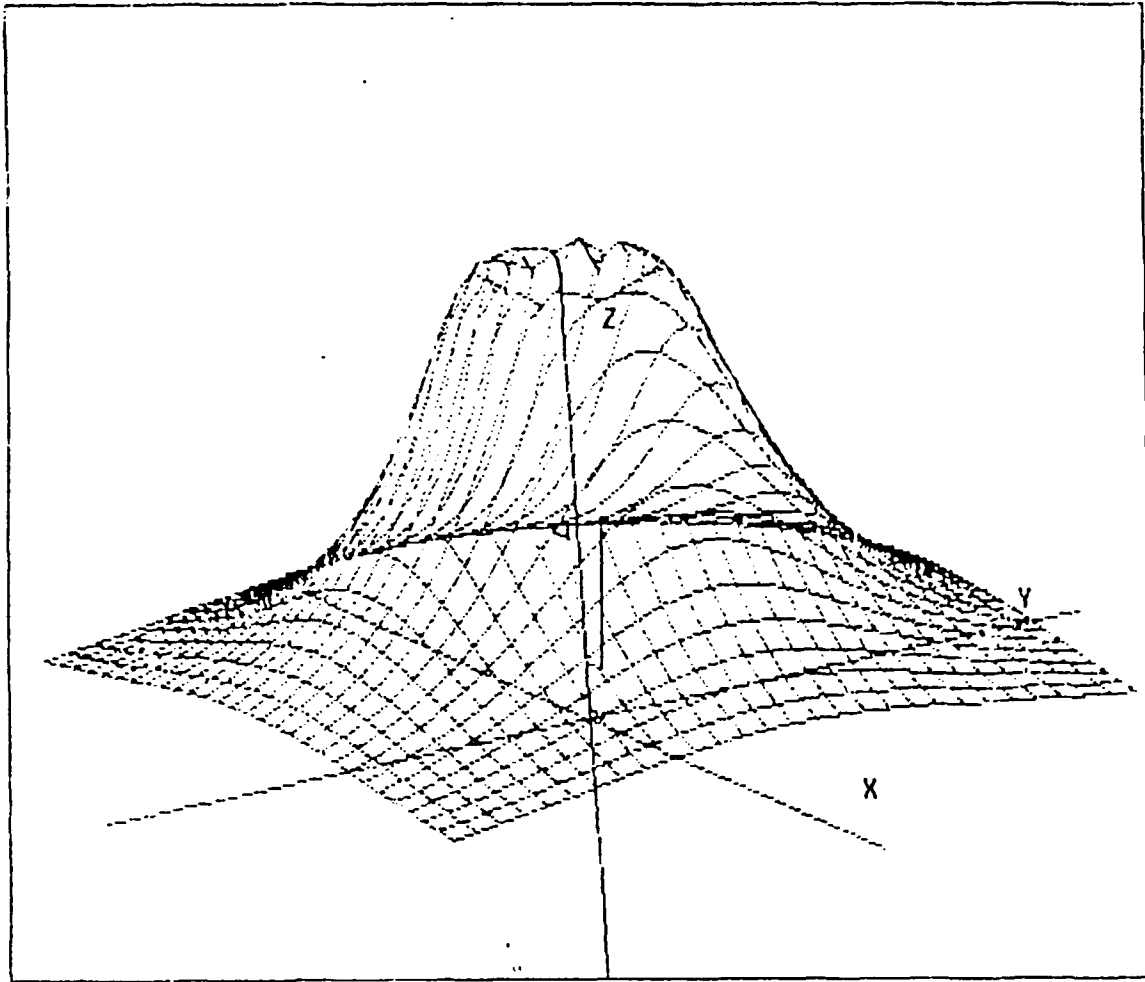


Figure 8. Single foil transition radiation at 30 Mev. Compare with the plot for single foil transition radiation at 40 MeV (Figure 4). In this case data extends to five times the predicted value of maximum intensity,  $1/\gamma$  in either direction on the X and Y-axes. The Z-axis still measures the relative intensity of the data with the top of the Z-axis corresponding to the maximum intensity.

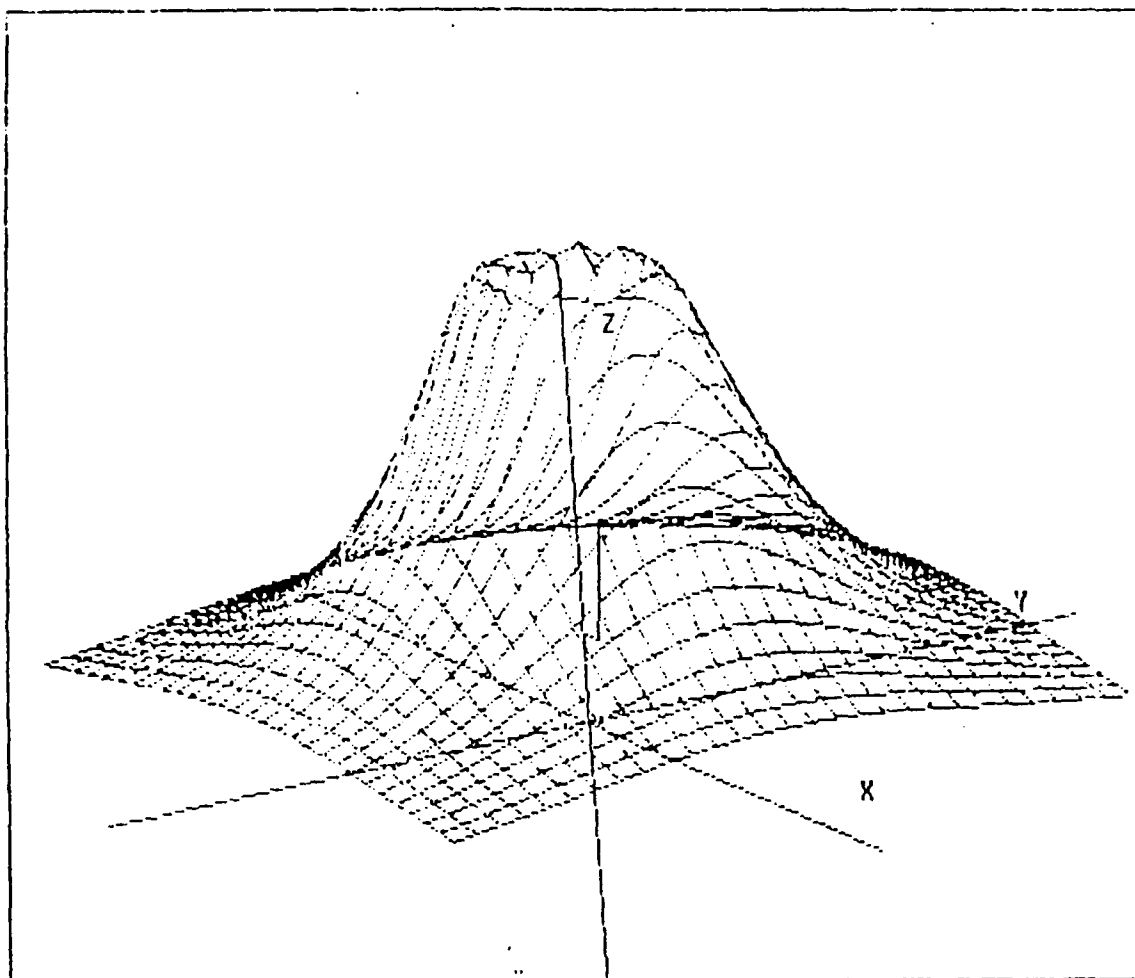


Figure 9. Single foil transition radiation at 60 Mev. The plot is nearly identical to the plot for 30 MeV (Figure 8), which is plotted on the same relative scale. That is, the data extends to five times the predicted value of maximum intensity,  $1/\gamma$  in either direction on the X and Y-axes. The Z-axis measures the relative intensity of the data with the top of the Z-axis corresponding to the maximum intensity.

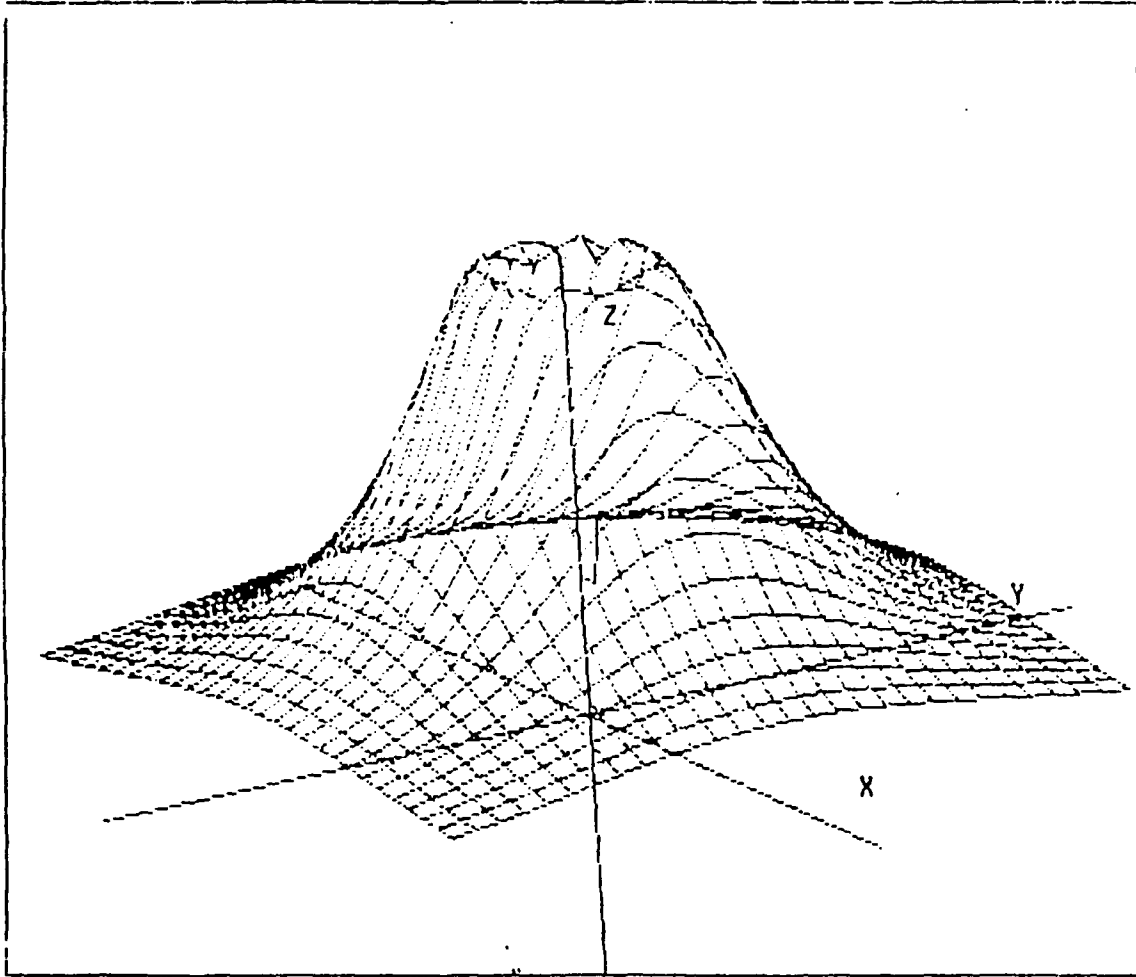


Figure 10. Single foil transition radiation at 90 Mev. Compare with the plot for 30 and 60 MeV (Figures 8,9), measured on the same relative scale. The plots appear to be identical. The shape of the single foil transition radiation pattern is independent to the energy. Intensity increases with energy increases while the angle at which the maximum intensity occurs decreases. The data extends to five times the predicted value of maximum intensity,  $1/\gamma$  in either direction on the X and Y-axes. The Z-axis still measures the relative intensity of the data with the top of the Z-axis corresponding to the maximum intensity.

$$f_{\parallel} = \frac{2 \epsilon \cos \theta}{\epsilon \cos \theta + \sqrt{\epsilon - \sin^2 \theta}}. \quad (3.3)$$

The fresnel coefficients must satisfy the continuity relationship:

$$1 + r_{\parallel} = f_{\parallel} \quad (3.4)$$

For metallic media in the visible region,  $|\epsilon| \gg 1$ , and equation (3.1) can be rewritten

$$I = |r_{\parallel}|^2 \frac{e^2 \sin^2 \theta}{4\pi^2 c (1 - \beta \cos \theta)^2}. \quad (3.5)$$

Since  $\beta \cong 1 - (1/2\gamma^2)$  for the extremely relativistic case

$$I = |r_{\parallel}|^2 \frac{e^2 \sin^2 \theta}{4\pi^2 c [1 - \cos \theta + (1/2\gamma^2) \cos \theta]^2}. \quad (3.6)$$

A second approximation was made by considering the angle theta sufficiently small such that  $\sin^2 \theta$  and  $\cos^2 \theta$  could be replaced by  $\theta^2$  and  $(1 - \theta^2/2)$ , respectively, leaving

$$I = \frac{e^2}{\pi^2 c} |r_{\parallel}|^2 \frac{\theta^2}{[\theta^2 + 1/\gamma^2]^2}. \quad (3.7)$$

Again, the preceding equations were for the specific case at hand of a vacuum to medium transition. The factor  $|r_{||}|^2$ , the reflectance of the medium, can be ignored for a medium to vacuum transition. Equation (3.7) showed the relationship of radiation intensity to energy and the angle theta. The nature of this relationship was shown by differentiating equation (3.7) with respect to theta:

$$\frac{dI}{d\theta} = \frac{e^2}{\pi^2 c} |r_{||}|^2 \frac{[2\theta(1/\gamma^2 - \theta^2)]}{(\theta^2 + 1/\gamma^2)^3}. \quad (3.8)$$

This equation demonstrated that the extrema occur for the theta equal zero direction and for theta equal  $1/\gamma$ . Using these values for theta in equation (3.7) showed that the radiation intensity is zero in the theta equal zero direction and is at a maximum for the theta equal  $1/\gamma$  direction. This angle of maximum radiation intensity decreased as energy increased. A look at Figures 3-7 showed that the relationship was qualitatively true. A close look at the data (Table I). in which the angle measured where maximum intensity actually occurred was compared with  $1/\gamma$  demonstrated excellent correlation.

The energy, the Lorentz factor  $\gamma$ , predicted angle of maximum intensity  $1/\gamma$ , and measured angle of maximum intensity  $\theta_m$ , for a beam divergence of .001 radians were tabulated in Table I. The maximum value of the total intensity ITOT, maximum value of parallel intensity IPAR, maximum value of perpendicular intensity IPERP, the value of parallel intensity at maximum total intensity  $IPAR(\theta_m)$ , and the value of perpendicular intensity at maximum total intensity  $IPERP(\theta_m)$ , were tabulated in Table II for comparison. Intensity

was calculated per unit frequency and solid angle in terms of the square of the charge divided by the speed of light. Energy was listed in units of MeV, angles were listed in units of radians. Additionally, parallel, perpendicular, and total intensities at the angle of maximum intensity as well as the maximum of the perpendicular intensity versus energy were plotted in Figure 11. The plot revealed that total and parallel intensity increased as a power function of energy.

TABLE 1. ACTUAL VS. ANGLE OF MAXIMUM INTENSITY

Energy (MeV)	$\gamma$	$1/\gamma$ (radians)	Actual $\theta_m$ (radians)
10	20.57	.0486	.0487
20	40.14	.0249	.0250
30	59.71	.0168	.0169
40	79.28	.0126	.0126
50	98.85	.0101	.0102
60	118.4	.0084	.0087
70	137.0	.0073	.0072
80	157.6	.0064	.0065
90	177.1	.0057	.0058
100	196.7	.0051	.0051
500	979.5	.0010	.0000

It was interesting to note that the maximum intensity at .5 GeV and 1.0 GeV occurred at the theta equal zero direction. A look at the data in Table II provides a clue as to why this occurred. As energy increased, the perpendicular component of intensity provided a greater proportion of the total intensity. It was found that the perpendicular component of intensity began to dominate over the parallel component at energies above 200 MeV. At .5 GeV and 1.0 GeV, the perpendicular component of intensity dominated over the parallel component of

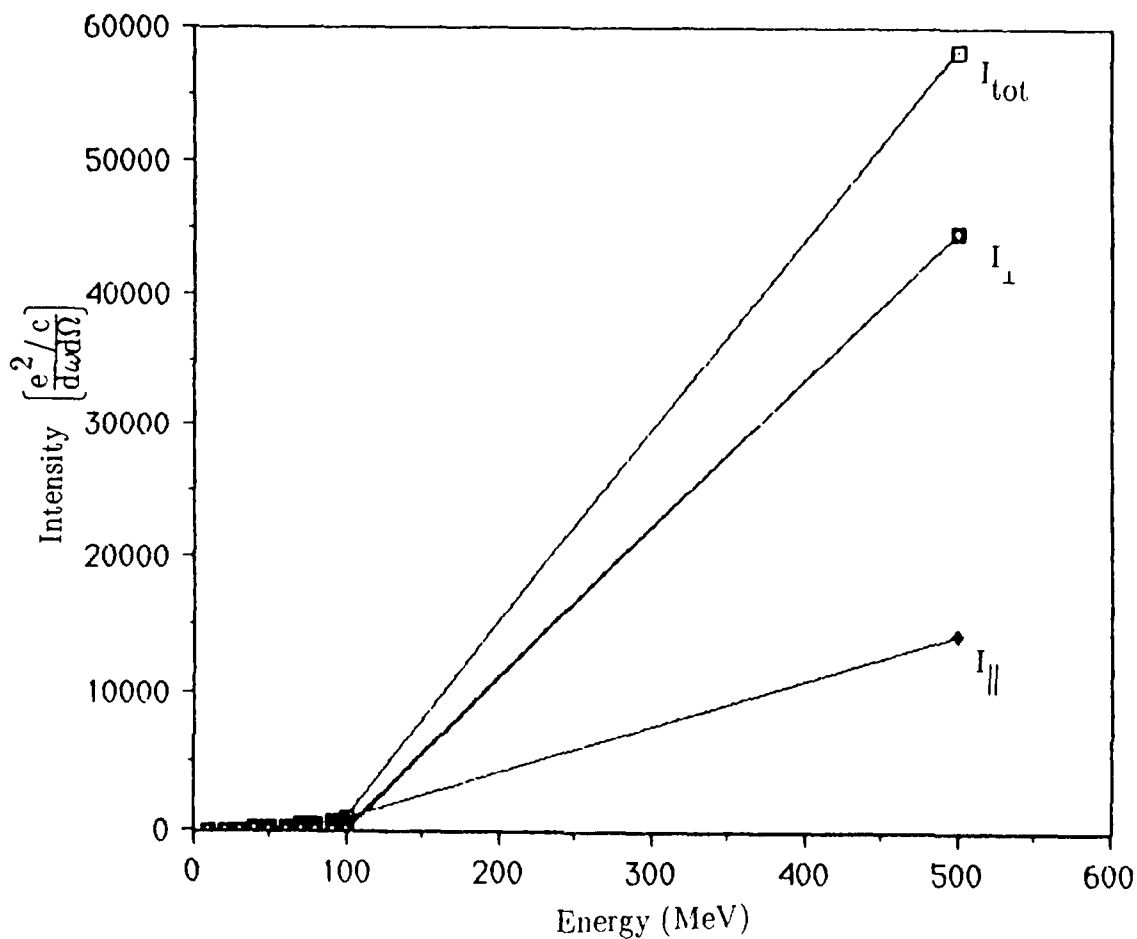


Figure 11. A plot of the components of intensity versus energy. It is apparent that the perpendicular component at the angle where the maximum intensity occurs is negligible at lower energies. However, the maximum value of the perpendicular component can not be ignored. This maximum value occurs on the axis of specular reflection, and thus tends to fill up the cone shape seen in Figures 3-5.

TABLE II. INTENSITIES

ENERGY (MeV)	ITOT $\left[\frac{e^2/c}{d\omega d\Omega}\right]$	IPAR $\left[\frac{e^2/c}{d\omega d\Omega}\right]$	IPERP $\left[\frac{e^2/c}{d\omega d\Omega}\right]$	IPAR( $\theta_m$ ) $\left[\frac{e^2/c}{d\omega d\Omega}\right]$	IPERP( $\theta_m$ ) $\left[\frac{e^2/c}{d\omega d\Omega}\right]$
10	9.571	9.567	0.171	9.567	.0043
20	36.51	36.45	.2479	36.45	.0618
30	80.83	80.52	1.209	80.52	.3036
40	142.5	141.6	3.740	141.6	.9617
50	221.7	219.4	8.979	219.4	2.296
60	318.1	313.5	18.34	313.5	4.580
70	432.3	423.2	33.53	423.2	9.106
80	564.1	549.3	56.42	549.1	15.01
90	713.5	689.9	89.13	689.9	23.63
100	881.4	843.0	133.9	843.0	38.36
500	58230	14230	44740	13480	44740
1000	467300	52090	415200	52090	415200

intensity in contributing to the total intensity. The components of radiation intensity behave quite differently from each other and contribute distinct profiles to the total intensity distribution. Wartski [Ref. 5], (Figure 12) showed that the perpendicular and parallel components of radiation intensity could be written:

$$I_{\parallel} = \frac{e^2}{4\pi^2 c} \left| \frac{\beta_{\parallel} \times \vec{n}}{1-\beta n} + r_{\parallel} \frac{\beta_{\parallel} \times \vec{n}'}{1-\beta n} - \frac{f_{\parallel} \beta_{\parallel} \times \vec{n}''}{\sqrt{\epsilon} (1-\beta n'' \sqrt{\epsilon})} \right|^2 \quad (3.9)$$

$$\left[ \frac{d^2 W}{d\omega d\Omega} \right]_{\perp} = I_{\perp} = \frac{e^2}{4\pi^2 c} \beta_{\perp}^2 \left| \frac{1}{1-\beta n} + r_{\perp} \frac{1}{1-\beta n'} - \frac{f_{\perp}}{\sqrt{\epsilon} (1-\beta n'' \sqrt{\epsilon})} \right|^2, \quad (3.10)$$

where  $\vec{n}$ ,  $\vec{n}'$ ,  $\vec{n}''$ , are as depicted in Figure 12 and  $\beta_{\parallel}$  and  $\beta_{\perp}$  are the projections of the  $\vec{v}/c$  vector on the plane of observation. Wartski [Ref. 5]

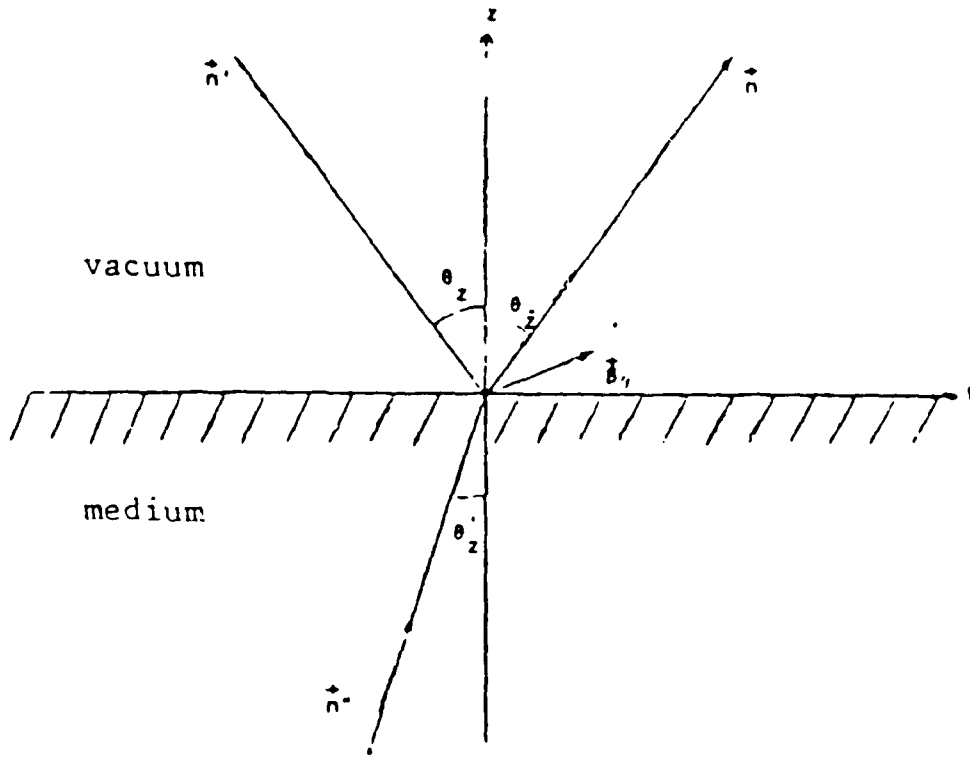


Figure 12. The the unit  $\vec{n}$ ,  $\vec{n}'$ ,  $\vec{n}''$ , and  $\vec{\beta}$  vectors in the plane of observation as depicted in Wartski [Ref. 5].

showed that for ultra-relativistic particles, where it is assumed that  $\sqrt{\epsilon} \gg 1$  in a vacuum to medium transition, the second term in equations (3.9) and (3.10) dominates as  $\vec{\beta} \cdot \vec{n}$  becomes close to one. In this case

$$I_{\parallel} = \frac{e^2}{4\pi^2 c} \left| \frac{\vec{\beta}_{\parallel} \times r_{\parallel} \vec{n}}{1 - \vec{\beta} \cdot \vec{n}'} \right|^2, \quad (3.11)$$

and

$$I_{\perp} = \frac{e^2}{4\pi^2 c} \beta^2 \left| r_{\perp} - \frac{1}{1 - \vec{\beta} \cdot \vec{n}'} \right|^2. \quad (3.12)$$

The maximum value of  $I_{\perp}$  does not occur at the same position as the maximum of total intensity except at very high energies where the perpendicular component of intensity becomes dominate and thus determines the location of the maximum total intensity. It was found that the energy where this occurs is in the neighborhood of about 200 MeV. A look at the perpendicular reflection coefficient reveals that the maximum of the perpendicular component of radiation intensity occurs when theta ( $\theta$ ), the angular separation from the observation angle (z-axis) is zero

$$r_{\perp} = \frac{\cos \theta - \sqrt{\epsilon - \sin^2 \theta}}{\cos \theta + \sqrt{\epsilon - \sin^2 \theta}} = \frac{1 - \sqrt{\epsilon}}{1 + \sqrt{\epsilon}} \Big|_{\theta=0} \quad (3.13)$$

For non-relativistic particles, the perpendicular component of the radiation intensity could be shown to be essentially zero while the parallel component of radiation intensity could be written

$$I_{\parallel} = \frac{e^2}{4\pi^2 c} \beta_z^2 \sin^2 \theta_z \left| 1 + r_{\parallel} - \frac{f_{\parallel}}{\sqrt{\epsilon}} \right|^2$$

$$= \frac{e^2}{\pi^2 c} \beta^2 \Big|_{\epsilon-1} \left| \frac{\sin^2 \theta \cos^2 \theta}{\epsilon \cos \theta + \sqrt{\epsilon - \sin^2 \theta}} \right|^2 \quad (3.14)$$

The  $\beta_z$  in equation (3.14) indicates that the radiation produced by a non-relativistic particle for an oblique angle is the same as that for

normal incidence at a velocity of  $\beta_z$  rather than  $\beta$ . It was clear from equation (3.14) that the parallel component of radiation intensity for a non-relativistic particle is proportional to the square of the energy as is the total intensity.

In the ultra-relativistic energy region,  $I_{\parallel}$  remains proportional to the square of the energy. Equation (3.12) indicates that  $I_{\perp}$  is also proportional to the square of the energy for lower energies. The contribution of  $I_{\perp}$  to the total energy is negligible at lower energies but becomes quite significant as energy increases, and increases asymptotically as  $\vec{\beta} \cdot \vec{n}$  approaches one. Figures 13-15 depict the perpendicular component of radiation intensity at 100, 250, and 500 MeV.

Analysis of equation (3.7) revealed that total intensity was proportional to the square of the energy. Figures 16-18 dramatically showed the dependence of radiation intensity on energy. The intensity distribution for these figures was scaled to the maximum intensity value of 100 MeV. The energies for these figures were 50 MeV to 90 MeV in increments of 20 MeV.

Finally, a closer look at Figures 8-10 reveals that the plots aren't quite identical in appearance. In each case the intensity distribution was calculated over an angular distribution of five times the predicted angle of maximum intensity of  $1/\gamma$  for the energies of 30, 60, and 90 MeV. Closer inspection revealed that the apex of the cone decreased in depth as energy increased. Obviously, the apex of the cone was not zero intensity at higher energies. This was due to the contribution of the perpendicular component of intensity to the total intensity distribution.

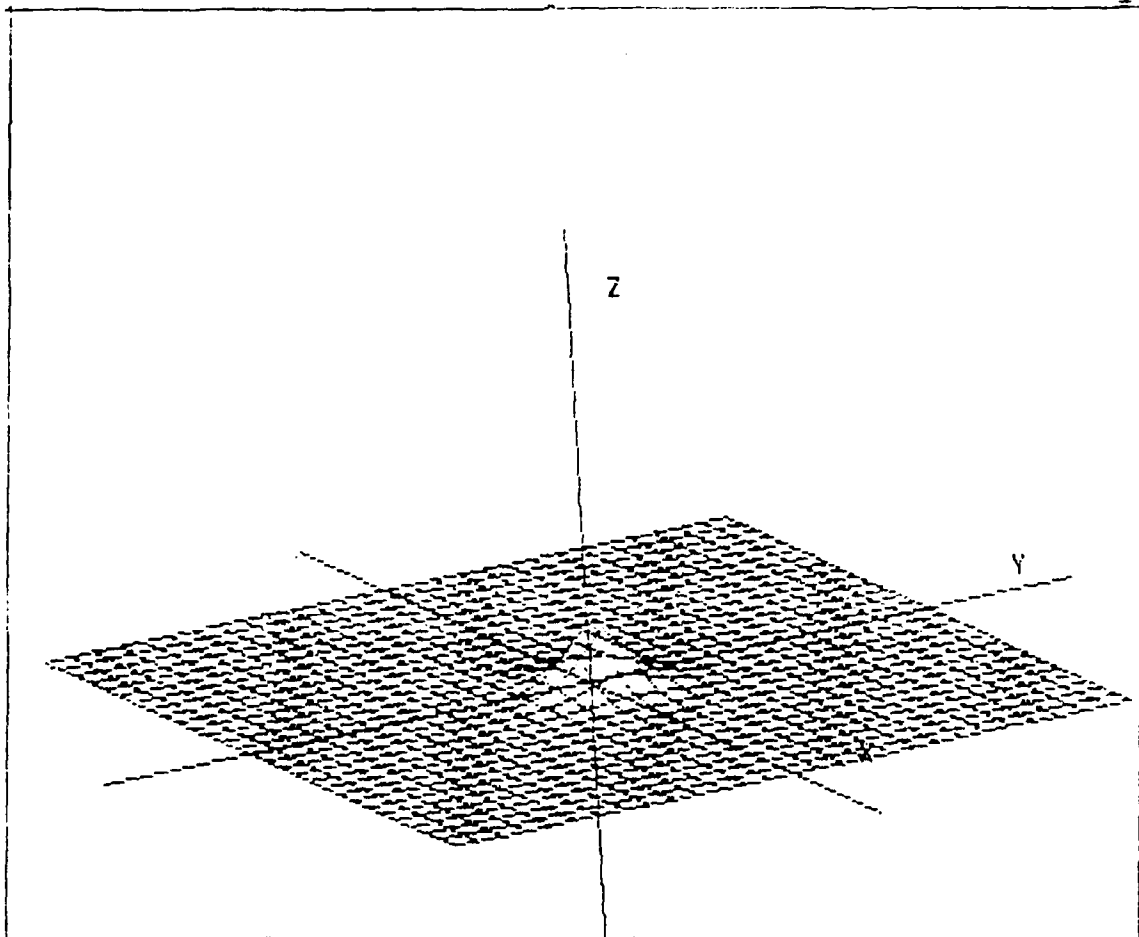


Figure 13. The perpendicular component of intensity at 100 MeV. The data extends to five times the predicted value of maximum intensity,  $1/\gamma$  in either direction on the X and Y-axes. The Z-axis measures the relative intensity of the data with the top of the Z-axis corresponding to the maximum total intensity.

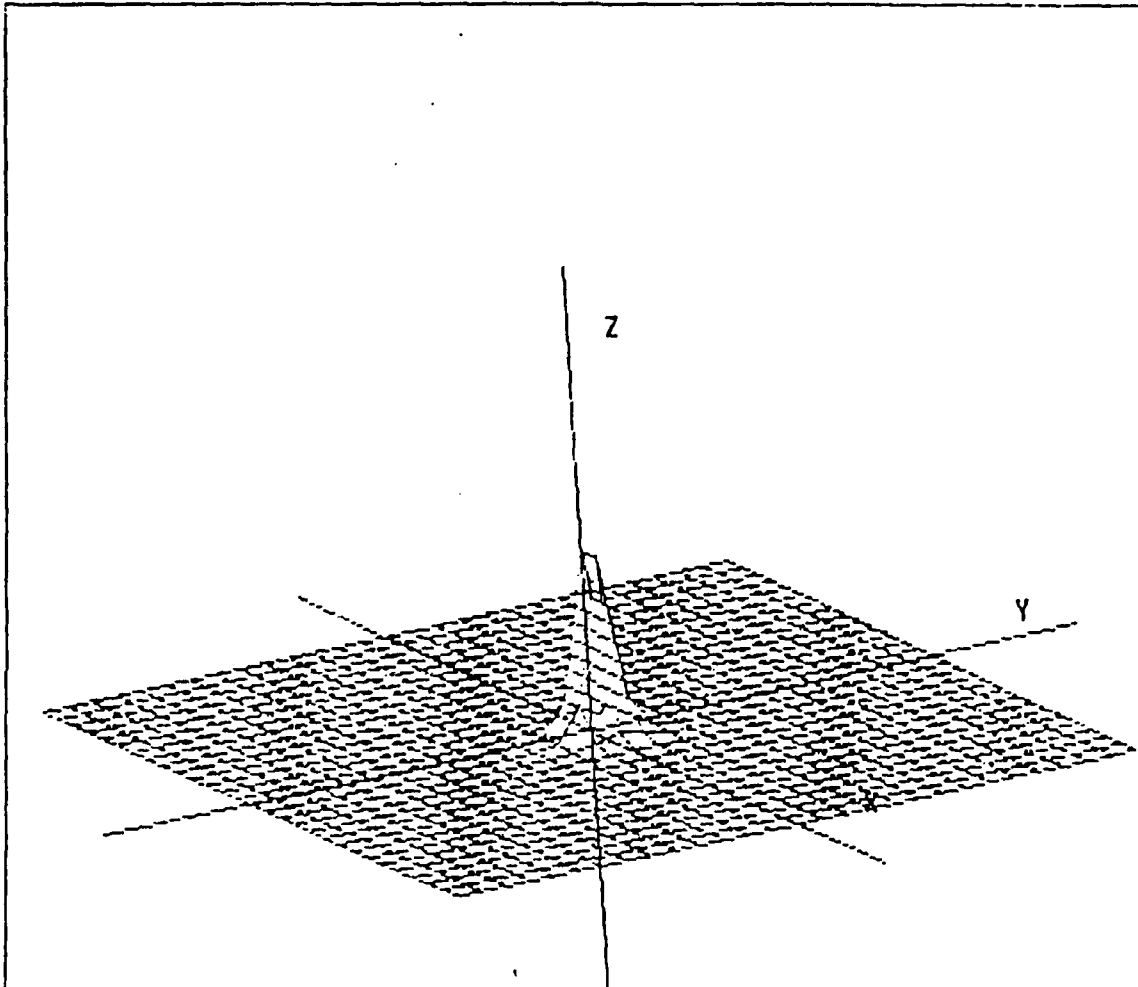


Figure 14. The perpendicular component of intensity at 250 MeV. The data extends to five times the predicted value of maximum intensity,  $1/\gamma$  in either direction on the X and Y-axes. The Z-axis measures the relative intensity of the data with the top of the Z-axis corresponding to the maximum total intensity.

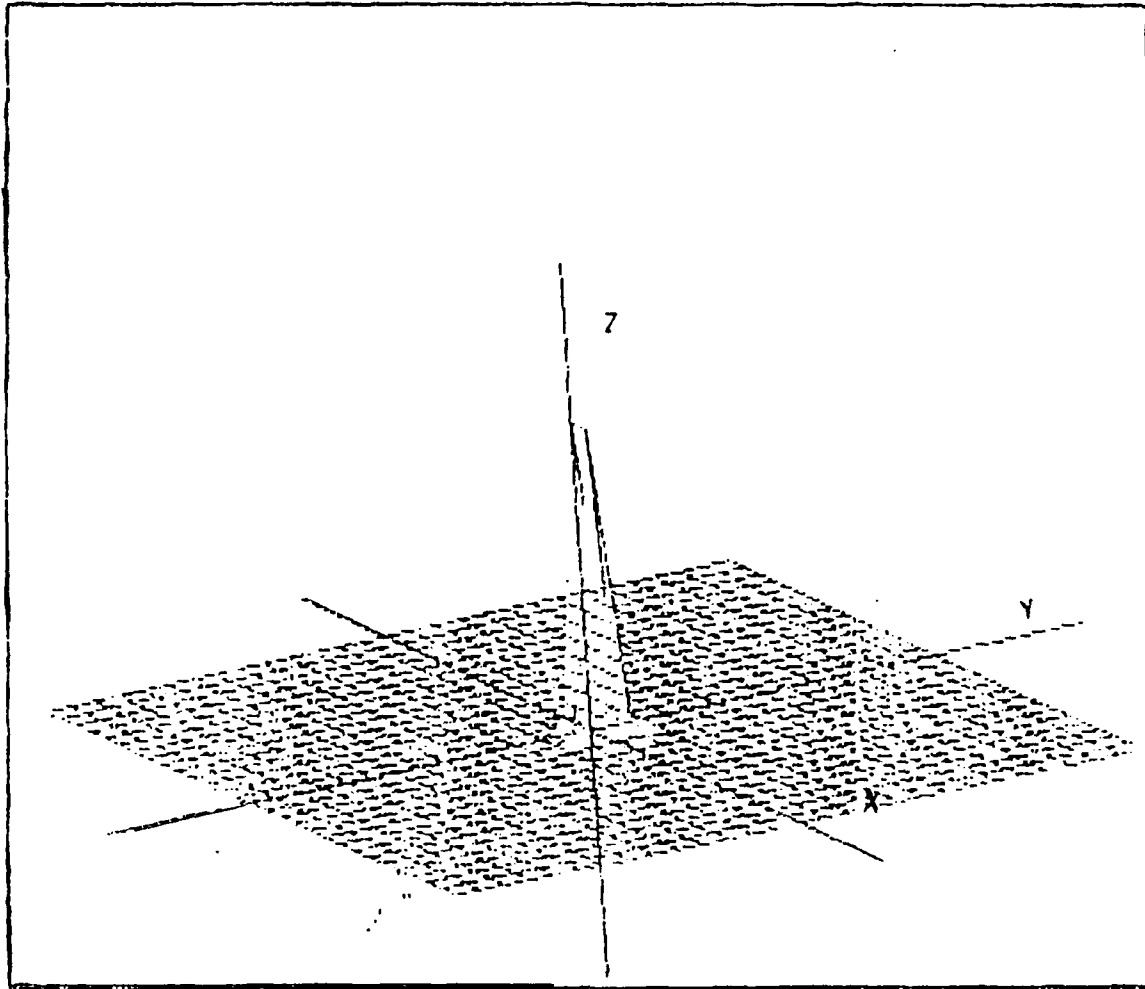


Figure 15. The perpendicular component of intensity at 500 MeV. The data extends to five times the predicted value of maximum intensity,  $1/\gamma$  in either direction on the X and Y-axes. The Z-axis measures the relative intensity of the data with the top of the Z-axis corresponding to the maximum total intensity.

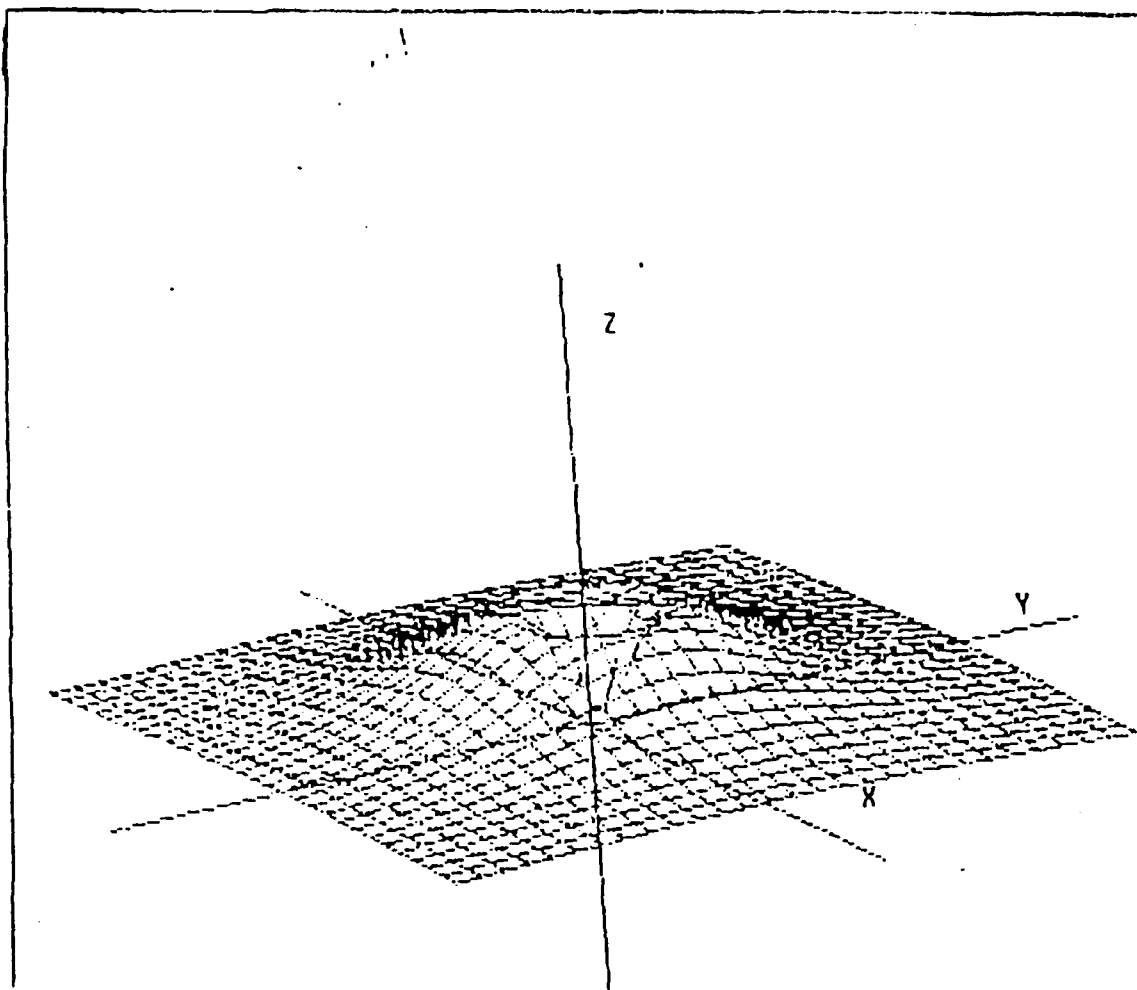


Figure 16. Single foil transition radiation intensity at 50 MeV. The data extends to five times the predicted value of maximum intensity,  $1/\gamma$  in either direction on the X and Y-axes. The Z-axis measures the intensity of the data relative to the maximum intensity obtained for 100 MeV using the default values of the program.

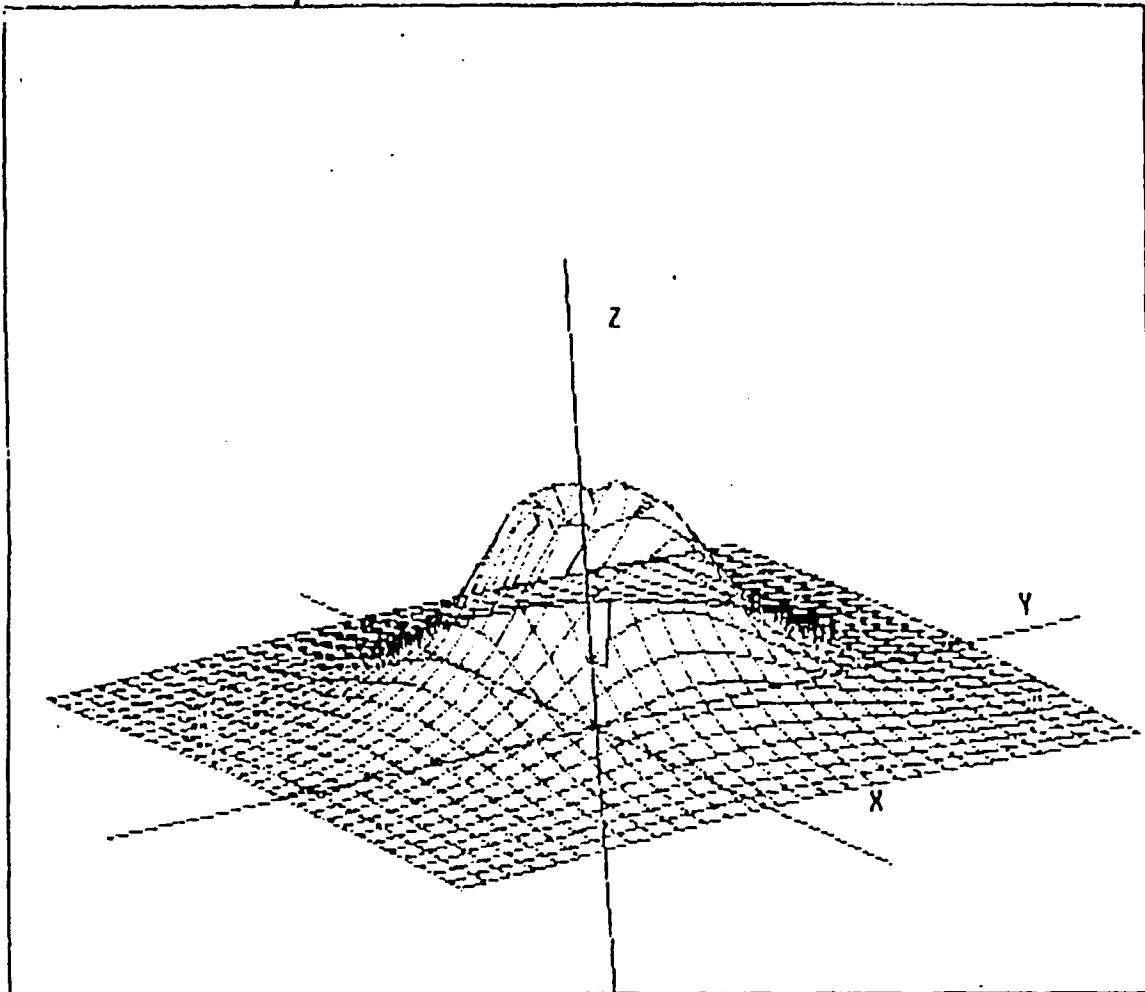


Figure 17. Single foil transition radiation intensity at 70 MeV. The data extends to five times the predicted value of maximum intensity,  $1/\gamma$  in either direction on the X and Y-axes. The Z-axis measures the intensity of the data relative to the maximum intensity obtained for 100 MeV using the default values of the program.

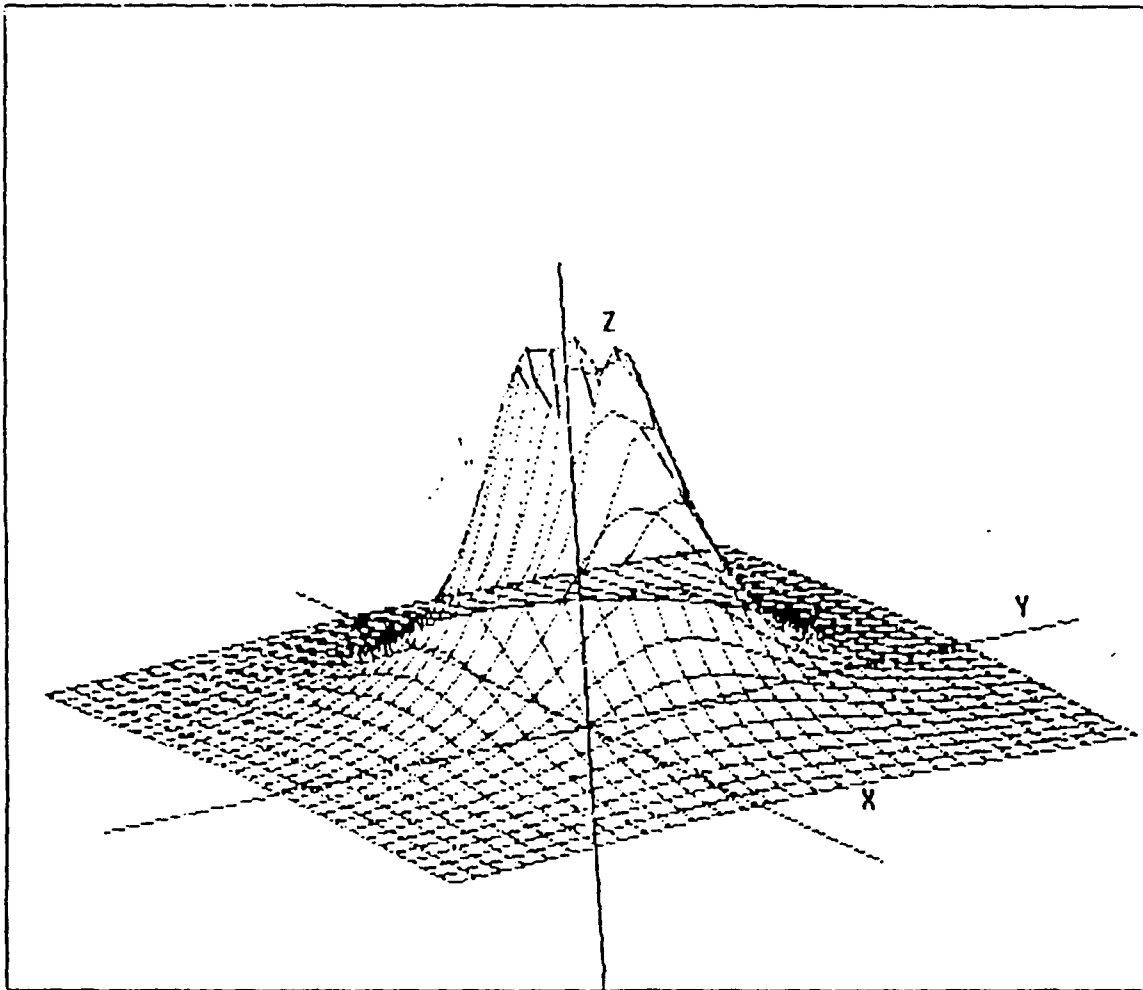


Figure 18. Single foil transition radiation intensity at 90 MeV. The data extends to five times the predicted value of maximum intensity,  $1/\gamma$  in either direction on the X and Y-axes. The Z-axis measures the intensity of the data relative to the maximum intensity obtained for 100 MeV using the default values of the program.

TABLE III. MULTIPLES OF  $1/\gamma$

Energy (MeV)	$\gamma$	$1/\gamma$ (radians)	$5/\gamma$ (radians)	$\theta_m$ (radians)
10	20.57	.0486	.2431	.0487
30	59.71	.0168	.0837	.0168
60	118.4	.0084	.0422	.0087
90	177.1	.0057	.0282	.0058

In summary, the angle of maximum intensity, total intensity, perpendicular component of intensity, and the parallel component of intensity were found to be very sensitive to changes in energy. The perpendicular component of intensity was found to be rather insignificant at energies below 50 MeV but quite dominate at energies above 200 MeV. The angle of maximum intensity, total intensity, and parallel component of radiation intensity would be the most useful parameters for diagnostic purposes of beam quality at lower energies. However the angular information is lost above 200 MeV when the perpendicular component of intensity becomes dominate.

## B. BEAM DIVERGENCE

The effect of beam divergence upon the transition radiation intensity distribution may be studied by assuming a Gaussian distribution of divergence angles. The Gaussian distribution of angles may be approximated by taking the root mean square average value and applying it to the transition radiation intensity equations (2.7) and (2.8) discussed in Chapter II.

$$I_{\parallel} = \frac{e^2}{c} \beta^2 (2\pi)^{-3/2} \sigma_x^{-1} \left[ |r_{\parallel}|^2 \operatorname{Re}[(\gamma + \sqrt{2}Z\sigma_x) \times W(Z) - \left[ \frac{2}{\pi\sigma_x^2} \right]^{1/2} - 2\operatorname{Re}(r_{\parallel}) \operatorname{Im} W(Z)] \right], \quad (2.7)$$

and

$$I_{\perp} = \frac{e^2}{c} \beta^2 (2\pi)^{-3/2} \sigma_x^{-1} \sigma_y^2 \gamma^2 |r_{\perp}|^2 \times \operatorname{Re}[(\gamma - \sqrt{2}Z/\sigma_x) W(Z) + \sigma_x^{-1} (2/\pi)^{1/2}]. \quad (2.8)$$

Recall that when writing the code for the single foil case, Rule [Ref. 7] programmed in the assumption that  $\sigma_x = \sigma_y = \sigma$  such that the total divergence angle is  $\sqrt{\sigma}$ . In this case, equations (2.7) and (2.8) may be rearranged to bring out the dependence on beam divergence more clearly.

$$I_{\parallel} = \frac{e^2}{c} \beta^2 (2\pi)^{-3/2} \left[ |r_{\parallel}|^2 \operatorname{Re}\left[\left(\frac{\gamma}{\sqrt{2}\sigma} + Z\right) \times W(Z) - \frac{1}{2\sigma^2} \left[ \frac{2}{\pi} \right]^{1/2} - \frac{2}{\sqrt{2}\sigma} \operatorname{Re}(r_{\parallel}) \operatorname{Im} W(Z) \right] \right], \quad (3.15)$$

$$I_{\perp} = \frac{e^2}{c} \beta^2 (2\pi)^{-3/2} \gamma^2 |r_{\perp}|^2 \times \operatorname{Re}[\sqrt{2}\sigma(\gamma - Z/\sigma) W(Z) + 2/\sqrt{\pi}]. \quad (3.16)$$

It is now clear that the parallel component of intensity should decrease with an increase in beam divergence. On the other hand, any increase in beam divergence should bring about a corresponding increase for the perpendicular component of intensity. Recall that the maximum intensity of the perpendicular component occurs on the axis of specular reflection. The maximum of the parallel component, however, occurs away from that axis at an angle equal to the inverse of

the Lorentz factor. Suppose the beam divergence would be permitted to become large enough for the perpendicular component to become comparable with, or even dominant over the parallel component. The angle at which the maximum intensity occurs would shift, eventually occurring on the axis of specular reflection whenever the perpendicular component dominates over the parallel component. The angular information provided by the parallel component would then be lost. Both components of intensity increase as a power function of energy so beam divergence effects should be more pronounced at higher energies.

The data in Table IV and in Figures 19–28 bear out the correctness of this analysis. Table IV contains a comparison of the total, parallel, and perpendicular intensities for various energies and rms beam divergence angles. Energy is listed in MeV, beam divergence, labelled Beam Div., is listed in radians. The intensities are per unit frequency and solid angle in terms of charge squared divided by the speed of light. The values for the parallel and perpendicular components of intensity are the maximum values obtained for that component. Since the maxima of the components of intensity do not occur in the same position, the sum of the values listed will not agree with the value of the total intensity. The angle  $\theta_m$  at which the maximum intensity occurs is in radians. It is included here to study the behavior of this parameter as the parallel and perpendicular components of intensity adjust roles to changes in beam divergence. Note that an increase in beam divergence is accompanied by a corresponding increase in the total and perpendicular intensities and a decrease in the parallel component of intensity. Whenever the beam divergence was large enough for the perpendicular component to dominate

over the parallel component, the maximum intensity occurred on the axis. This can be seen in Table IV in that whenever the value of IPERP was larger than that of IPAR, the value of  $\theta_m$  was zero.

The data for Figures 19–28 was normalized to the maximum intensity for the energy plotted. The top of the z-axis corresponds to the value of the maximum intensity. The horizontal width of the data in the plots of Figures 19–26 was fixed at 0.05 radians as measured in either direction along the axis from the z-axis. The ends of the X and Y axes correspond to a value of .0625 radians. The horizontal width of the data in the plots of Figures 27 and 28 was set at a value of five times the predicted angle of maximum intensity. This option was chosen to preserve clarity at high energies.

The effects of beam divergence on the intensity distribution are clearly seen in Figures 19–28. Figures 19–23 depict the effects of increasing beam divergence at 10 MeV. A general flattening of the intensity distribution seems to occur. However, recall that the predicted angle of maximum intensity for this energy is .049 radians while the data is calculated out to .05 radians. Thus Figures 19–23 provide a close look at the region where the perpendicular component of intensity becomes more and more dominant. The perpendicular component of intensity appears to become completely dominant when the beam divergence was increased to just over .0250 radians.

Figures 24–26 depict the shape of a gaussian distribution at an energy of 40 MeV as the beam divergence is increased from 0.0010 to 0.0060 radians. In this case the predicted angle of maximum intensity at .0126 radians is much less than the .0500 radians over which the data is calculated. Therefore, the effects of beam divergence on the parallel, as well as the perpendicular, component of intensity can

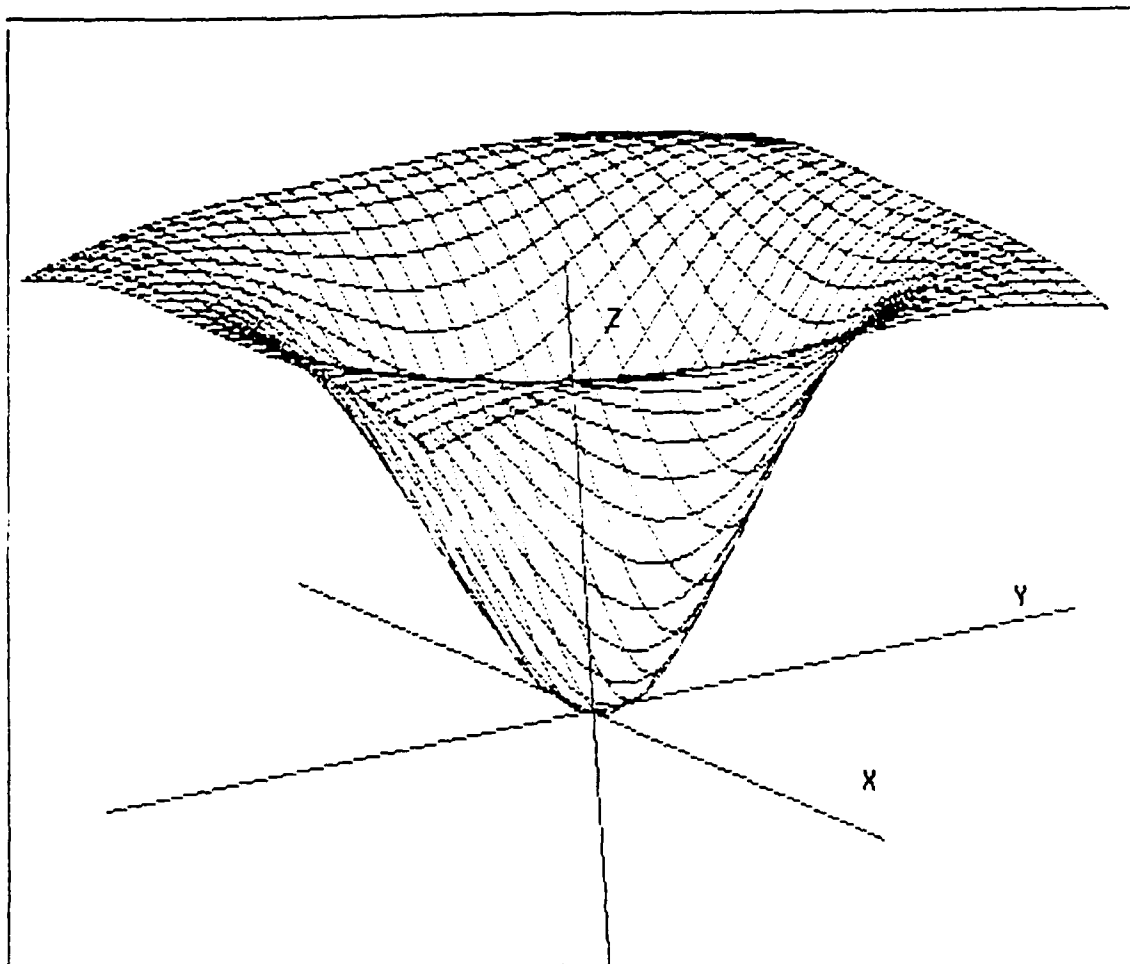


Figure 19. Single foil transition radiation pattern at 10 MeV for an rms beam divergence angle of  $1.000\text{E}-3$  radians. The data extends to .05 radians in the X-Y plane. The top of the Z-axis corresponds to the maximum intensity of the data.

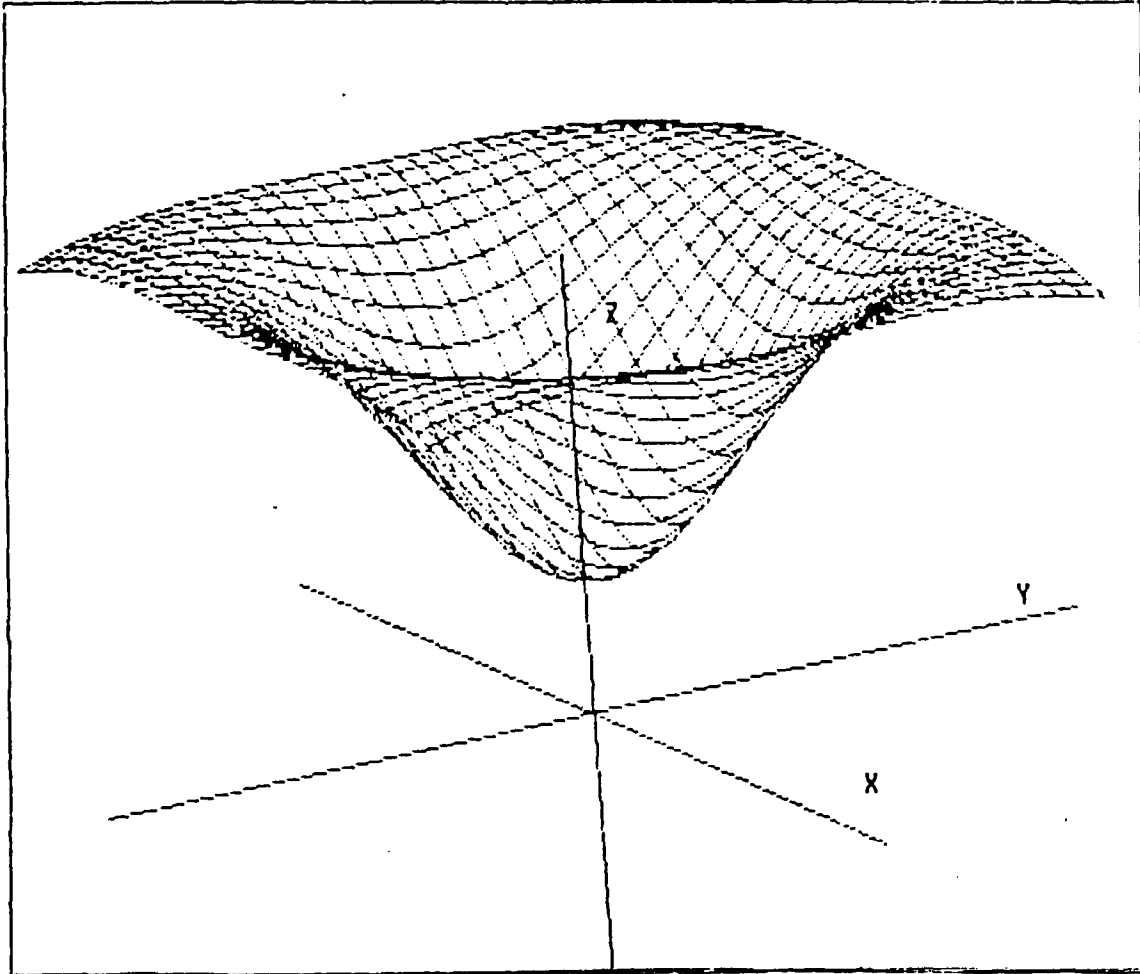


Figure 20. Single foil transition radiation pattern at 10 MeV for an rms beam divergence angle of  $1.000\text{E}-2$  radians. The depth of the cone is much shallower than in the previous figure. The data extends to .05 radians in the X-Y plane. The top of the Z-axis corresponds to the maximum intensity of the data.

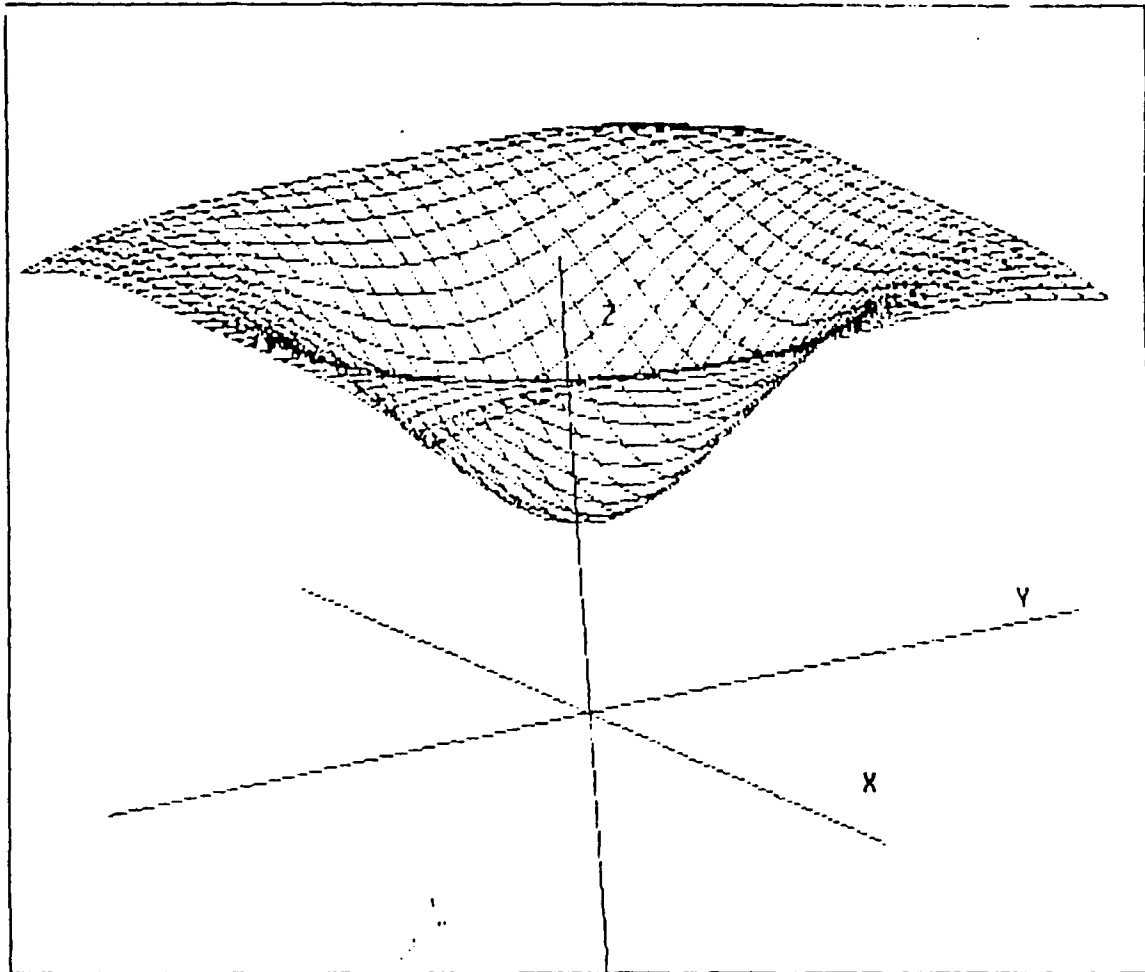


Figure 21. Single foil transition radiation pattern at 10 MeV for an rms beam divergence angle of  $1.250\text{E}-2$  radians. Note that the depth of the cone continues to decrease with an increase in beam divergence. The data extends to .05 radians in the X-Y plane. The top of the Z-axis corresponds to the maximum intensity of the data.

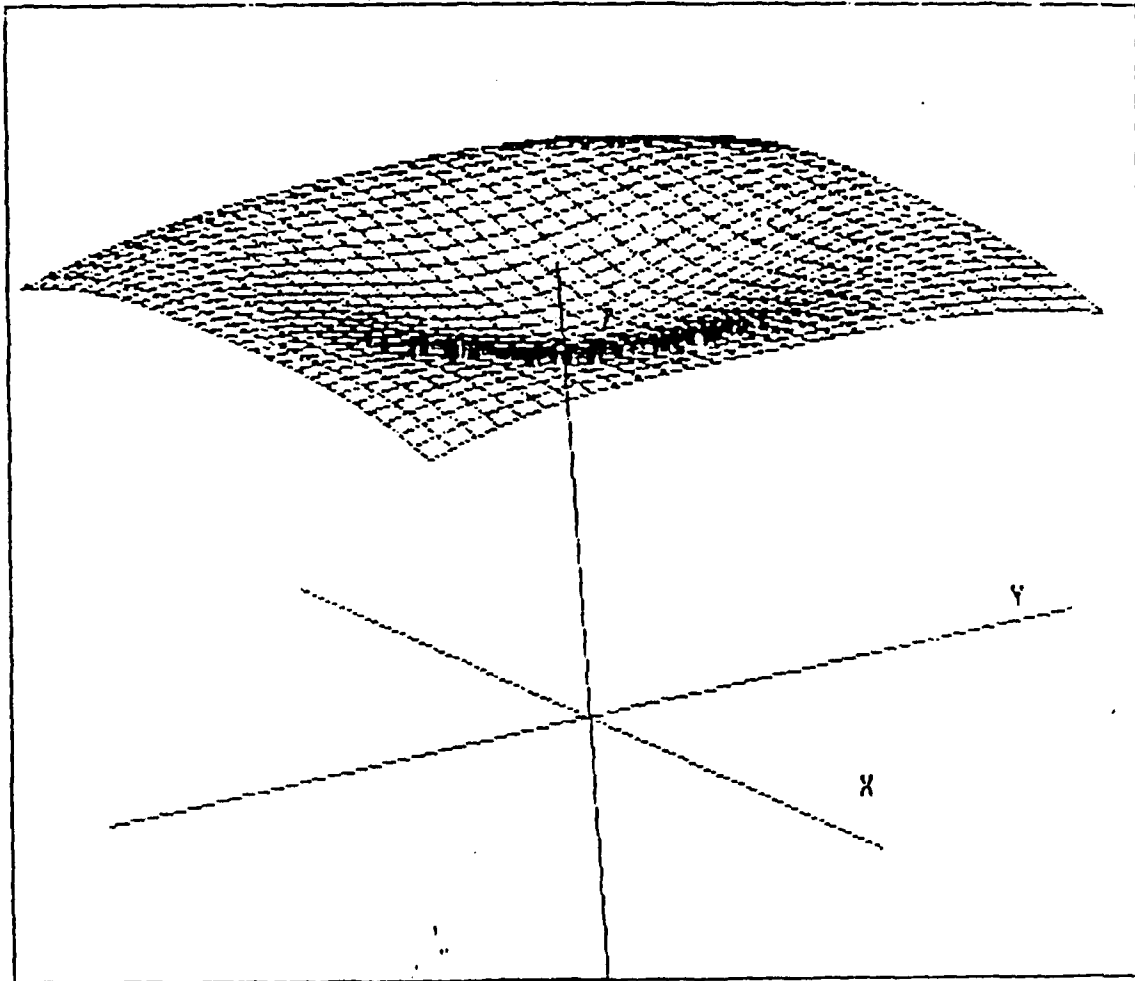


Figure 22. Single foil transition radiation pattern at 10 MeV for an rms beam divergence angle of  $2.000E-2$  radians. What's left of the cone appears to be little more than a dimple. Note that the angle at which the maximum intensity occurs for an energy of 10 MeV is  $.049$  radians while the data presented here extends to  $.05$  radians in the X-Y plane. The region depicted then coincides with the region in which the perpendicular component of intensity becomes more and more dominant over the parallel component. The top of the Z-axis corresponds to the maximum intensity of the data.

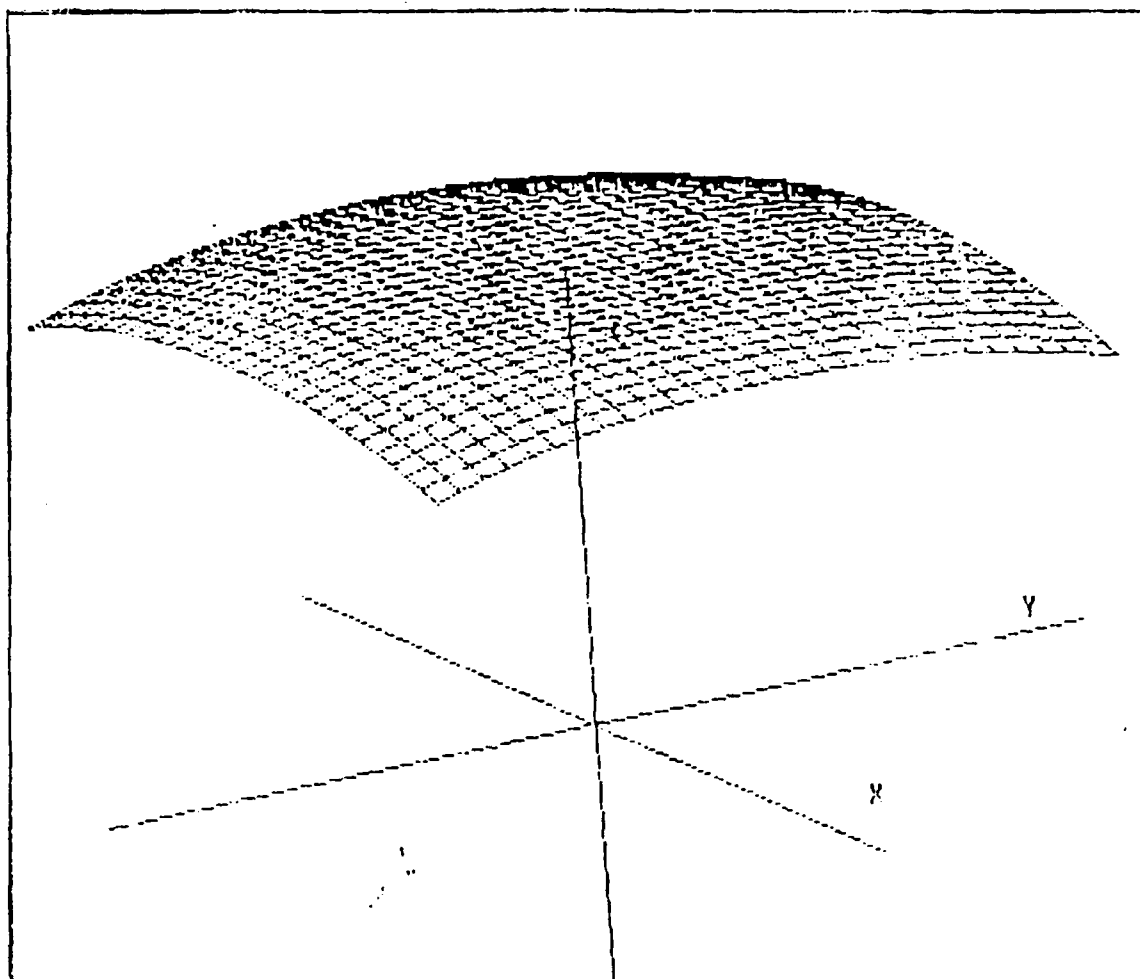


Figure 23. Single foil transition radiation pattern at 10 MeV for an rms beam divergence angle of  $2.500\text{E}-2$  radians. All the angular information of the TR pattern has been completely washed out by the effects of beam divergence. The data extends to .05 radians in the X-Y plane. The top of the Z-axis corresponds to the maximum intensity of the data.

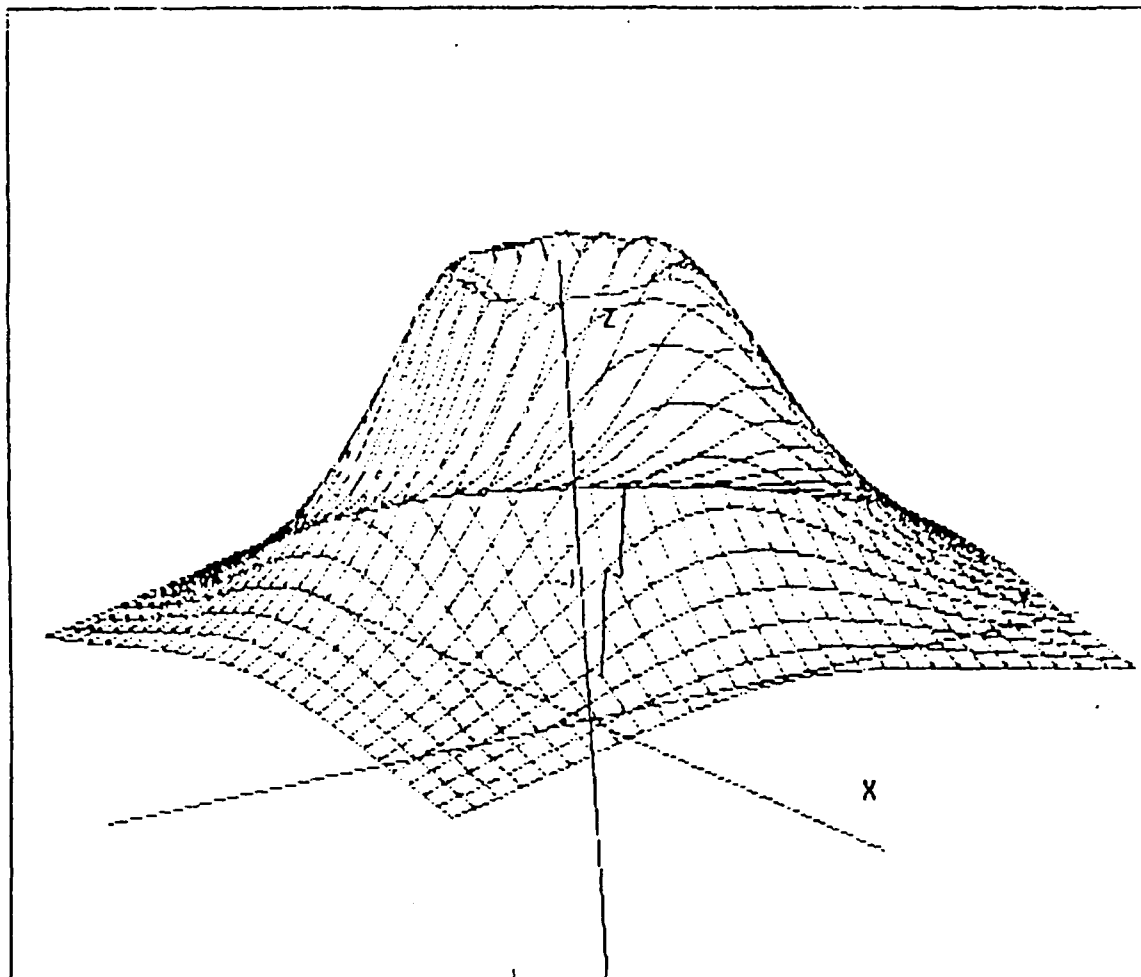


Figure 24. Single foil transition radiation pattern at 40 MeV for an rms beam divergence angle of  $1.000\text{E}-3$  radians. The maximum intensity occurs at an angle of  $.0126$  radians while the data presented extends to  $.05$  radians in the X-Y plane. The top of the Z-axis corresponds to the maximum intensity of the data.

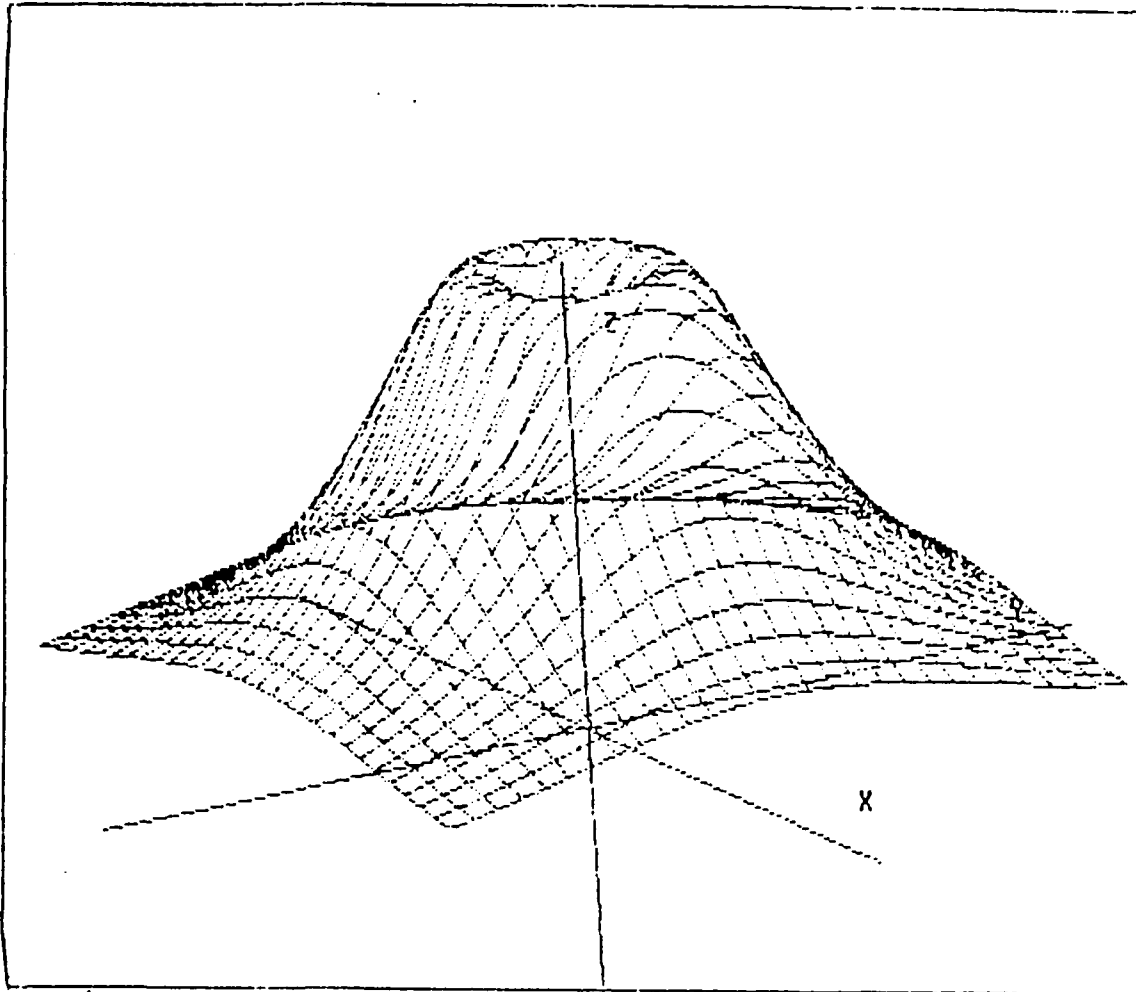


Figure 25. Single foil transition radiation pattern at 40 MeV for an rms beam divergence angle of  $5.000E-3$  radians. Note that the rim around the cone is more rounded than in the previous figure and that the depth of the cone has significantly decreased. The increase in the perpendicular component, which is at a maximum on the axis, is responsible for the decreasing depth of the cone. The data extends to .05 radians in the X-Y plane. The top of the Z-axis corresponds to the maximum intensity of the data.

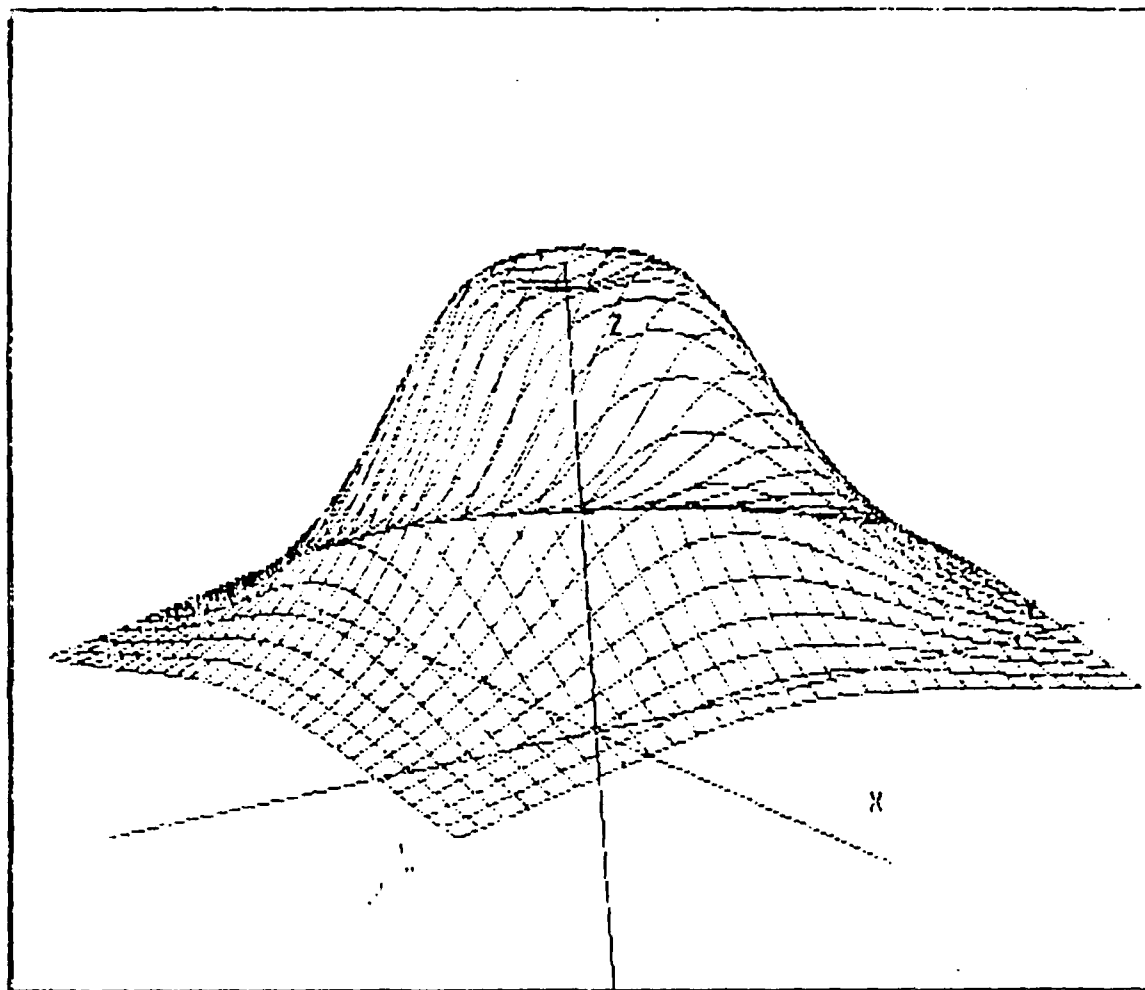


Figure 26. Single foil transition radiation pattern at 40 MeV for an rms beam divergence angle of  $6.000\text{E}-3$  radians. The angular information has been nearly washed out by the beam divergence. The perpendicular component of intensity is nearly equal to the parallel component of intensity. The data extends to .05 radians in the X-Y plane. The top of the Z-axis corresponds to the maximum intensity of the data.

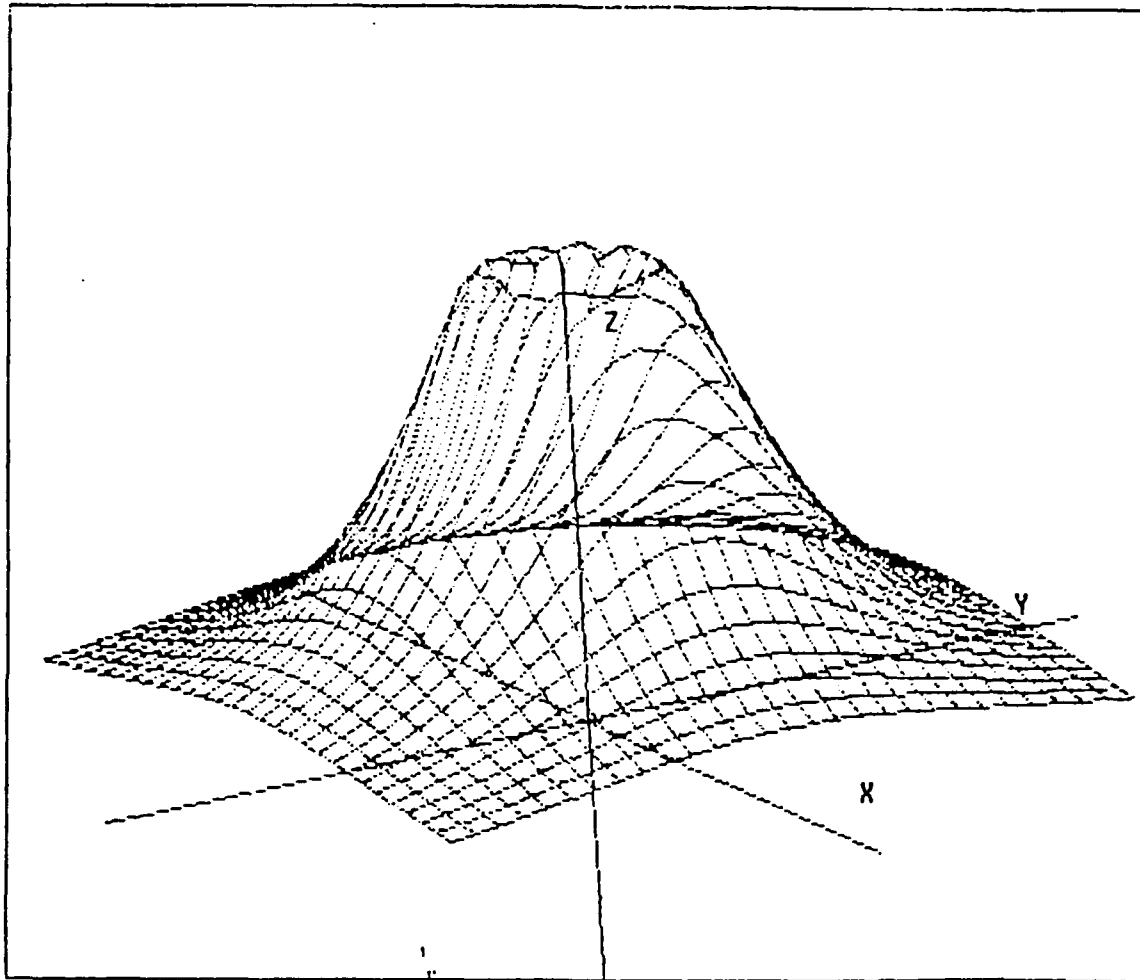


Figure 27. Single foil transition radiation pattern at 100 MeV for an rms beam divergence angle of  $1.500\text{E}-3$  radians. The data extends to five times the predicted angle of maximum intensity, i.e.  $\pm 5/\gamma$  in the X-Y plane. This option was chosen to preserve clarity at this high energy. The top of the Z-axis corresponds to the maximum intensity of the data.

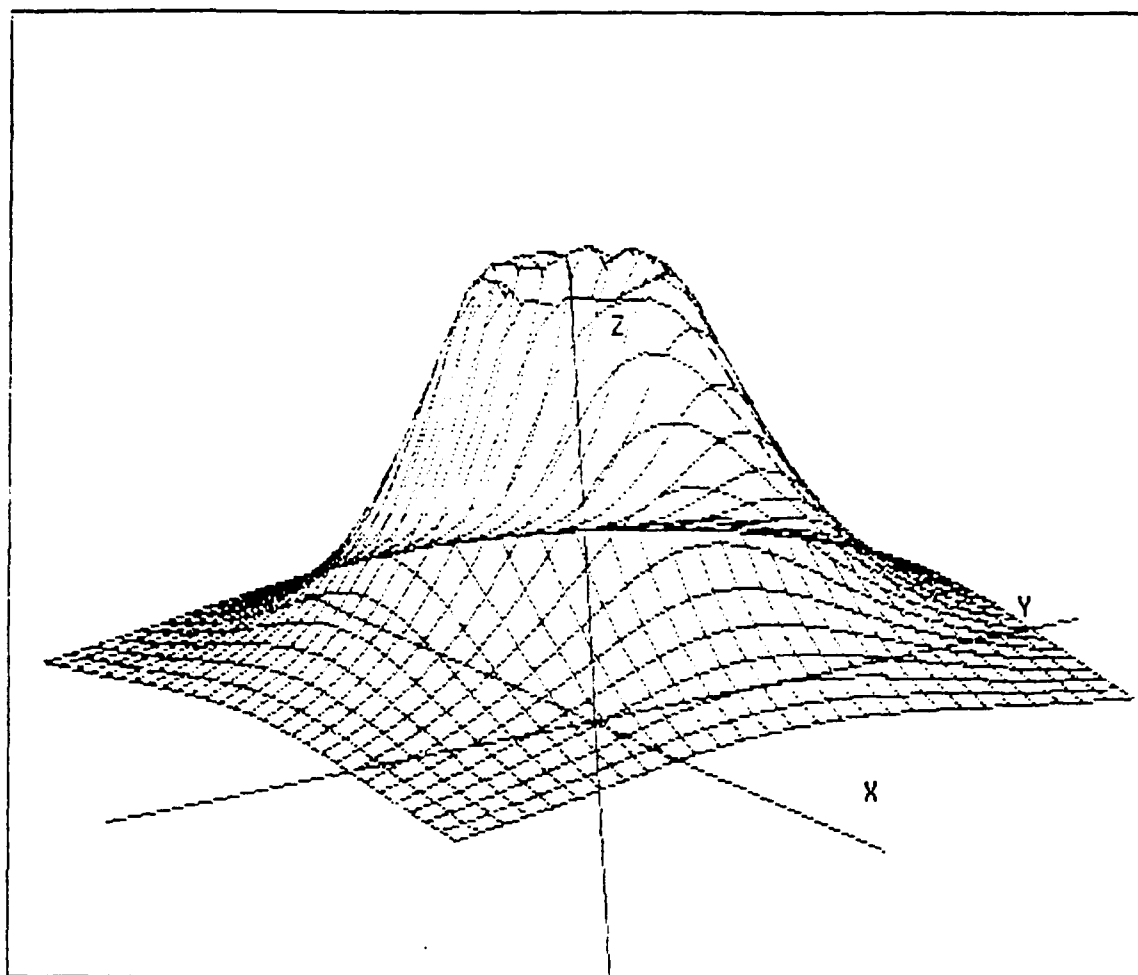


Figure 28. Single foil transition radiation pattern at 100 MeV for an rms beam divergence angle of  $3.000\text{E}-3$  radians. All the angular information has been washed out by the effects of beam divergence. Note the apparent gaussian distribution of the data. The data extends to  $\pm 5/\gamma$  radians in the X-Y plane. The top of the Z-axis corresponds to the maximum intensity of the data.

TABLE IV. BEAM DIVERGENCE VS INTENSITIES

Energy (MeV)	Beam Div. (radians)	ITOT $\left[\frac{e^2}{d\omega d\Omega}\right]$	IPAR $\left[\frac{e^2}{d\omega d\Omega}\right]$	IPERP $\left[\frac{e^2}{d\omega d\Omega}\right]$	$\theta_m$ (radians)
10	1.000E-3	9.571	9.567	1.711E-2	.0487
10	2.000E-3	9.571	9.554	6.826E-2	.0485
10	3.000E-3	9.573	9.534	0.1529	.0488
10	4.000E-3	9.574	9.506	0.2703	.0488
10	5.000E-3	9.578	9.471	0.4193	.0488
10	6.000E-3	9.582	9.428	0.5987	.0490
10	7.000E-3	9.588	9.378	0.8069	.0490
10	8.000E-3	9.597	9.322	1.042	.0490
10	9.000E-3	9.609	9.259	1.304	.0491
10	1.000E-2	9.625	9.191	1.589	.0490
10	2.000E-2	10.37	8.318	5.425	.0423
10	2.500E-2	12.00	7.853	7.781	.0178
10	3.000E-2	15.11	7.424	10.29	0.000
40	2.500E-3	143.2	137.2	22.07	.0126
40	5.000E-3	152.5	124.9	75.96	.0114
40	6.000E-3	166.4	119.5	102.4	.0082
40	7.500E-3	214.8	111.9	144.9	0.000
100	5.000E-4	877.8	868.7	35.21	.0051
100	1.500E-3	895.2	810.2	281.1	.0050
100	2.000E-3	937.1	770.0	461.7	.0046
100	3.000E-3	1310	690.3	881.6	0.000

be seen. In Figures 24–26 the parallel component of intensity increasingly dominates the distribution at and near the z-axis while the parallel component of intensity continues to dominate the intensity distribution farther out from the axis. The overall intensity distribution approximates a Gaussian distribution once the beam divergence is large enough for the perpendicular component to provide the maximum overall intensity on the axis of specular reflection. The point at which this occurs for 40 MeV is for an rms beam divergence angle of just over 0.060 radians. For 100 MeV, this point occurred between 0.0020 and 0.0030 radians. Figures 27 and 28 display the intensity distribution at 100 MeV for rms beam divergence angles of 0.0015 and 0.0030 radians.

In summary, increased beam divergence increases the perpendicular component of intensity while decreasing the parallel component. The angle of maximum intensity decreases as the parallel and perpendicular components adjust in response to the increase in beam divergence. This can result in the eventual loss of all angular information as the intensity distribution approximates a Gaussian distribution. The effect is more pronounced at higher energies and thus a beam divergence that may be negligible at low energies may have significant effect at higher energies. Beam divergence has a detrimental affect on beam quality, especially at higher energies and should be minimized to preserve angular information from transition radiation.

### C. DIELECTRIC CONSTANT

As has been stated before, transition radiation occurs when a charged particle in motion encounters a boundary between media. The intensity of the radiation emitted is dependent upon the dielectric properties of the media involved. The majority of the study of transition radiation here has assumed a vacuum to medium transtion. That assumption simplifies the analysis and the formulas involved. Now, however, it is more useful to study the equation for the total intensity per unit frequency and solid angle in which neither medium is assumed to be a vacuum.

The classic case, as developed by Frank and Ginsberg [Ref. 1], is to assume that the particle travelling through a medium which is characterized by adielectric constant  $\epsilon_1$  transits an interface to another medium characterized by a dielectric constant  $\epsilon_2$ . The trajectory of the particle is assumed to be normal to the

interface. Frank and Ginsberg [Ref. 1] developed expressions for the transition radiation intensity in both media. The intensity observed in the first medium per unit frequency and solid angle at an angle  $\theta_1$  from the the normal is

$$I_1 = \frac{e^2 \beta^2 \sqrt{\epsilon_1} \sin^2 \theta_1 \cos^2 \theta_1}{\pi^2 c} (\epsilon_2 - \epsilon_1)^2 \quad (3.16)$$

$$\times \left| \frac{(1 - \beta^2 \epsilon_1 + \beta \sqrt{\epsilon_2 - \epsilon_1} \sin^2 \theta_1)}{(1 - \beta^2 \epsilon_1 \cos^2 \theta_1)(1 - \beta \sqrt{\epsilon_2 - \epsilon_1} \sin^2 \theta_1)(\epsilon_2 \cos \theta_1 + \sqrt{\epsilon_1 \epsilon_2 - \epsilon_1^2} \sin^2 \theta_1)} \right|$$

The intensity per unit frequency and solid angle observed in the second medium at an angle  $\theta_2$  to the normal may be found from the above expression by substituting  $-\beta$  for  $\beta$  and interchanging the subscripts 1 and 2. In either case it is clear that the intensity observed in the medium is proportional to the square of the difference of the dielectric constants of the two media.

Actually the dielectric constant isn't really a constant at all. It is really a slowly-varying function of wavelength that may be considered a constant when considering short ranges of wavelength. The dielectric constant is complex, consisting of both a real and imaginary part that are related to the refractive index  $n$  and the absorption coefficient  $\kappa$  of the medium. Letting  $\epsilon_1$  represent the real part of the dielectric constant  $\epsilon$  and  $\epsilon_2$  the imaginary part, the following relations define the dielectric constant;

$$\epsilon = \epsilon_1 + i\epsilon_2, \quad (3.17)$$

$$\epsilon_1 = n^2 - \kappa^2, \quad (3.18)$$

$$\epsilon_2 = 2n\kappa. \quad (3.19)$$

Values for the refractive index and absorption coefficient at discrete wavelengths for some metals were found in the Handbook of Chemistry and Physics [Ref. 12]. The available information on the dielectric constants of the metals limited the data analysis on this subject to three significant figures. TABLE V lists the optical wavelength, refractive index  $n$ , absorption coefficient  $\kappa$ , real part of the dielectric constant  $\epsilon_1$ , and the imaginary part of the dielectric constant  $\epsilon_2$ , for aluminum Al, gold Au, and silver Ag. Note that the value listed the real part of the dielectric constant is the absolute value of the result of equation (3.18).

Some of the results obtained by this method required verification. The formulas listed in equations (3.18) and (3.19) were also found in Wartski [Ref. 5], and in Bennett and Bennett [Ref. 13] which also provided a table of optical constants at infrared wavelengths for gold, silver, and aluminum. The dielectric constants calculated from that table for the infrared wavelengths appeared to be consistent with those obtained in Table V.

Table VI provides the results of applying the dielectric constants listed in Table V to the single foil case at an energy of 100 MeV. Recall that the total intensity should be proportional to the square of the modulus of the difference of the dielectric constants of the two media. For the single foil case, the first media was assumed to be a vacuum which is characterized by dielectric constant of one, ie  $\epsilon = 1 + i0$ . The total intensity ITOT per unit frequency and solid angle in terms of charge squared divided by the speed of light is listed for aluminum Al, gold Au, and silver Ag, as a function of wavelength (listed in angstroms), and the square of the modulus of the difference between the dielectric constant of the metal and of the

TABLE V. DIELECTRIC CONSTANT AT OPTICAL WAVELENGTHS

Metal	Wavelength (angstroms)	n	$\kappa$	$\epsilon_1$	$\epsilon_2$
Al	5890	1.44	3.69	11.5	10.6
Au	4410	1.18	1.56	1.04	3.70
Au	5890	0.47	6.02	36.0	5.66
Ag	5000	0.17	17.1	292	5.88
Ag	5890	0.18	20.6	424	7.28

vacuum  $(\epsilon_2 - \epsilon_1)^2$ . The dielectric constant of the metal for the wavelength listed is the same as that listed for the same wavelength in Table V.

TABLE VI. SINGLE FOIL DIELECTRIC CONSTANT VS. TOTAL TRANSITION RADIATION INTENSITY AT 100 MEV.

Metal	Wavelength (angstroms)	$(\epsilon_1 - \epsilon_2)^2$	ITOT $\left[ \frac{e^2/c}{d\omega d\Omega} \right]$
Al	5890	138	881
Au	4410	8.08	684
Au	5890	1250	845
Ag	5000	84700	964
Ag	5890	179000	970

The data in Table VI clearly indicates that the total intensity does indeed increase whenever the square of the modulus of the difference in dielectric constants is increased. Figures 29–31 depict the intensity distributions of aluminum, gold, and silver at a wavelength of 5890 angstroms and energy of 100 MeV. The data in each plot is normalized to the maximum value, represented by the top of the z-axis. The data extends five times the predicted angle of maximum intensity in the x–y plane. Since the data in each case is plotted on the same relative scale, Figures 29–31 appear nearly identical.

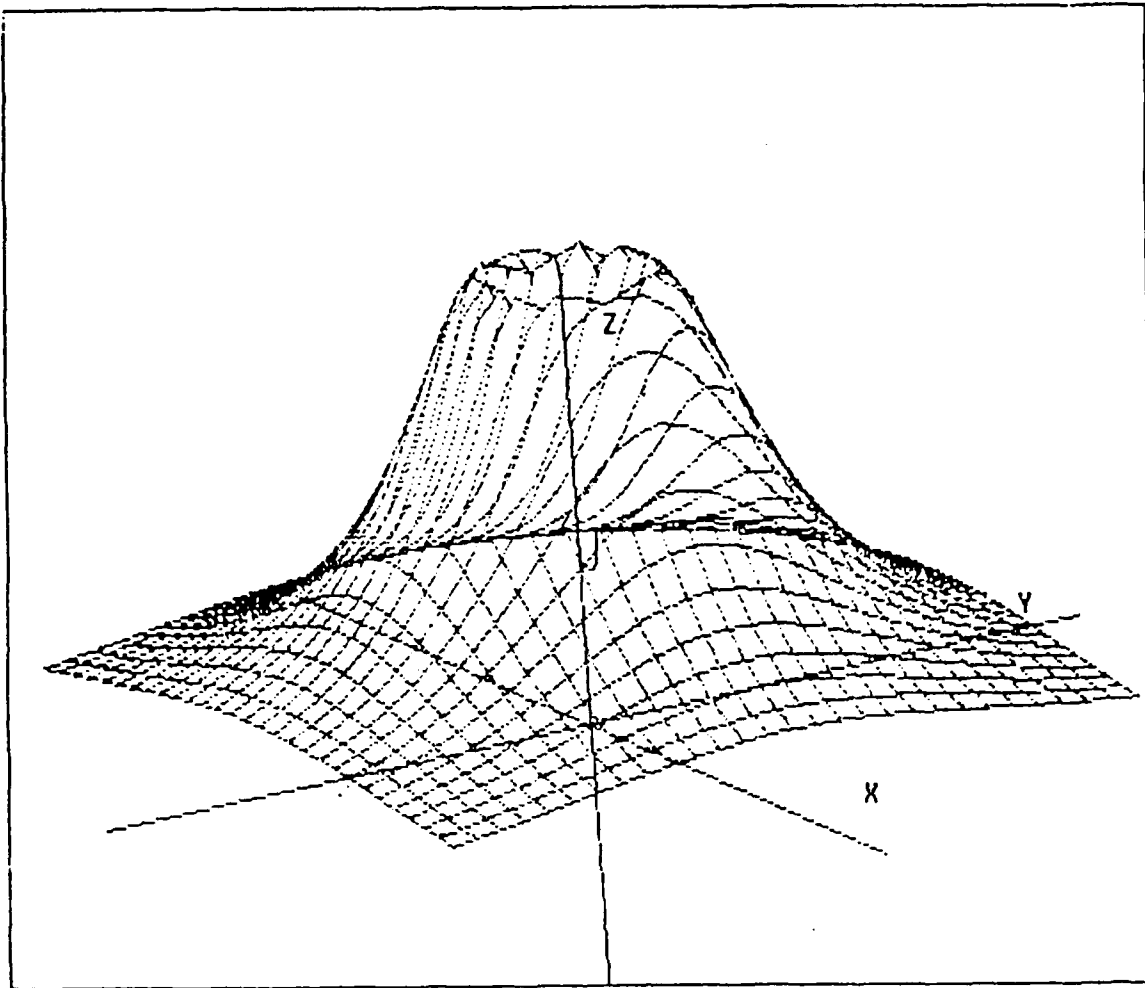


Figure 29. The single foil transition radiation intensity distribution for aluminum at 100 MeV at a wavelength of  $5890 \text{ \AA}$ . The data extends to  $\pm 5/\gamma$  radians in the X-Y plane. The top of the Z-axis corresponds to the maximum intensity of the data.

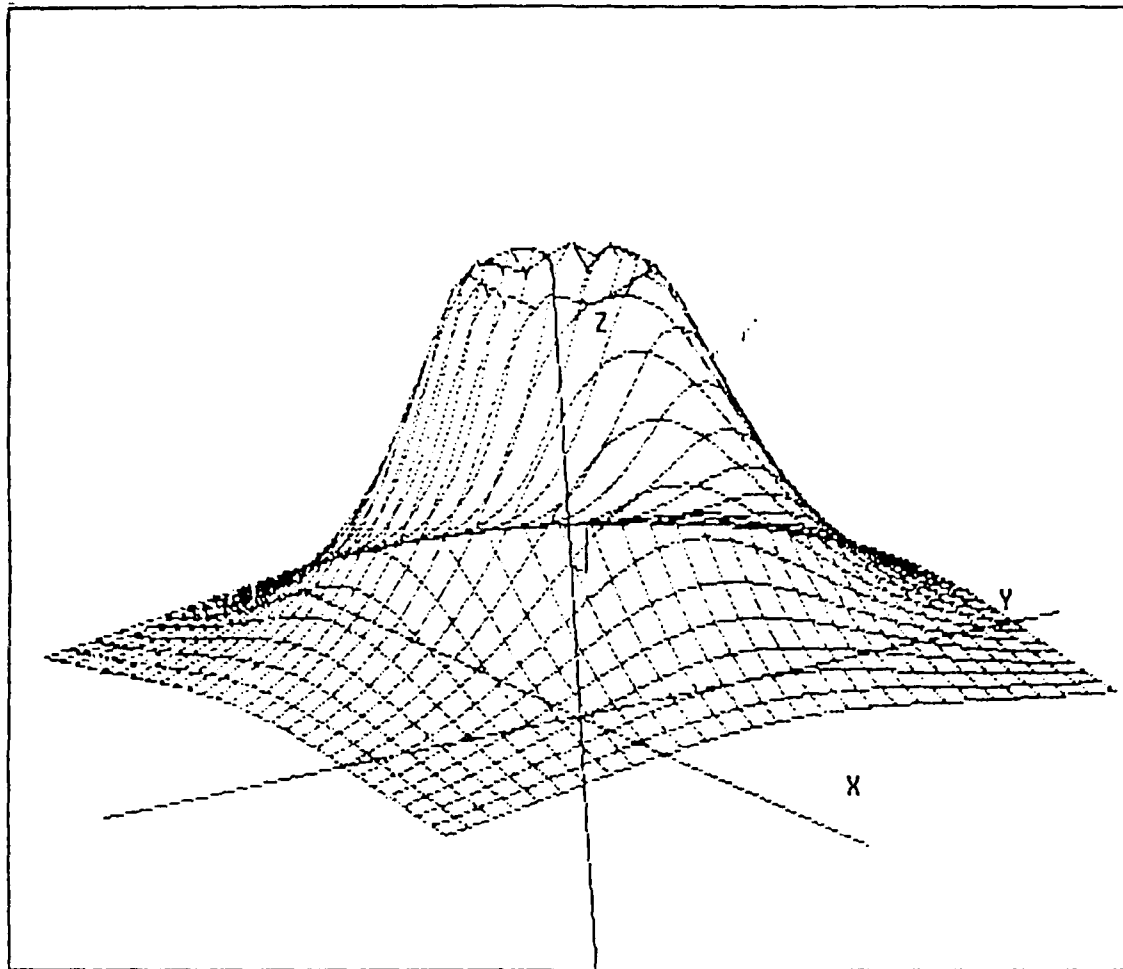


Figure 30. The single foil transition radiation intensity distribution for gold at 100 MeV at a wavelength of  $5890 \text{ \AA}$ . The data extends to  $\pm 5/\gamma$  radians in the X-Y plane. The top of the Z-axis corresponds to the maximum intensity of the data.

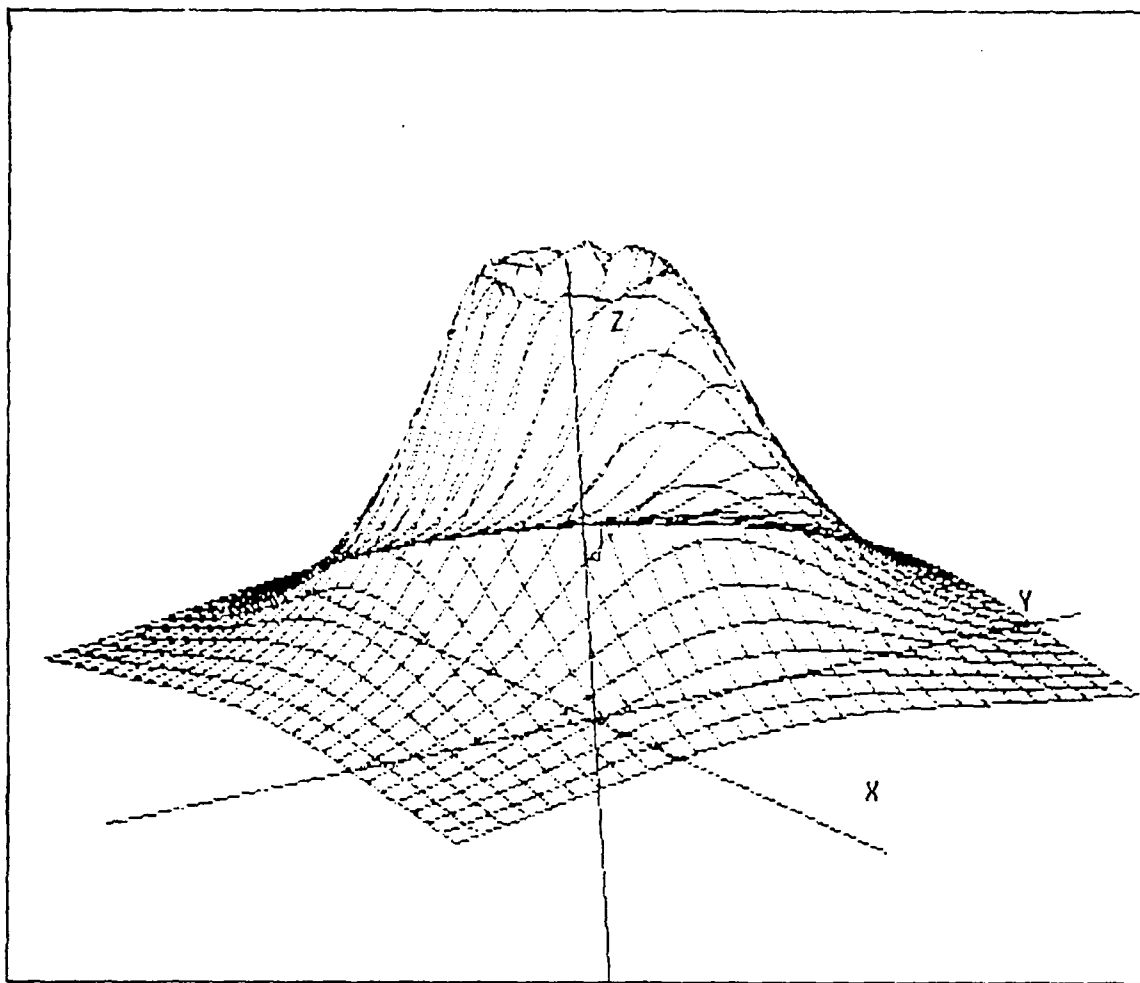


Figure 31. The single foil transition radiation intensity distribution for silver at 100 MeV at a wavelength of  $5890 \text{ \AA}$ . Note that this plot is nearly identical to the plots for aluminum and gold (Figures 29, 30). Dielectric permittivity does not affect the angular distribution of transition radiation. It does have a significant effect on the intensity. The data extends to  $\pm 5/\gamma$  radians in the X-Y plane. The top of the Z-axis corresponds to the maximum intensity of the data.

## IV. COHERENT TRANSITION RADIATION

The two-foil interferometer program COHER3 was used to study the effects of energy, beam divergence, and dielectric constant on coherent transition radiation for comparison with the results obtained from the single foil case. The interferometer program permits the study of a finite optical bandwidth of wavelength and thus also of frequency. In addition, it promotes a better understanding of the concept of coherence length and its importance in determining the separation between foils to obtain coherent addition of transition radiation from successive foils.

### A. COHERENCE LENGTH

It is necessary to begin the study of the two-foil interferometer with a discussion of coherence length. This is due to the fact that the distance between the foils of the interferometer in relation to the coherence length, has a profound effect upon the resulting interference pattern. Recall from chapter one that the coherence length in a medium is defined

$$L_m = \frac{\beta\lambda}{2\pi} \frac{1}{|1 - \beta\sqrt{\epsilon}\cos\theta|} \quad (4.1)$$

Chapter I also described how the forward transition radiation from the back of the first foil and the backward transition radiation emitted from the front surface of the second foil differ in phase by

$$\phi = \left(\frac{2\pi L}{\lambda\beta}\right)(1-\beta\cos\theta) = L/L_v, \quad (4.2)$$

where  $L$  is the distance between the foils and  $L_v$  is the coherence length in a vacuum. Obviously, the interference pattern generated by the interferometer is highly dependent upon the phase difference and thus the ratio of the distance between the foils and the coherence length. For the radiation patterns to add coherently, the distance between the foils should be an integer multiple of the coherence length in a vacuum for that energy. Wartski [Ref. 5] showed that the coherence length on the axis of specular reflection, i.e.  $\theta = 0$ , is proportional to the square of the energy

$$L = \frac{\lambda}{2\pi} \gamma^2. \quad (4.3)$$

Table VII displays the coherence length on the axis of specular reflection at various energies for a wavelength of  $\lambda = 5890$  angstroms. This wavelength was chosen because it was the only wavelength in the visible spectrum for which the optical constants for determining the dielectric constant were available for gold, silver, and aluminum. The default value of the two-foil interferometer program for the distance between the foils is 1.20 centimeters.

Figures 32 and 33 demonstrate the impact of coherence length on the interference pattern from a two-foil interferometer. For both cases the energy is 30 MeV and the data in the X-Y plane is spread over  $\pm 3/\gamma$  radians from the Z-axis. The top of the Z-axis corresponds to the maximum value of the data. In Figure 32 the distance between the foils is 1.20 centimeters while in Figure 33 the distance is equal to the coherence length of .034 centimeters. All angular information available

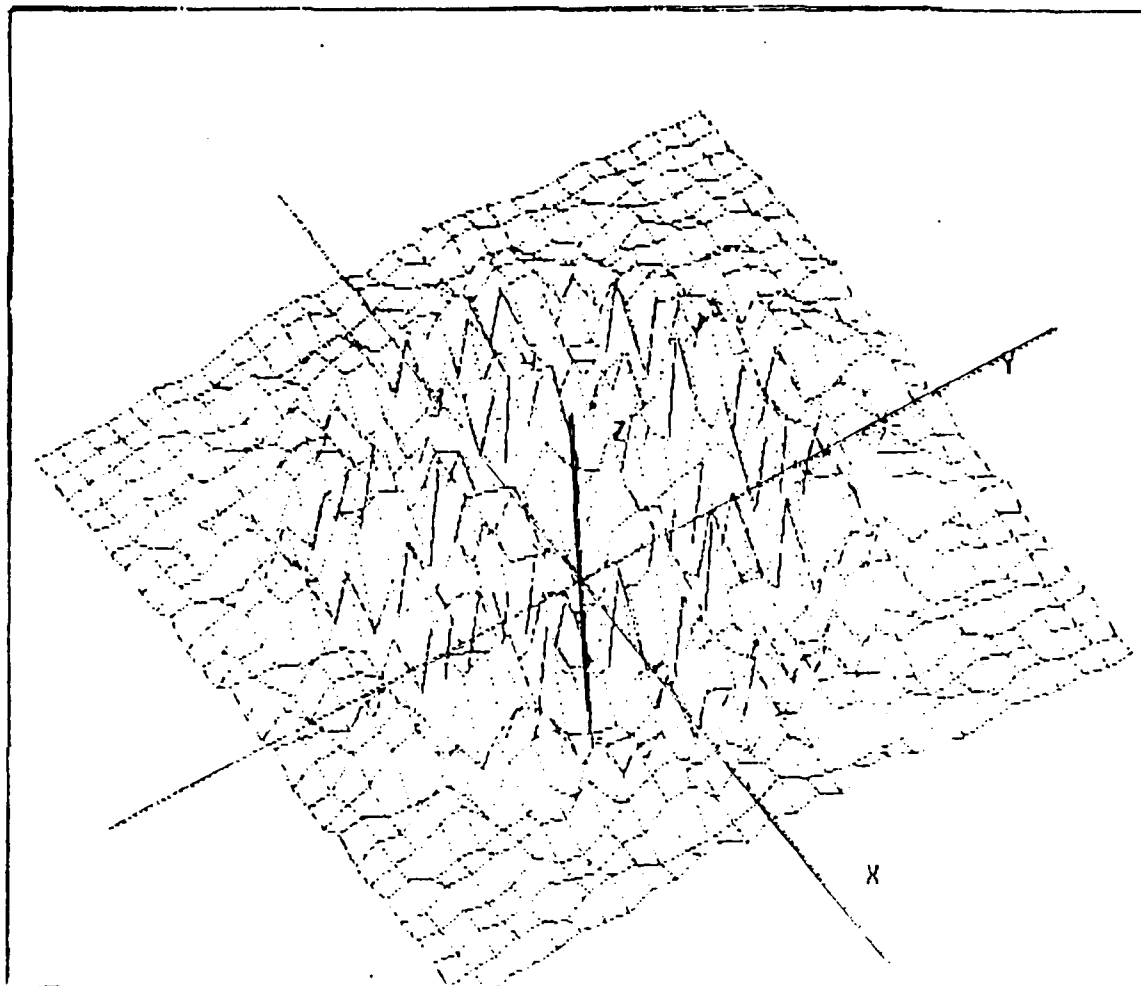


Figure 32. Two-foil interferometer interference pattern at 30 Mev for a clear front foil and gold back foil. Distance between foils is 1.20 cm. while coherence length is .034 cm. at 30 McV for a wavelength of  $5890 \text{ \AA}$ .

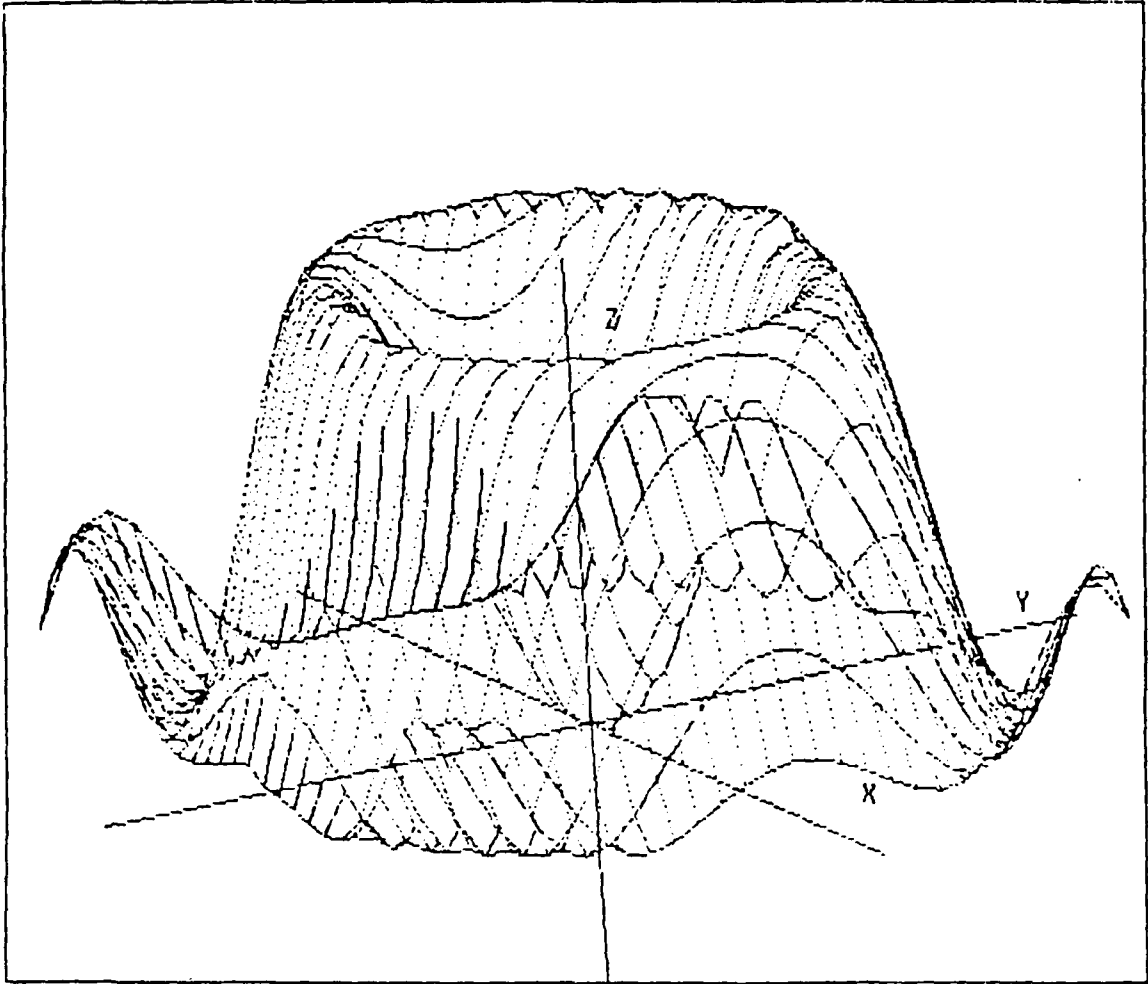


Figure 33. Two-foil interferometer interference pattern at 30 Mev for a clear front foil and gold back foil. Distance between foils is equal to the coherence length of .034 cm. at 30 MeV for a wavelength of  $5890 \text{ \AA}$ .

in Figure 33, where the distance between the foils is equal to the coherence length, is lost in Figure 32. Not surprisingly the intensities for each case were completely different. A numerical comparison of the intensities would not be meaningful since one case is coherent and the other is not.

TABLE VII. COHERENCE LENGTH VS. ENERGY FOR  $\lambda = 5890 \text{ \AA}$

Energy (MeV)	Coherence Length (cm)
10	.004
20	.015
30	.034
40	.059
50	.092
60	.131
70	.178
80	.233
90	.294
100	.363
150	.813
200	1.44

## B. ENERGY

The discussion on coherence length demonstrated the effect of energy on the considerations for determining foil separation as a function of energy and coherence length. Table VIII demonstrates the effect of energy on the angle at which maximum intensity occurs, the parallel and perpendicular components of intensity and the total intensity for comparison with the effects of the single foil case. The intensities listed are for the maximum of each component and therefore should not be summed to obtain the maximum total intensity, ITOT. The angle at which the maximum intensity occurred is much greater than the  $1/\gamma$  angle predicted for the

TABLE VIII. ENERGY EFFECTS ON INTERFEROMETER  
TRANSITION RADIATION

Energy (MeV)	$1/\gamma$ (radians)	Actual $\theta_M$ (radians)	ITOT $\left[\frac{e^2/c}{d\omega d\Omega}\right]$	IPAR $\left[\frac{e^2/c}{d\omega d\Omega}\right]$	IPERP $\left[\frac{e^2/c}{d\omega d\Omega}\right]$
20	.0249	.0730	31.92	31.92	.0008
60	.0084	.0536	900.3	900.3	.1615
100	.0051	.0277	2046	2046	.8868

single foil case. A comparison with the intensities in Table II of Chapter III indicates that the intensities for the interferometer case are much more sensitive to increases in energy than for the single foil case. The fact that the intensity of TR can be increased through the use of a stack of plates is well known and has proven to be a useful tool in studying transition radiation [Ref. 2-4]. Ginsburg and Tsytovich [Ref. 1] and Garibian [Ref. 4] showed that a condition of resonance occurs when the distance between successive foils is such that the transition radiation fields from the foils add coherently. This condition is met when the distance between the foils is an integer multiple of the coherence length. If the distance between the foils does not meet this criteria, the intensity is then a function of the number of boundaries per unit length. For this study the separation distance between the foils was set equal to the vacuum coherence length for the energy listed.

Figures 34-36 depict coherent TR patterns at 60 and 100 MeV. The data is spread over an angular distribution of five times the predicted angle of maximum intensity for the single foil case. The top of the Z-axis corresponds to the maximum value of the total intensity.

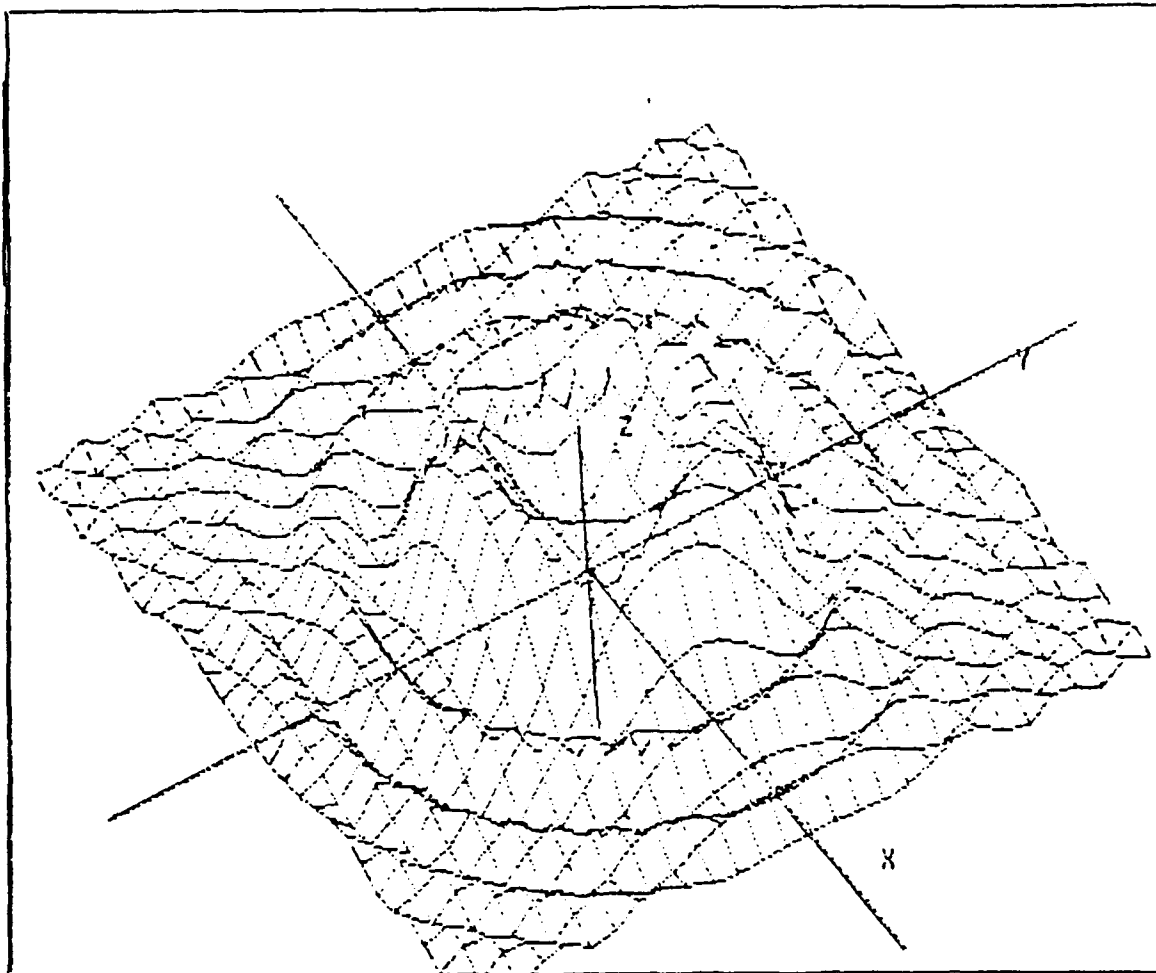


Figure 34. Coherent TR interference pattern at 60 MeV for a wavelength of  $5890 \text{ \AA}$ . Separation distance between foils was 1.31 mm. The Z-axis measures relative intensity. The top of the Z-axis corresponds to the maximum intensity in units of charge squared divided by the speed of light per unit frequency and solid angle. Angular information is depicted in the X-Y plane. The data extends to five times the predicted angle of maximum intensity (in radians) for the single foil case.

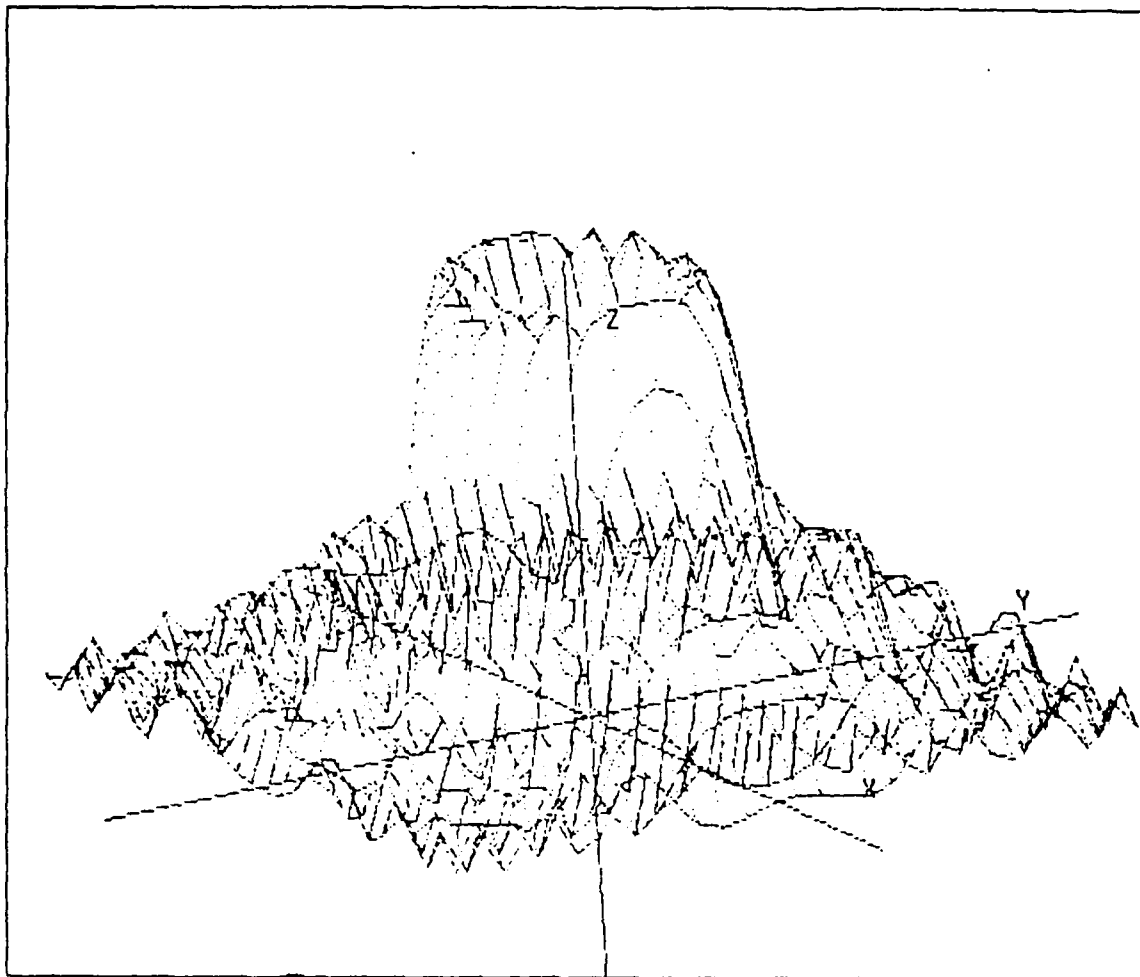


Figure 35. Another view of coherent TR interference pattern at 60 MeV for a wavelength of  $5890 \text{ \AA}$ . Separation distance between foils was 1.31 mm. The Z-axis measures relative intensity. The top of the Z-axis corresponds to the maximum intensity in units of charge squared divided by the speed of light per unit frequency and solid angle. Angular information is depicted in the X-Y plane. The data extends to five times the predicted angle of maximum intensity (in radians) for the single foil case.

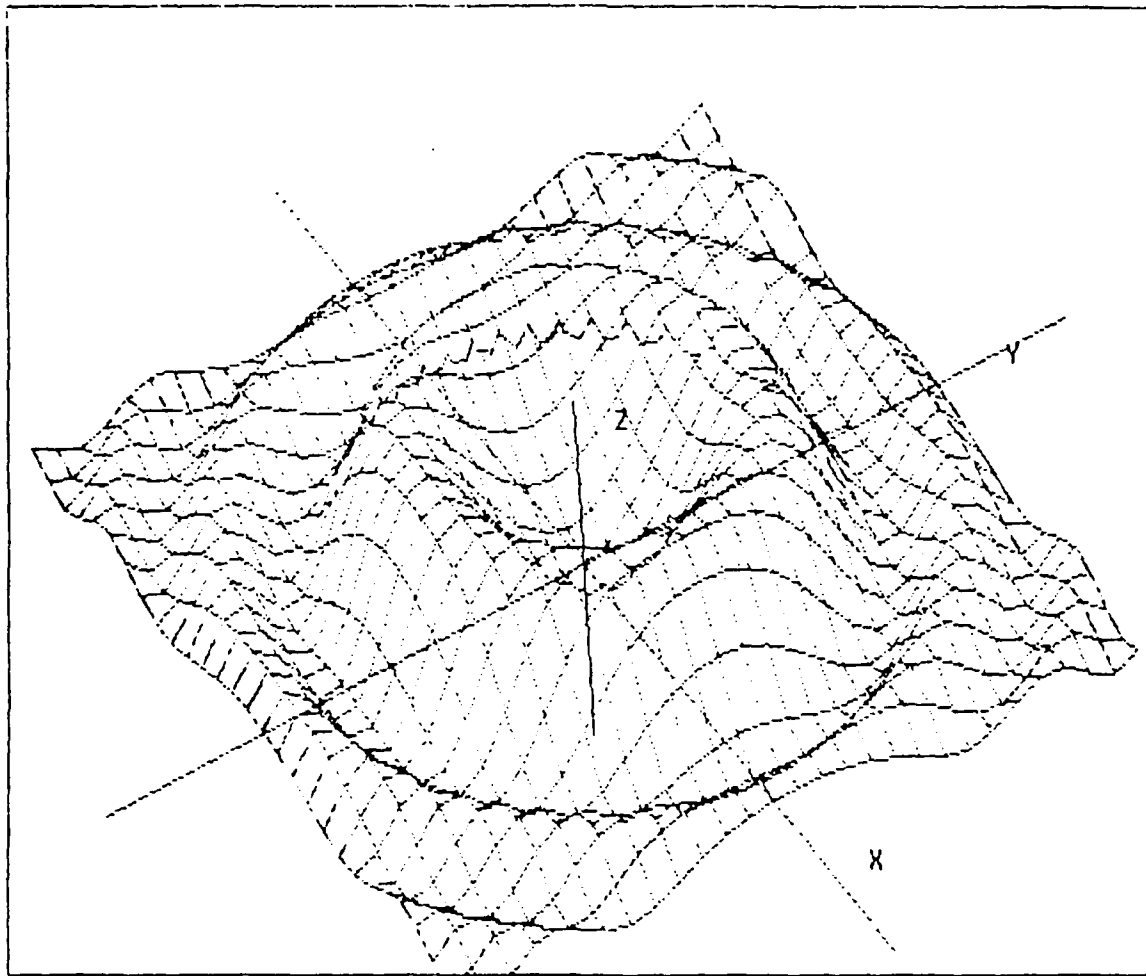


Figure 36. Coherent TR interference pattern at 100 MeV for a wavelength of  $5890 \text{ \AA}$ . Separation distance between foils was 3.63 mm. The Z-axis measures relative intensity. The top of the Z-axis corresponds to the maximum intensity in units of charge squared divided by the speed of light per unit frequency and solid angle. Angular information is depicted in the X-Y plane. The data extends to five times the predicted angle of maximum intensity (in radians) for the single foil case.

The characteristics of the surface plot are quite different than that of the single foil case. A series of fringes surround the central cone of maximum intensity. The positions of these relative maximum and minimum intensities are described by Wartski [Ref. 5] in terms of an interference order  $p$  which is defined

$$p = \frac{L}{\lambda\beta}(1-\beta\cos\theta) = \frac{L}{2\pi L_V}, \quad (4.4)$$

where  $L_V$  is the coherence length in a vacuum and  $L$  is the distance between the foils. For the relativistic case, this may be approximated as

$$p = \frac{L}{2\lambda}(\gamma^{-2} + \theta^2). \quad (4.5)$$

Local minima,  $\theta_m$ , occur whenever  $p$  is an integer,  $k$ . Local maximum intensities,  $\theta_\mu$ , occur whenever  $p = k \pm 1/2$ . The order of interference at the center, that is on the axis of specular reflection is defined to be

$$p_0 = \frac{L}{2\lambda} \gamma^{-2}. \quad (4.6)$$

The angle for which the local maxima and minima intensities occur can be described by

$$\theta_{M,m} = \frac{2\lambda}{L} (p - p_0), \quad (4.7)$$

for  $p = k \pm 1/2$  and  $p = k$ , respectively.

The intensities for the coherent interferometer case increase with an increase in energy. The intensities for the incoherent case depend upon the number of boundaries per unit length as well as upon intensity. The maximum intensity occurs at the inner most fringe which is located at a much greater angle than that predicted for the single foil case. The locations of maxima and minima are described in terms of an order of interference  $p$ , wavelength  $\lambda$ , and distance between foils  $L$ . The order of interference was shown to be inversely proportional to the square of the Lorentz factor  $\gamma$ .

### C. BEAM DIVERGENCE

The effects of beam divergence were studied for energies of 10, 40, and 100 MeV for comparison with beam divergence effects at those energies for the single foil case. Although an increase in beam divergence decreases the visibility of the fringes, the beam divergence required to wipe out all angular information was found to be much greater than that required for the single foil case. Coherent transition radiation is less susceptible to the effects of beam divergence because of the amplified intensities due to resonance.

Table IX contains a comparison of the total, parallel, and perpendicular intensities for a few rms beam divergence angles. In all cases, the rms beam divergence angle in the X-Z plane and in the Y-Z plane were set equal to each other, i.e.  $\sigma_x = \sigma_y$ . In this case the total beam divergence angle is  $\sqrt{2}\sigma$ , which is the value listed in the table in radians. Energy is listed in MeV, the intensities are per unit frequency and solid angle in terms of charge squared divided by the speed of

light. As in the single foil case, the values listed for each component of intensity are the maximum attained for that component and do not necessarily add up to the maximum overall intensity, labelled ITOT.

TABLE IX. BEAM DIVERGENCE VS COHERENT OPTICAL TRANSITION RADIATION INTENSITIES AT  $\lambda = 5890 \text{ \AA}$

Energy (MeV)	Beam Div. (radians)	ITOT $\left[\frac{e^2}{d\omega d\Omega}\right]$	IPAR $\left[\frac{e^2}{d\omega d\Omega}\right]$	IPERP $\left[\frac{e^2}{d\omega d\Omega}\right]$	Actual $\theta_m$ (radians)
10	1.41E-2	23.27	23.01	.7195	.2654
10	2.83E-2	21.87	20.79	2.685	.2654
10	4.24E-2	20.72	18.14	5.650	.2627
10	5.66E-2	20.72	15.76	9.356	.2581
10	8.49E-2	26.75	12.50	18.15	.0000
40	7.07E-2	308.2	293.6	37.07	.0688
40	8.49E-2	300.1	278.7	51.94	.0695
40	1.41E-1	2587	69.93	2517	.0000
100	2.83E-3	1877	1788	224.9	.0277
100	4.24E-3	1768	1560	472.7	.0274
100	7.07E-3	1889	1186	1145	.0270

An increase in beam divergence resulted in a corresponding increase in the perpendicular component of intensity and decrease in the parallel component of intensity. Also the total intensity tended to decrease until the perpendicular component of intensity became comparable to or greater than the parallel component. The maximum intensity occurred on the axis of specular reflection when the perpendicular component of intensity dominated the intensity distribution. The physics behind this was explained for the single foil beam divergence in Chapter III.

The effect of beam divergence on the coherent transition radiation interference pattern is depicted in Figures 37–43. For all the figures, the angular information depicted in the X–Y plane extends to five times the predicted angle of maximum intensity in radians for the single foil case at the same energy. Intensity is measured along the Z–axis. The top of the Z–axis corresponds to the maximum intensity in units of charge squared divided by the speed of light per unit frequency and solid angle.

The apparent inconsistency that appears in these plots is due to a forced asymmetry built into the program. When a beam of particles encounters a boundary at an oblique angle, the resulting transition radiation is asymmetric in that one side of the pattern will be more intense than the other. This asymmetry was simulated in the two–dimensional program by changing the sign of the observation angle on opposite sides of the axis of specular reflection. That technique was carried *on into the three–dimensional simulation*. Obviously, a refinement of the method is needed, but the solution is not a simple one. The inconsistency could be removed by neglecting the asymmetry introduced by the beam encountering the boundary at angle.

Figures 37–40 depict the effect of beam divergence on the fringe pattern at an energy of 10 MeV. As the beam divergence is increased, the fringes become less visible. Note that the central cone becomes more shallow as well as the perpendicular component of intensity increases. All the angular information is lost when the beam divergence angle becomes sufficiently large for the perpendicular component of intensity to dominate the intensity distribution. However, the beam

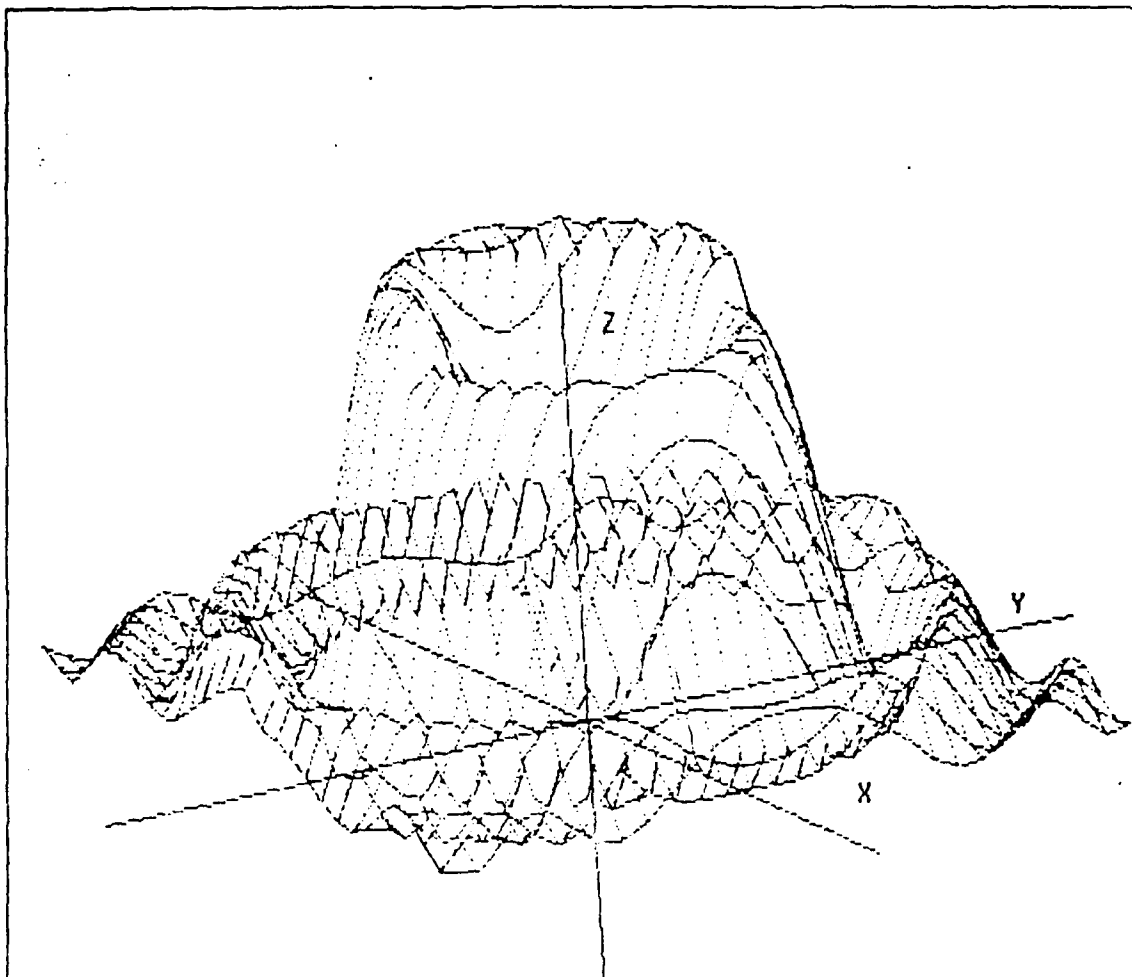


Figure 37. Coherent transition radiation at 10 MeV for an rms beam divergence angle of  $1.41E-2$  radians. The apparent inconsistency is due to a crude approximation of the asymmetry arising from the charged particles encountering the boundary at an oblique angle. The angular information depicted in the X-Y plane extends to five times the predicted angle of maximum intensity in radians for the single foil case at the same energy. Intensity is measured along the Z-axis. The top of the Z-axis corresponds to the maximum intensity in units of charge squared divided by the speed of light per unit frequency and solid angle.

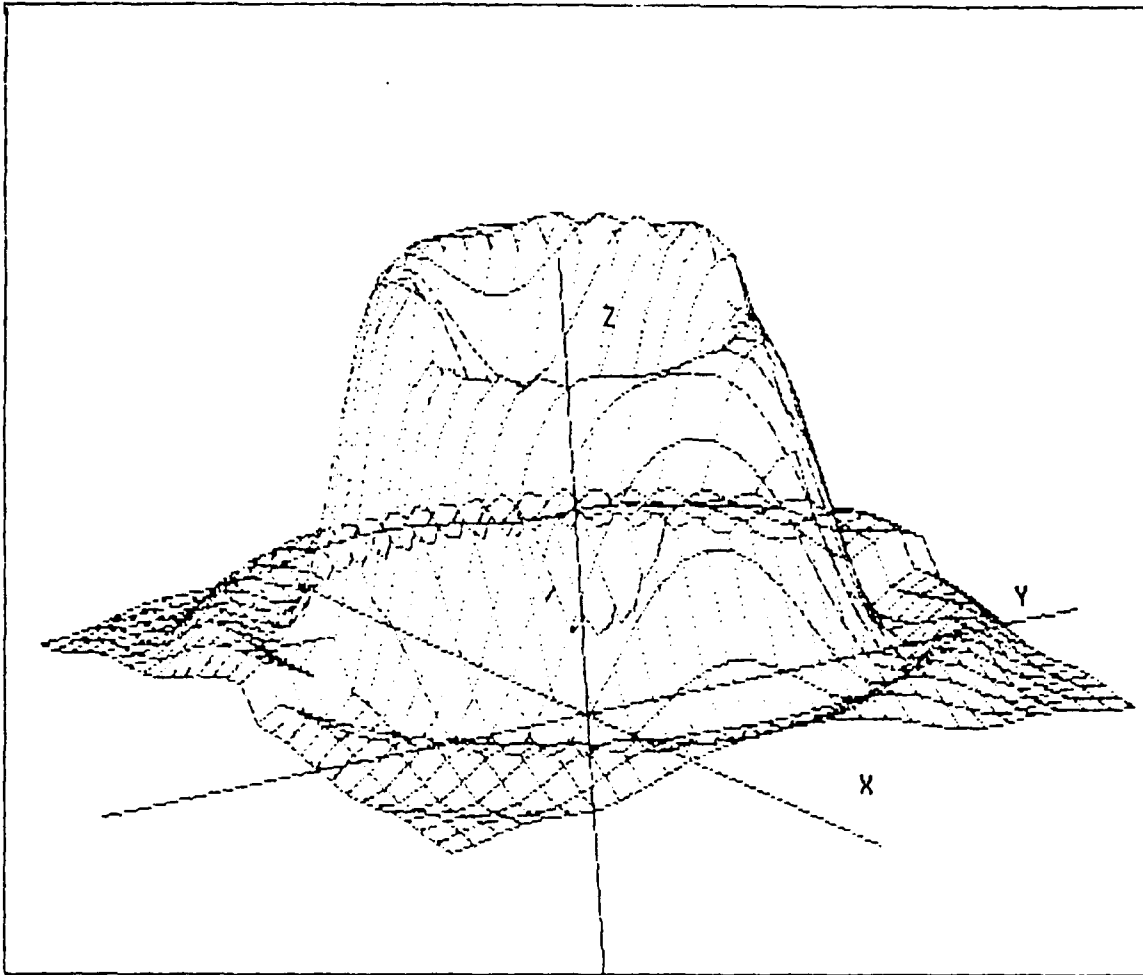


Figure 38. Coherent transition radiation at 10 MeV for an rms beam divergence angle of  $2.83E-2$  radians. Note the relative amplitudes of the outer fringes is much less than those of Figure 37. The angular information depicted in the X-Y plane extends to five times the predicted angle of maximum intensity in radians for the single foil case at the same energy. Intensity is measured along the Z-axis. The top of the Z-axis corresponds to the maximum intensity in units of charge squared divided by the speed of light per unit frequency and solid angle.

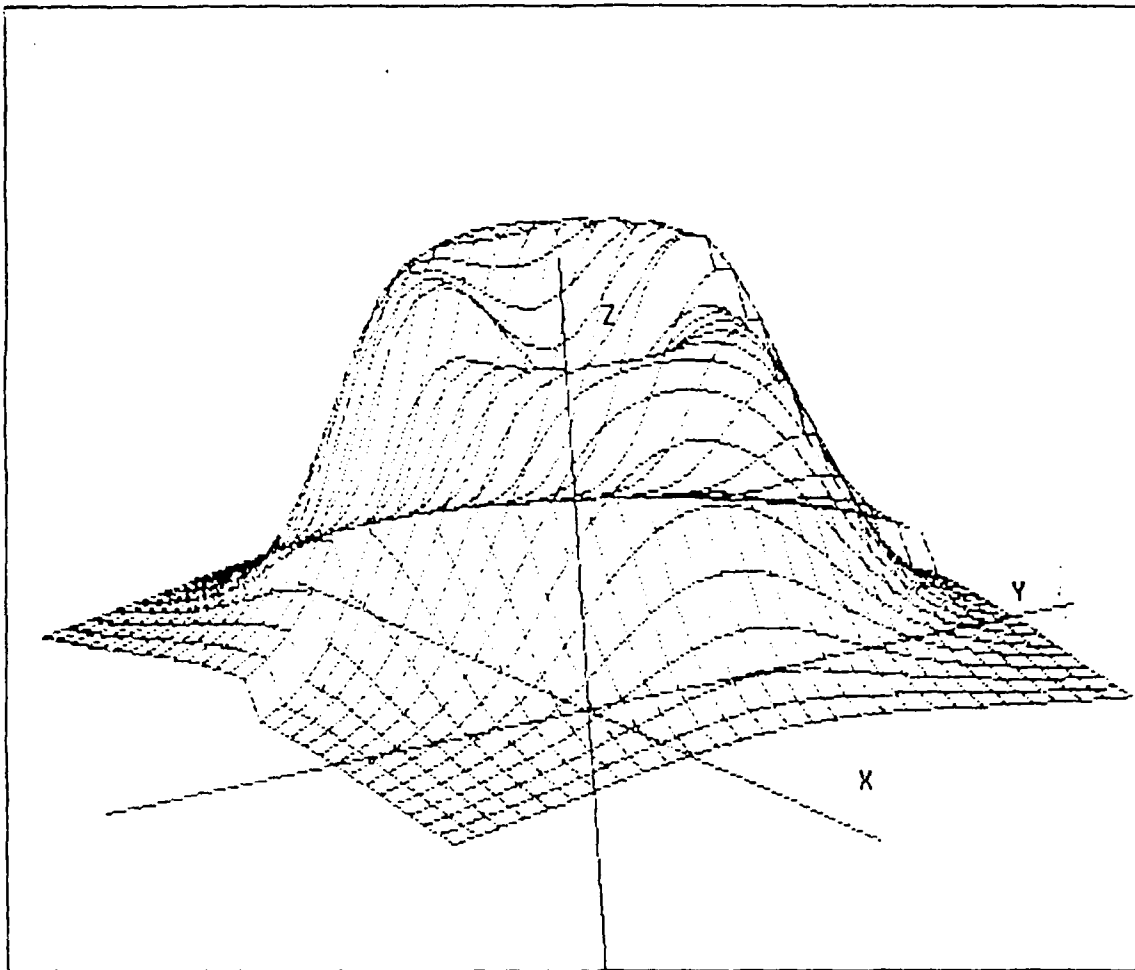


Figure 39. Coherent transition radiation at 10 MeV for an rms beam divergence angle of  $5.66E-2$  radians. Note that the outer fringes are no longer visible. Compare with Figures 37 and 38. Note also the general spreading and smoothing of the intensity distribution. The angular information depicted in the X-Y plane extends to five times the predicted angle of maximum intensity in radians for the single foil case at the same energy. Intensity is measured along the Z-axis. The top of the Z-axis corresponds to the maximum intensity in units of charge squared divided by the speed of light per unit frequency and solid angle.

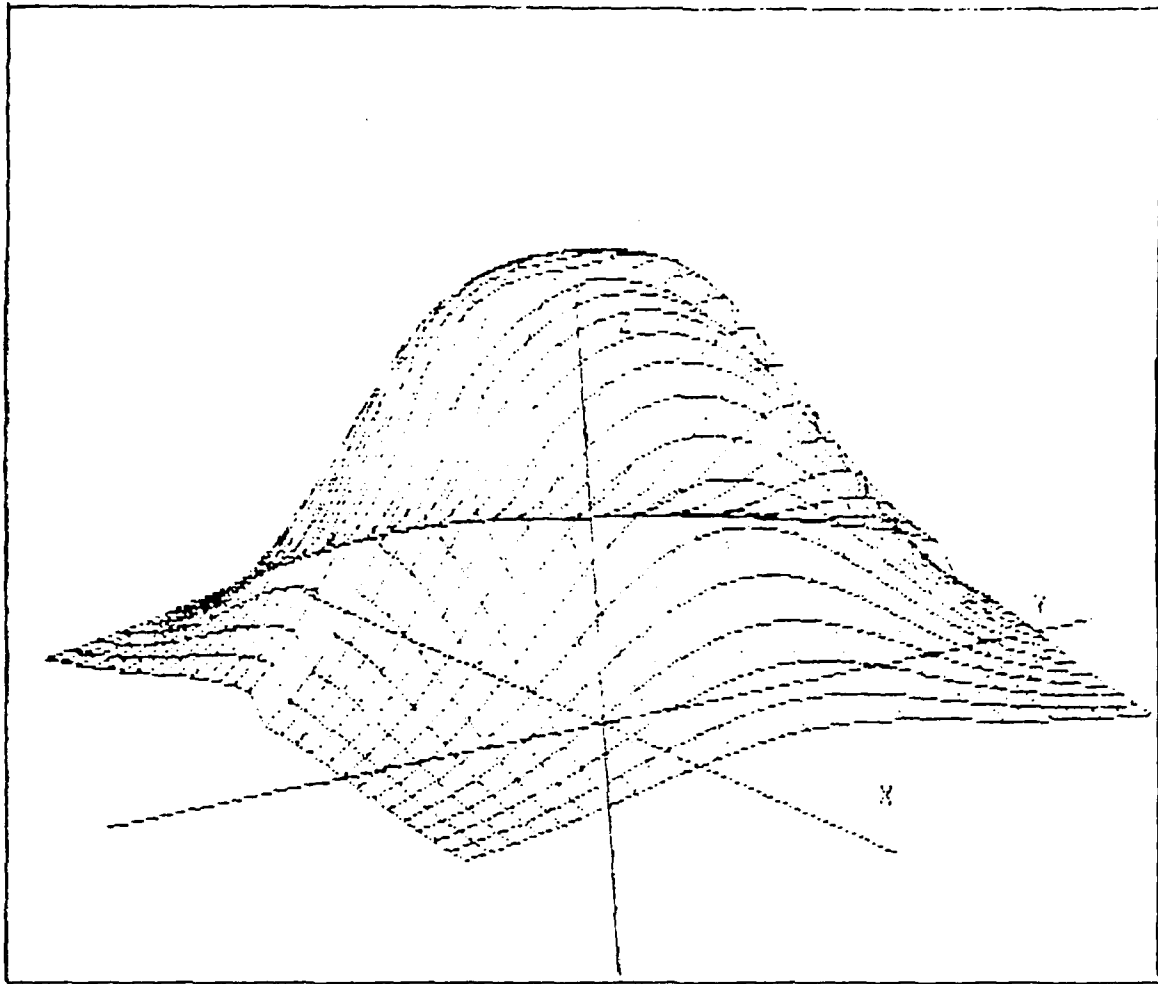


Figure 40. Coherent transition radiation at 10 MeV for an rms beam divergence angle of  $8.49\text{E}-2$  radians. The beam divergence has washed out all angular information. However a beam divergence angle of little more than  $2.50\text{E}-2$  radians accomplished the same effect for the single foil case. The angular information depicted in the X-Y plane extends to five times the predicted angle of maximum intensity in radians for the single foil case at the same energy. Intensity is measured along the Z-axis. The top of the Z-axis corresponds to the maximum intensity in units of charge squared divided by the speed of light per unit frequency and solid angle.

divergence angle at which this occurs is significantly higher than that for the single foil case. Figure 40 depicts the intensity distribution when the beam divergence angle is sufficiently large enough for this phenomenon to occur.

Figures 41 and 42 depict the effect of beam divergence on the interference pattern at 40 MeV. Here again, the fringe pattern becomes less visible as the beam divergence is increased. Finally, Figure 43 depicts the case where the beam divergence is nearly large enough for the angular information to be completely washed out. The beam divergence angle of  $7.07\text{E}-3$  radians required for this is well over twice that required of the  $3.00\text{E}-3$  radians for the single foil case at the same energy of 100 MeV.

In general, beam divergence has the same effect on the components of intensity as for the coherent transition radiation case as for single foil transition radiation. As in the single foil case, the effects of beam divergence are amplified at higher energies. An increase in beam divergence decreases the visibility of the fringes. However, the effect of resonance causes coherent transition radiation to be less susceptible to the loss of angular information due to beam divergence.

#### D. DIELECTRIC CONSTANTS

The intensity of transition radiation emitted when a charged particle transits from one medium to another is dependent upon the dielectric constant of each media. It was shown in Chapter III that the intensity is directly proportional to the square of the modulus of the difference between the dielectric constants of the two media. As in the single foil case, a vacuum to medium transition was assumed. The

dielectric constants for gold Au, silver Ag, and aluminum Al at a wavelength of  $5890 \text{ \AA}$  were used to study the effect on coherent transition radiation at 100 MeV.

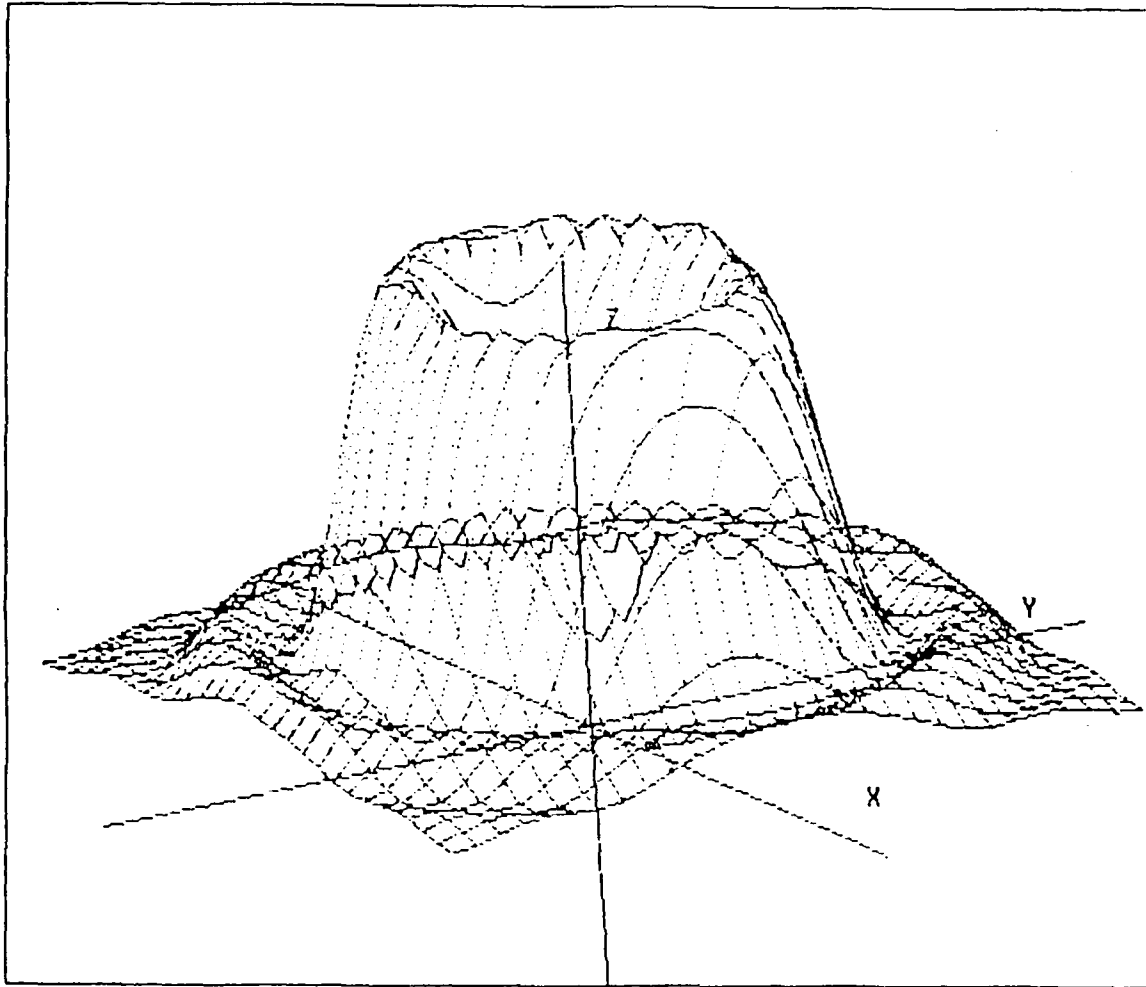


Figure 41. Coherent transition radiation at 40 MeV for an rms beam divergence angle of  $7.07E-3$  radians. The angular information depicted in the X-Y plane extends to five times the predicted angle of maximum intensity in radians for the single foil case at the same energy. Intensity is measured along the Z-axis. The top of the Z-axis corresponds to the maximum intensity in units of charge squared divided by the speed of light per unit frequency and solid angle.

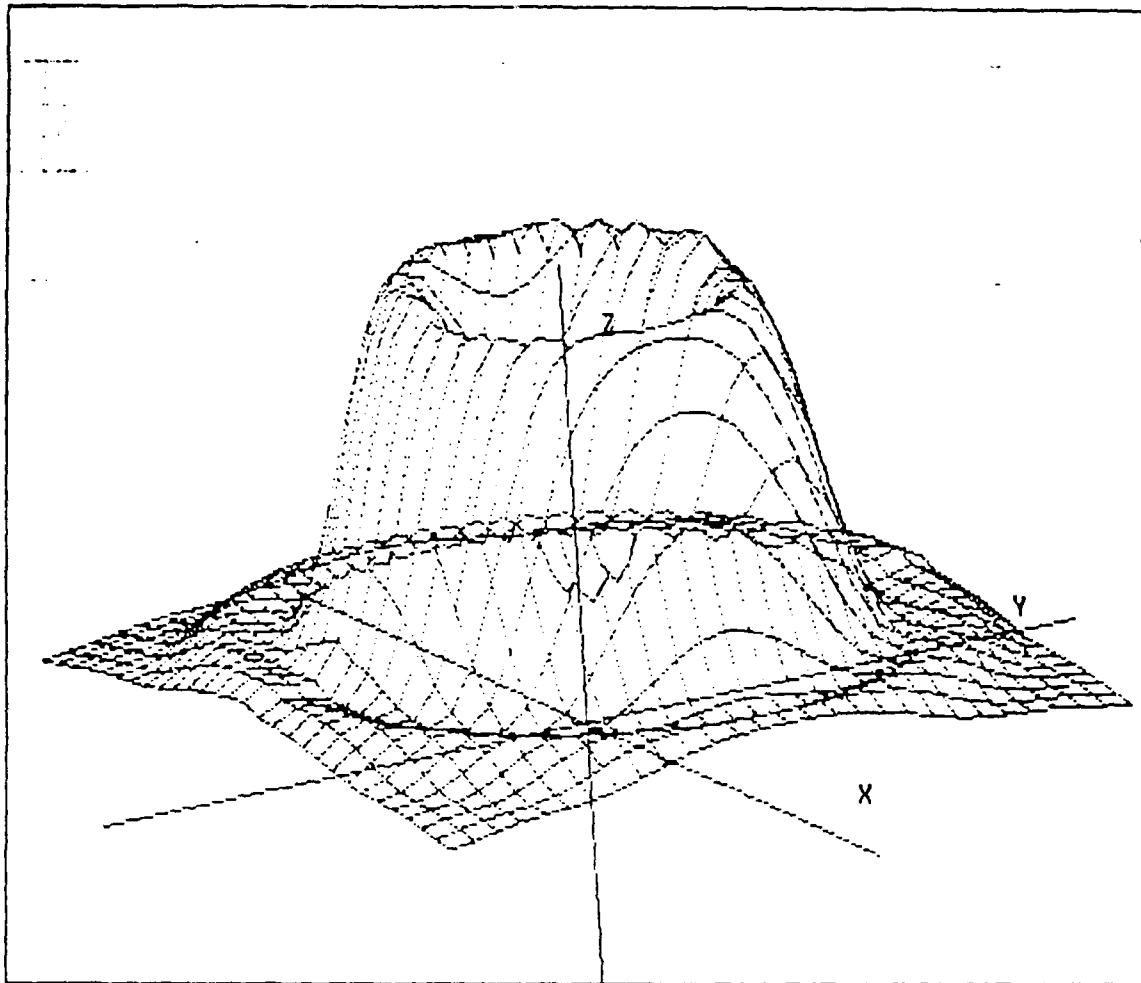


Figure 42. Coherent transition radiation at 40 MeV for an  $\mu$ s beam divergence angle of  $8.49\text{E}-3$  radians. Note the decrease of the outer fringe amplitudes as compared to those in Figure 41. The angular information depicted in the X-Y plane extends to five times the predicted angle of maximum intensity in radians for the single foil case at the same energy. Intensity is measured along the Z-axis. The top of the Z-axis corresponds to the maximum intensity in units of charge squared divided by the speed of light per unit frequency and solid angle.

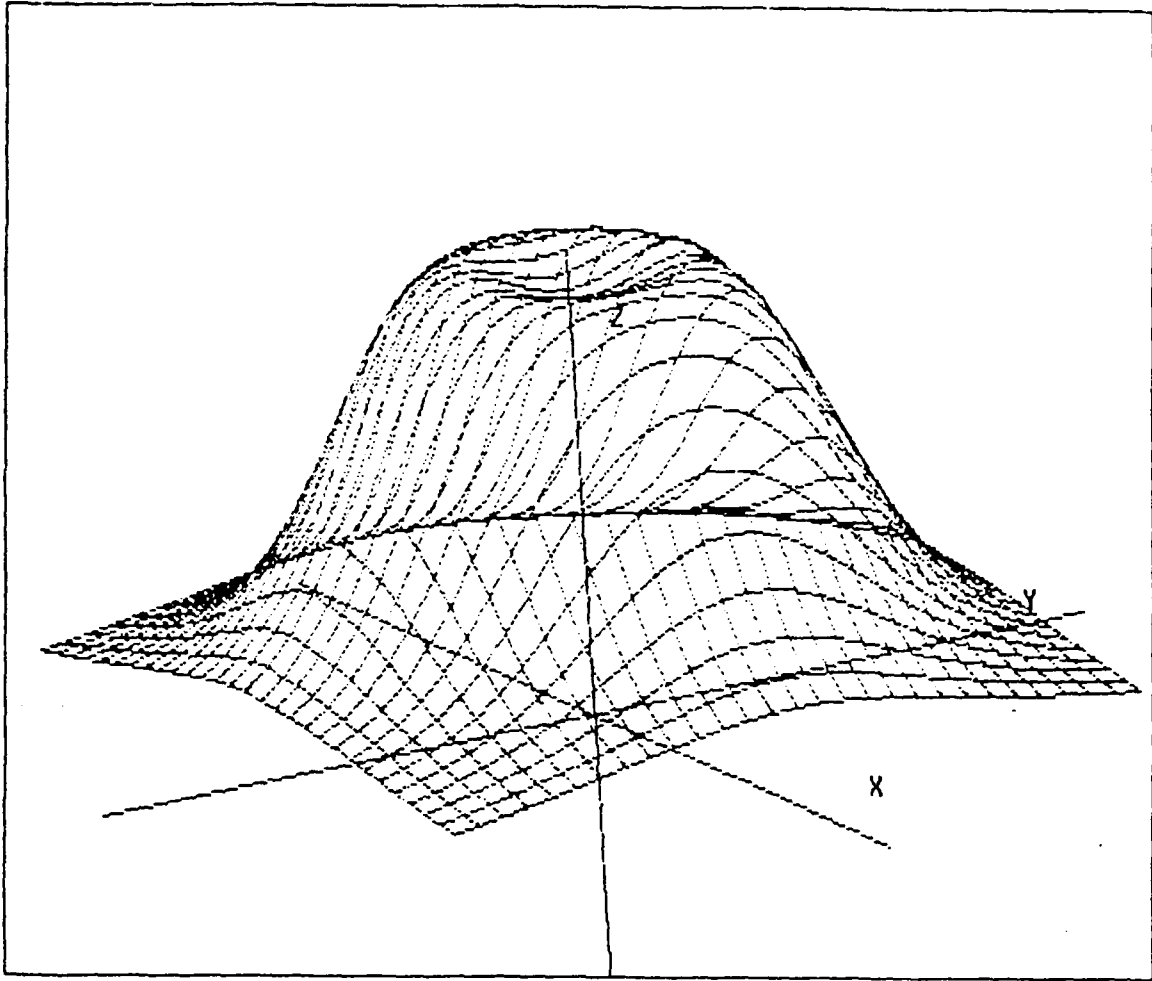


Figure 43. Coherent transition radiation at 100 MeV for an rms beam divergence angle of  $7.07E-3$  radians. The beam divergence angle is nearly great enough to wash out all angular information. However, a beam divergence angle of only  $3.00E-3$  radians was able to produce the same effect for the single foil case. The resonance effects in coherent transition radiation reduces the susceptibility to loss of angular information caused by beam divergence. The angular information in the X-Y plane extends to five times the predicted angle of maximum intensity in radians for the single foil case at the same energy. Intensity is measured along the Z-axis. The top of the Z-axis corresponds to the maximum intensity in units of charge squared divided by the speed of light per unit frequency and solid angle.

The results of applying the dielectric constants found in Table V of Chapter III for the parameters discussed here are presented in Table X for comparison with the results of the single foil case. The total intensity ITOT is presented in units of charge squared divided by the speed of light per unit frequency and solid angle.

TABLE X. DIELECTRIC CONSTANT VS. INTENSITY FOR COHERENT TRANSITION RADIATION AT 100 MEV AND  $\lambda=5890 \text{ \AA}$

Metal	$(\epsilon_1 - \epsilon_2)^2$	ITOT $\left[ \frac{e^2/c}{d\omega d\Omega} \right]$
Aluminum Al	138	1757
Gold Au	1250	1964
Silver Ag	179000	2256

The intensities for the coherent transition radiation case are much greater than that for the single foil case. This effect is again attributable to resonance. It is clear that the intensity for the coherent case is indeed proportional to the square of the difference between the dielectric constants between the two media. Figure 44 depicts the coherent transition radiation interference pattern for silver at 100 MeV over an angular distribution of  $\pm 5/\gamma$  radians from the Z-axis. The data is normalized so that the top of the Z-axis corresponds to the maximum value of intensity.

#### E. FINITE BANDWIDTH

Wartski [Ref. 5] found that variations in wavelength, and thus frequency, affected the visibility of the interference pattern fringes from the interferometer.

The pattern fringes became less visible as the bandwidth of wavelength increased. Wartski showed that the relation between intensity per unit solid angle and a bandwidth of wavelength could be expressed

$$I = |r_{\parallel}(\Delta\lambda)|^2 \frac{e^2}{\pi} \left[ \frac{L}{\lambda} \right]^2 \frac{\Delta\lambda \sin^2 \theta}{\lambda^2 p^2} \times \left\{ 1 - \frac{\sin(\pi p \Delta\lambda / \lambda)}{\pi p \Delta\lambda / \lambda} \right\} \cos 2\pi p, \quad (4.8)$$

where  $\Delta\lambda$  is the bandwidth of wavelength,  $L$  is the distance between foils, and  $p$  is the order of interference. An expression for the intensities of the maxima and minima may be found by substituting  $p=k\pm 1/2$  or  $p=K$  respectively.

For this study, the dielectric constants of gold at wavelengths of 4410 Å and 5890 Å was used. The coherent transition radiation distribution was studied at 30 MeV for a single wavelength of 4410 Å, and for a two percent (88 Å) and fifteen percent (66 Å) bandwidth centered on this wavelength. A similar study was done at 150 MeV around a wavelength of 5890 Å. It was found that an increase in bandwidth resulted in very slight fluctuations of intensity. There also appeared to be a slight shift in the fringe patterns for the 30 MeV case.

Figures 45–48 depict the effect of two percent and fifteen percent wavelength bandwidths at 30 and 150 MeV. The data is normalized so that the top of the Z-axis corresponds to the maximum intensity. The X–Y plane is used to plot the angular information in terms of the predicted angle of maximum intensity,  $1/\gamma$ , for the single foil case. The data extends to  $\pm 5/\gamma$  on the X and Y axes. A close comparison of the fringe patterns at 30 MeV for the four percent bandwidth in

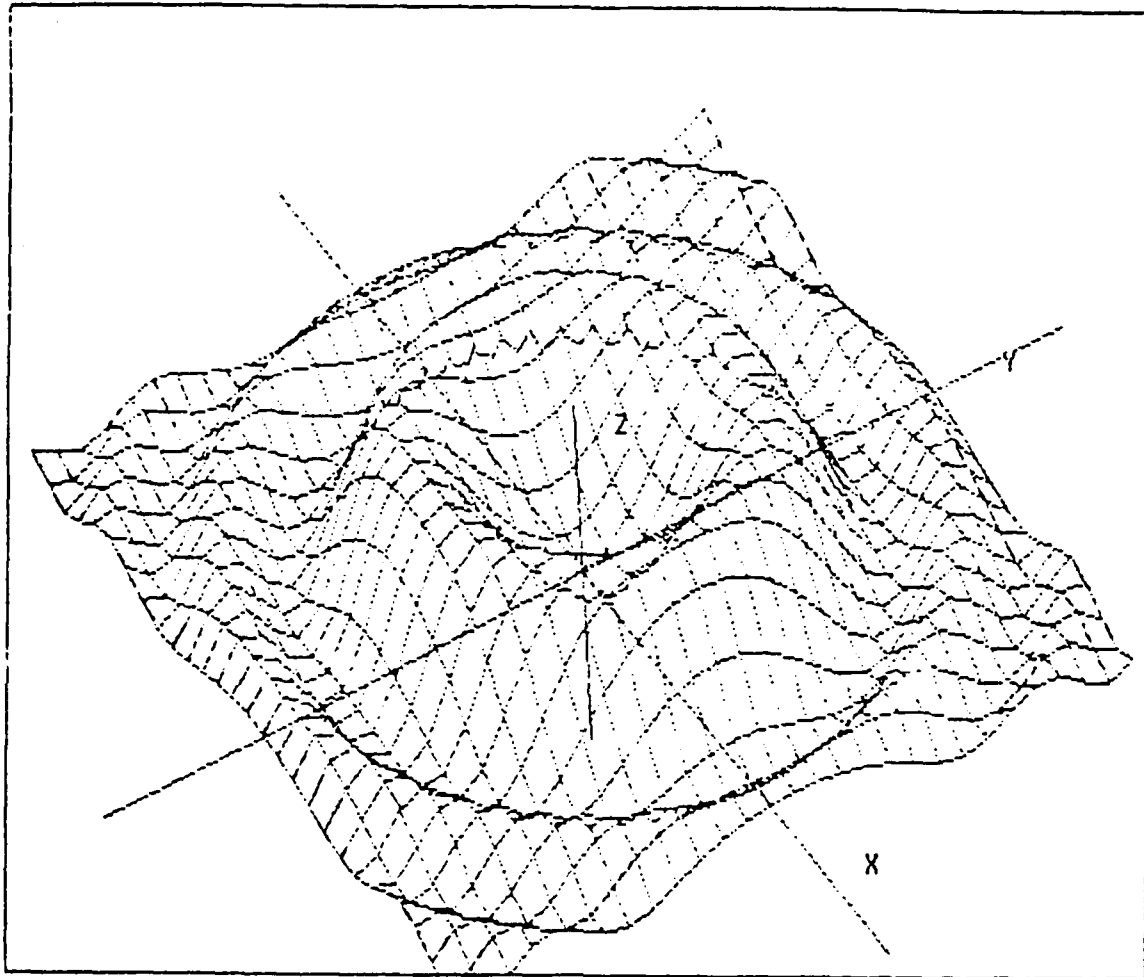


Figure 44. Coherent TR interference pattern for silver at 100 MeV and a wavelength of  $5890 \text{ \AA}$ . The patterns for silver and gold at the same energy and wavelength are nearly identical despite the difference in dielectric permittivity. The reason for this is that the data in each case is plotted on a relative scale. The intensity is normalized so that the top of the Z-axis corresponds to the maximum intensity. The data in the X-Y plane extends to five times the predicted angle of maximum intensity for the single foil case at 100 MeV.

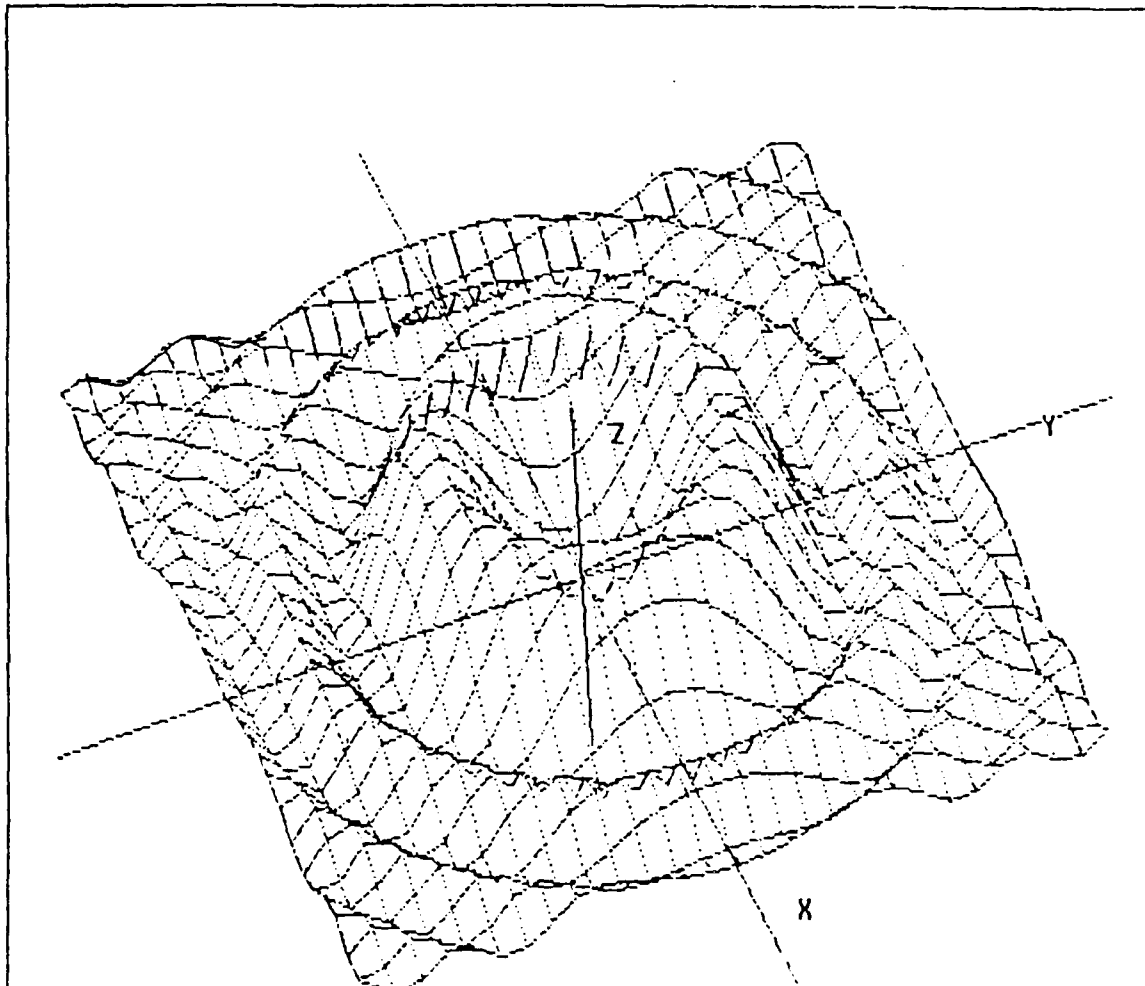


Figure 45. Coherent TR interference pattern at 30 MeV for a four percent wavelength bandwidth centered at  $4410 \text{ \AA}$ . The data is normalized so that the top of the Z-axis corresponds to the maximum intensity. The X-Y plane is used to plot the angular information in terms of the predicted angle of maximum intensity,  $1/\gamma$ , for the single foil case. The data extends to  $\pm 5/\gamma$  on the X and Y axes.

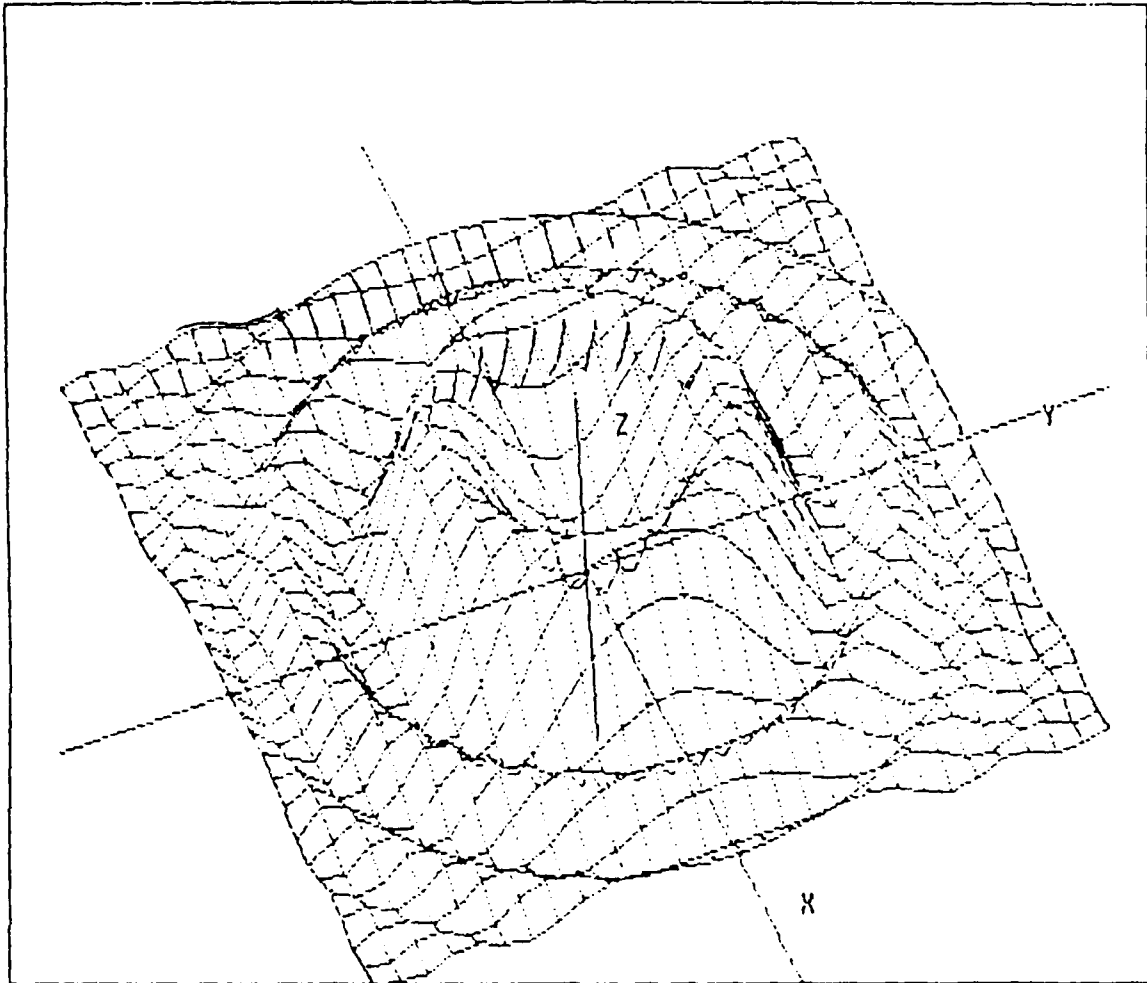


Figure 46. Coherent TR interference pattern at 30 MeV for a fifteen percent wavelength bandwidth centered at  $4410 \text{ \AA}$ . A close comparison of the fringe patterns here with those in Figure 45 reveals that the fringe patterns become slightly less visible as the bandwidth is increased. The data is normalized so that the top of the Z-axis corresponds to the maximum intensity. The X-Y plane is used to plot the angular information in terms of the predicted angle of maximum intensity,  $1/\gamma$ , for the single foil case. The data extends to  $\pm 5/\gamma$  on the X and Y axes.

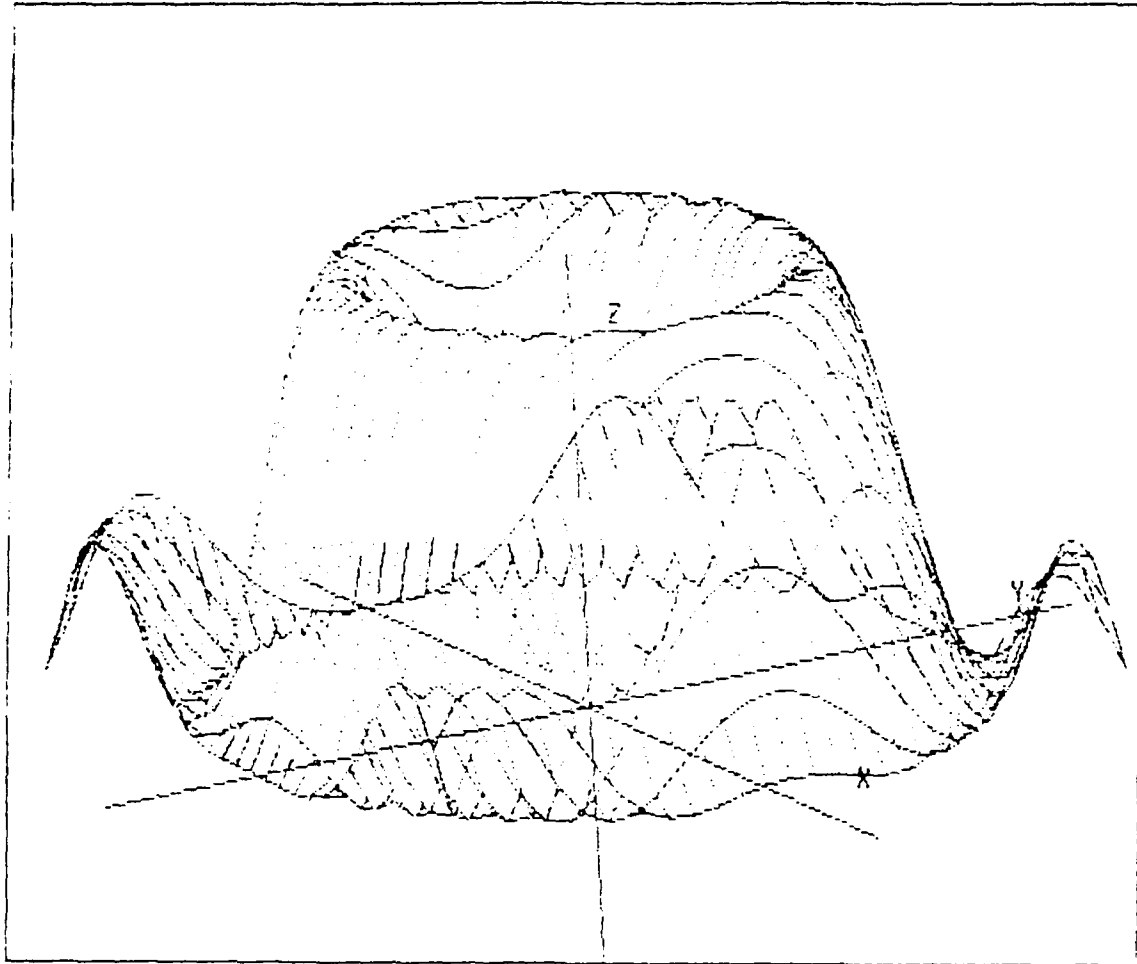


Figure 47. Coherent TR interference pattern at 150 MeV for a four percent wavelength bandwidth centered at  $5890 \text{ \AA}$ . The data is normalized so that the top of the Z-axis corresponds to the maximum intensity. The X-Y plane is used to plot the angular information in terms of the predicted angle of maximum intensity,  $1/\gamma$ , for the single foil case. The data extends to  $\pm 5/\gamma$  on the X and Y axes.

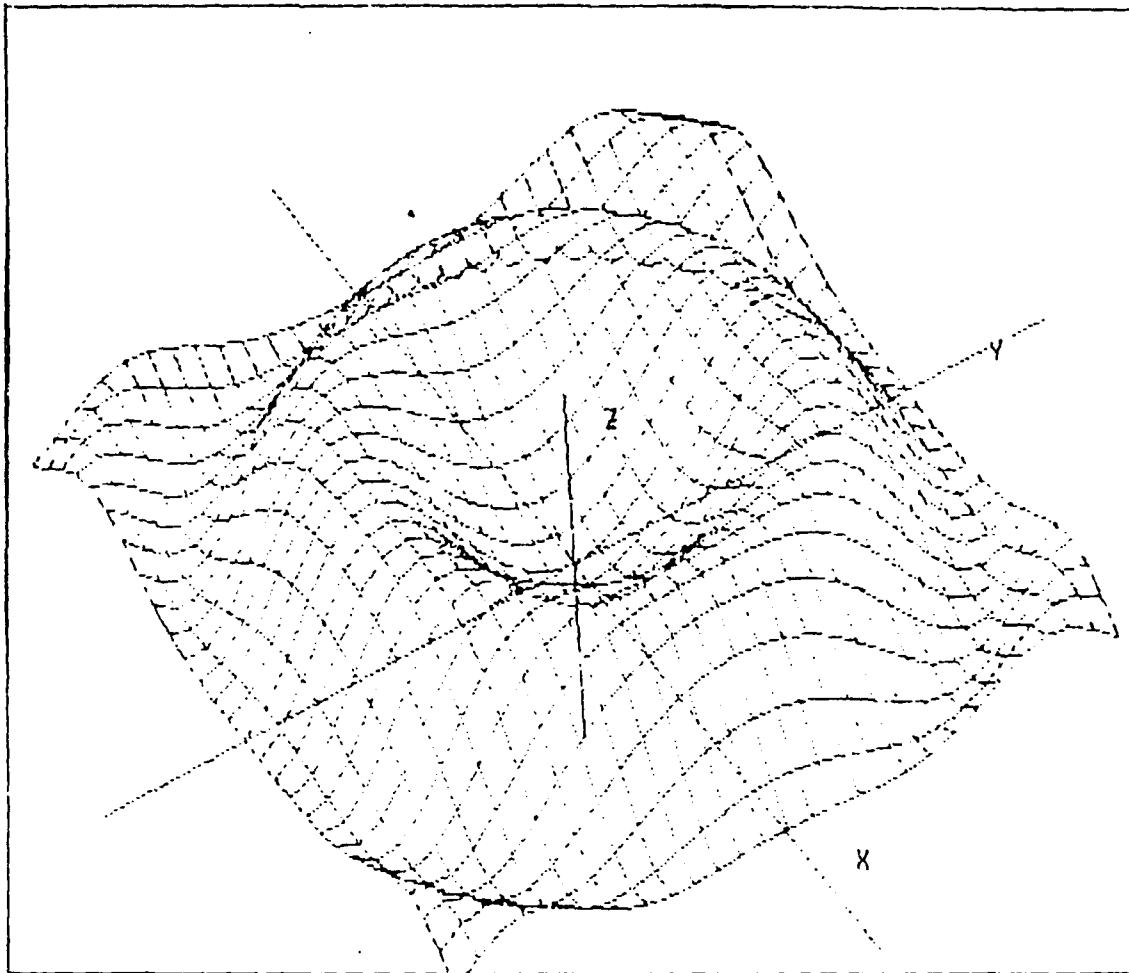


Figure 48. Coherent TR interference pattern at 150 MeV for a fifteen percent wavelength bandwidth centered at  $5890 \text{ \AA}$ . This pattern is indistinguishable from that of the four percent bandwidth presented in Figure 47. The data is normalized so that the top of the Z-axis corresponds to the maximum intensity. The X-Y plane is used to plot the angular information in terms of the predicted angle of maximum intensity,  $1/\gamma$ , for the single foil case. The data extends to  $\pm 5/\gamma$  on the X and Y axes.

Figure 45 and the fifteen percent bandwidth in Figure 46 reveals that the outer fringes become slightly less visible as the bandwidth is increased. However, no such difference could be found for the same case at 150 MeV (Figures 47,48).

In summary, a finite bandwidth of wavelength, and thus frequency, results in slight variations of intensity. An increase in bandwidth produces a small increase in intensity. Angular information such as fringe pattern is relatively unaffected except for large bandwidths.

## RECOMMENDATIONS AND CONCLUSIONS

The programs used in this study provide an effective tool for studying the characteristics of optical transition radiation to aid in interpretation of experiments. They provide an inexpensive method of obtaining a thorough understanding of optical transition radiation and its potential use for charged particle beam diagnostics. Such an understanding has already been promoted through the results of this study.

The nature of the energy effects on angular distribution and polarization was thoroughly explored. Other factors affecting the intensity and distribution of transition radiation were also investigated. It was shown that beam divergence affects the angular distribution of intensity, particularly at higher energies. However, the effects of beam divergence can be more sensitively investigated through the use of a stack of foils spaced at intervals comparable with the coherence length. Metals characterized by dielectric permittivities much greater than one can be used to enhance the intensity of transition radiation. The finite bandwidths of the observed wavelength have little effect on the distribution of transition radiation unless the bandwidth is excessively large.

Further improvements can be made on the programs used in this study. For the single foil and two-foil interferometer TR programs, the asymmetry representing the effect of a charged particle encountering a boundary at an oblique angle requires refinement. A cosine dependence was discussed in which the asymmetry could be introduced at one point and then "rotated" around the axis. The asymmetry factor could then be multiplied by the cosine of the angle of rotation. Some means

of labelling or indicating units of measure on the axes for the plots in the SON OF SURF3D program is also recommended. The SON OF SURF3D program should also be fully developed for commercial use.

Finally, software should be developed to measure and present actual data in three dimensions for comparison with the theoretical data presented here. A program compatible with SON OF SURF3D under development for that purpose had to be abandoned due to the time constraints on this study. Such a program would be a necessary step in actually applying the optical transition radiation as a diagnostic for charged particle beams.

## LIST OF REFERENCES

1. Frank, I., and Ginsberg, V., "Radiation of a Uniformly Moving Electron Due to Its Transition from one Medium into Another," Journal of Physics, Vol. IX, No. 5, 1945, pp. 353-362.
2. Ginzburg, V. L., and Tsytovich, V. N., "Several Problems of the Theory of Transition Radiation and Transition Scattering," Physics Reports, v. 49, No. 1, 1979.
3. Ter-Mikaelian, M. L., High-Energy Electromagnetic Processes in Condensed Media, (Wiley-Interscience, New York, 1972).
4. Garibian, G. M., "Theoretical Foundations of Transition Radiation," Soviet Physics JETP, Vol 10, 1960.
5. Wartski, L., Study on the Optical Transition Radiation Produced by 30 to 70 Mev Energy Electrons. Application to the Diagnosis of Beams of Charged Particles, Ph.D. Dissertation, The Universite de Paris-Sud, Centre D'Orsay, France, 1976.
6. Fiorito, R. B., and others, "Optical Transition Radiation Diagnostics for Low Emittance, High Energy. Charged Particle Beams," paper presented at EPAC Proceedings of the European Particle Accelerator Conference, June 7-11, 1988.
7. Iversen, S. G., and others, "Charged Particle Beam Divergence Measurements Using Transition Radiation," IEEE Particle Accelerator Conference, March 16-19, 1987, pp 573-575.
8. Rule, D. W., and Fiorito, R. B., "Transition Radiation Diagnostics for Intense Charged Particle Beams," Nuclear Instruments and Methods in Physics Research B24/25, 1987, pp 901, 904.
9. Naval Surface Warfare Center Report TR 84-134, "The Use of Transition Radiation as a Diagnostic for Intense Beams," by D. W. Rule and R. B. Fiorito, July 1984.
10. Gilmore, D., "SURF / SURF 87 Documentation", Dogstar Software, Inc. 1987.
11. Media Cybernetics and IMSI, TurboHalo, 1<sup>st</sup>ed., August 1986.
12. Handbook of Chemistry and Physics, 38<sup>th</sup>ed., pp 2703-2705, Chemical Rubber Publishing Company, 1956.
13. Bennett, H. E., and Bennett, J. M., "The Validity of the Drude Theory for Silver, Gold, and Aluminum in the Infrared," paper presented at International Colloquium Colloquium on Optical Properties and Electronic Structure of Metals and Alloys, September 13-16, 1965, pp 175-188.

## APPENDIX A

### USER'S MANUAL

This appendix is intended to aid the operator in using the transition radiation programs TR3 and COHER3 and the three-dimensional graphics program SON OF SURF3D. While the content was written so as to be readily understandable to the inexperienced computer user, a basic understanding of MS-DOS procedures is assumed. This appendix is written in two parts. The two transition radiation programs, being very similar in use are treated as one unit. A description for the use of each was taken up to the point of invoking the use of the graphics program. The final section is written so that the user would be able to begin with a data file from either transition radiation program, plot it out in three dimensions, and vary all the plotting parameters in any combination so as to obtain the most satisfactory plot for the case at hand.

#### A. THE TRANSITION RADIATION PROGRAMS

The transition radiation programs were written in Fortran and compiled using the Ryan-McFarland fortran compiler. Both programs should be installed on the hard disk under the directory C:\FORT>. If not previously compiled, the programs may be compiled from within the C:\FORT> directory using the command RMFORT TR3 /N or RMFORT COHER3 /N. This command causes and object file to be formed which is used by the PLINK command. PLINK86 FI

TR3 or PLINK86 FI COHER3 at the C:\FORT> prompt, to form an execute file. The programs are then ready for use by typing either TR3 or COHER3 for the program desired.

### 1. Overview

Program execution begins upon typing either TR3 or COHER3 at the C:\FORT> prompt. The user is then faced with the following messages in succession:

```
ENTER NAME OF 3-D GRAPHICS FILE
EXAMPLE: GRAPH.DAT
[entry]
ENTER NAME OF CORRESPONDING PARAMETER FILE
EXAMPLE: PRMTRS.DAT
[entry]
WHAT IS THE DESIRED BEAM ENERGY IN MEV?
PLEASE INCLUDE A DECIMAL PLACE.
[entry]
```

Once the above entries are made, a menu list of current parameters appears. This menu list for the COHER3 program differs a bit from that of the TR3 program as should be expected. The menu list for the TR3 and the COHER3 programs are depicted in Figures 49 and 50, respectively. The user has the option of accepting the current default parameters or changing one, any combination, or all the parameters. In order to change any parameter, the user need only type the appropriate number, press return/enter, and follow the directions. In all cases, after the new parameter is entered, the parameter change menu reappears indicating the new parameters. Once all the parameters are to the user's satisfaction, the user accepts the current parameters by entering the appropriate number as indicated in order to continue with the program.

The last entry required of the user provides the user with a choice of polarization. The parallel component of intensity only, the perpendicular component of intensity only, or the sum of the two for the total, non-polarized intensity may be plotted. The decided choice is entered by typing the appropriate number and pressing return/enter.

CHOOSE DESIRED POLARIZATION.  
ENTER APPROPRIATE INTEGER FOR DESIRED POLARIZATION

1 NO POLARIZATION—TOTAL INTENSITY  
2 PARALLEL.  
3 PERPENDICULAR

Once the choice of polarization is entered, the program begins calculations that take approximately seven to ten minutes (assuming a math co-processor is installed). Progress is indicated by the program through displaying the current record number over which the calculations are being done. There are a total of 64 records corresponding to rows of data. The data is organized into 64 rows (records) and 64 columns (fields) for use with the graphics program. All data for the graphics file is normalized after the intensities for all the data points are calculated. The output includes the graphics file of normalized data, a corresponding parameter file, a file containing the non-normalized intensity data in terms of charge squared divided by the speed of light (per unit frequency and solid angle), and a scratch file used for interim calculations.

## 2. Required entries

The program is executed by typing TR3 or COHER3 at the C:\FORT> prompt. The following message then appears upon the screen:

ENTER NAME OF 3-D GRAPHICS FILE  
EXAMPLE: GRAPH.DAT

The required entry here is the name of the actual file that will be used by the SON OF SURF3D graphics program. It is suggested that some sort of mnemonic device be used for key characteristics of the file for ease in later identification. Table XI demonstrates the standard format used in conjunction with this thesis.

TABLE XI. GRAPHICS FILE LABELLING SCHEME

AXXXENNN.DAT	A	Either T for TR3 single-foil program or C for COHER3 interferometer program.
	.DAT	Extension required by graphics program.
	ENNN	Indicated energy in MeV.
	XXX	Specified key characteristics.
	3	Standard defaults. ie T3E10.DAT
	AN	RMS Beam angle altered, N indicated variation number for that energy. ie CA2E30.DAT for second variant at 30 MeV.
	F	scattering foil present. ie TFE50.DAT
	DXX	Dielectric constant altered. ie CDAL for dielectric constant of Aluminum.
	NG	Data calculated over angular distance of N times $1/\gamma$ from axis. ie T5GE70.DAT
	N	Data normalized to maximum value for total intensity at 100 MeV. ie CNE90.DAT
	PERP	Perpendicular component of intensity only selected for plots. ie TPERPE5.DAT
	PAR	Parallel component of intensity only selected for plots. ie CPARE15.DAT
	B	Finite bandwidth, wavelengths altered COHER3 program only. ie CBE80.DAT
	TH	Foil thickness altered, COHER3 program only. ie CTHE50.DAT
	DL	Distance between foils altered, COHER3 program only. ie CDLE90.DAT.

Combinations of key characteristics are also possible. For example, TF5GNE80.DAT indicates the presence of a scattering foil, calculations over an angular distance of  $\pm(5/\gamma)$  from the axis, and data normalized to 100 MeV.

Upon entering the name of the graphics file, the operator is requested to enter the name of the associated parameters file.

ENTER NAME OF CORRESPONDING PARAMETER FILE  
EXAMPLE: GRAPHP.DAT

The name of the parameter file should be similar enough to the name of the graphics file to avoid confusion at a later date. For this thesis a P for parameters was tagged on to the name of the graphics file. For example, C5GE60P.DAT or C5GP60.DAT for the parameter file corresponding to the C5GE60.DAT graphics file.

One word of caution. The computer doesn't read beyond the first nine letters of a file name. The file name plus three-letter extension should never exceed twelve letters. The programs will run using filenames entered in excess of nine characters. However, the files in which the only difference in name occurs beyond the ninth character will not appear in the directories and the data will be lost. It may occasionally become necessary to abbreviate the name of the graphics and parameter file to prevent this from happening.

Once the name of the parameter file has been entered, the user is requested to enter the energy in MeV. Since the analytic solutions were obtained through the use of small angle approximations for angles represented by the inverse of the Lorentz factor, analysis at lower energies must be considered less exact. Energies at which the inverse of the Lorentz factor is greater than 0.1, that is energies less than about 5 MeV should be treated as rough approximations. Angular information, which is important for purposes of beam diagnostics, is lost

above about 200 MeV without a polarizing filter. No such filter is built into these programs therefore their analysis above 200 MeV is of little value for beam diagnostics. The energy entry should include a decimal point.

Once the output files have been named and the desired energy entered, a menu for changing data parameters appears on the screen. Figures 49 and 50 depict the menus for the TR3 single-foil and the COHER3 interferometer programs respectively.

The current values are:

1 RMS beam angle is 0.001 radians/sqrt(2).

2 IFOIL is 0.

A value of one indicates that a scattering foil is present. A value of zero indicates that there is a target foil only.

3 The dielectric constant of the medium is  
0.618 + 5.47i.

This program assumes a vacuum to medium transition.

4 Angular measurement is over 0.05 radians.

5 Normalization is to the maximum total intensity for the energy entered for this run.

The option is to normalize to the maximum total intensity for an energy of 100 MeV.

In all cases, parallel intensity will be normalized to its own maximum value for the energy entered for this run.

6 Accept current parameters.

Enter the number without the decimal for the value you wish to change. Enter 6 for no changes.

Figure 49. Parameter change menu for the single foil TR3 program

THE CURRENT PARAMETERS ARE:

- 1 RMS beam angle in the X-Z plane is .000210 radians  
RMS beam angle in the Y-Z plane is .000210 radians
- 2 IFOIL is 0. A value of 1 indicates  
that a scattering foil is present. A value of  
zero indicate absence of scattering foil.
- 3 The optical constants for the back metallic foil  
are  $.618 + 5.47i$ .
- 4 The optical constants for the front clear foil  
are  $1.48 + 0.00i$ .
- 5 Angular measurement is over 0.05 radians
- 6 Normalization is to the maximum total  
intensity for the enery entered for this run.  
The option is to normalize to the maximum total  
intensity for an energy of 100 MeV.
- 7 Minimum wavelength is 4500 angstroms.  
Maximum wavelength is 4500 angstroms.
- 8 Foil thickness is .005 centimeters.
- 9 Distance between foils is 1.20 centemeters.
- 10 Accept current parameters.

Enter the number without the decimal for the value  
you wish to change. Enter 10 to accept parameters.

Figure 50. Parameter change menu for interferometer COHER3 program

The user has the option of accepting the current default parameters or changing one, any combination, or all the parameters. In order to change any parameter, the user must first type the appropriate number, then press return/enter. The user will then be directed to enter the new value. Each of these parameters will now be discussed in detail.

Any parameter may be changed simply by entering the integer value that appears next to the parameter the user wishes to change. The first parameter option in both programs is RMS beam angle. Upon entering a 1 to change this parameter, the message 'PLEASE ENTER NEW VALUE FOR RMS BEAM ANGLE' appears. The appropriate entry is entered in terms of radians. Not all the

particles within the beam travel parallel to each other. The particles tend to diverge at various angles within the beam. The rms beam angle is the mean of a Gaussian distribution of these angles of divergence. For the TR3 program it is assumed that the distribution of divergence in the X-Z plane ( $\sigma_x$ ) is the same as in the Y-Z plane ( $\sigma_y$ ) such that  $\sigma_x = \sigma_y = \sigma$ . In that case the total RMS beam angle of divergence is equal to  $\sqrt{2}\sigma$ . The value entered for the TR3 program should be in terms of radians/ $\sqrt{2}$ . The COHER3 program does not make that assumption and allows separate values to be entered for  $\sigma_x$  and  $\sigma_y$ . The values entered for the COHER3 program should be in radians.

Option 2 in both programs allows for the inclusion of a separate scattering foil. The message 'ENTER NEW VALUE FOR IFOIL' appears when this option is selected. The only valid entries for this option are 0 and 1. As indicated, a value of 1 here indicates the presence of the scattering foil. The presence of the scattering foil slightly affects the distribution of the parallel component of TR intensity. It does not affect the perpendicular component of intensity. A value of 0 here indicates that a scattering foil is not present.

The ability to change the dielectric constants of the mediums is offered in option 3 for the single foil TR3 program and by options 3 and 4 of the interferometer COHER3 program. Upon selecting any of these options, the user is first asked to enter the value of the real component, then asked to enter the imaginary component. In effect, this allows the user to change the material of the target foil. Option 4 of the COHER3 program allows the user to substitute another material for the clear front foil figured into the program. Values for dielectric

constants may be found in the CRC Handbook of Chemistry and Physics [Ref 9]. Both the real and imaginary parts of the dielectric constant should be entered as real numbers.

Option 4 of the TR3 program and 5 of the COHER3 program allow the user to change the angular range over which the data is calculated. Two different means are allowed for this option. The predicted angle of maximum intensity is that of the inverse of the Lorentz factor in radians. The user has the option of entering a multiple of this angle or entering a value for this angle in radians directly. Upon selection of this option, the following menu appears.

Choose option

- 1 Angle that is  $N^*(1/\text{Lorentz factor})$
- 2 Enter angle in radians manually.

Choosing option 1 results in the message 'Enter N, for  $N^*(1/\text{Lorentz factor})$ '. The preferred entry is an integer. Choosing this option causes calculations of intensity to be over an integer multiple of the predicted angle of maximum intensity. This option aids the comparison of energy distributions over a wide range of energies. Choosing option 2 results in the message 'Enter desired angle in radians'. Obviously, the desired number is a real value of radians for the desired angle. Using this option to choose the same angle for a range of energies aids in examining the angular dependence of the intensity distribution on energy.

The ability to normalize data to the maximum intensity value attained at 100 MeV is offered by options 5 and 6 of the TR3 and COHER3 programs respectively. This option allows for ease of study of relative intensities as a function

of energy. Choosing this option is irreversible. Once chosen, there is no way of going back to normalizing the data to its own maximum intensity for that energy. Upon entering the appropriate number to choose this option, the parameter change menu appears with the message 'Normalization will be to 100 MeV.' in place of this option.

Option 7 of the COHER3 program allows the user to change the range of wavelengths over which calculations are made. Selection of this option results in the following messages:

```
ENTER NEW MINIMUM WAVELENGTH.  
[entry]  
ENTER NEW MAXIMUM WAVELENGTH.  
[entry]
```

The user should enter the minimum and maximum wavelengths in angstroms. This option provides for the rare opportunity to study the effects of finite bandwidth on the distribution of TR intensity. The traditional development of transition radiation theory is built upon an evaluation of integrals that assumes a Dirac function for frequency bandwidth. However, a finite frequency bandwidth has always been encountered while obtaining real data which may account for the small differences between theoretical and actual data.

Choosing option 8 of the COHER3 program results in the message: ENTER NEW VALUE FOR FOIL THICKNESS IN CENTIMETERS. This is for the thickness of the front clear foil through which the beam must travel before

encountering the back metallic foil. This option provides the opportunity to study the effects of front foil thickness on the interference pattern between the forward radiation from the front foil and the backward radiation from the rear metallic foil.

Option 9 of the COHER3 program allows the user to specify the distance between foils in centimeters. This option not only provides the user the ability to study coherence length, but is a necessity since the interference pattern is highly dependent on the distance between foils with respect to the coherence length. The convention has been to define coherence length as the distance a particle travels in the time it takes the particle to "see" the phase of its associated electromagnetic wave change by one radian [Ref. 5]. This phase difference was chosen so that the particle's field and the radiation fields add coherently, hence the name "coherence length".

The programs allow the user to alter any or all data parameters in any order or combination. Every time a user chooses an option other than ACCEPT CURRENT PARAMETERS a message appears which attempts to clearly specify the appropriate entry. Once that entry is made, the parameter change menu reflecting the new values reappears on the screen. This allows the user to review all the parameter values before continuing on with the program. Once satisfied with the current parameters, the user must select ACCEPT CURRENT PARAMETERS (option 6 for the TR3 program, option 10 for the COHER3 program) in order for the program to continue.

Having accepted the current parameters, the user is requested to make one last selection. The transition radiation intensities are calculated by computing the parallel and perpendicular components separately. Total intensity is then the

sum of the two components. The user is provided the option of plotting either the total intensity or either component of intensity. This allows the user to study the effects of each parameter on the components of intensity separately. The user selects the desired component (polarization) by entering the appropriate integer as specified on the following menu:

**ENTER APPROPRIATE INTEGER FOR DESIRED POLARIZATION**

- 1 NO POLARIZATION—TOTAL INTENSITY
- 2 PARALLEL
- 3 PERPENDICULAR

Once the selection is entered, the program will run its course, indicating progress by listing the current record number over which calculations are being made. recall that the data is organized into sixtyfour records each containg sixty four fields of data for use with the graphics psrogram. The intensities are normalized for the graphing purposes after all the other calculations have been completed.

## **B. THE THREE-DIMENSIONAL GRAPHICS PROGRAM**

The three-dimensional graphics program used in conjunction with the transition radiation programs is SON OF SURF3D which was written by Don Gilbert of DogStar Software. SON OF SURF3D is an improved version of SURF3-D / SURF87 that is not yet fully developed for public release at the time of this writing. The SURF3-D / SURF87 and the improved SON OF SURF3D are three dimensional plotting programs that are written in Turbo Pascal and use TurboHALO graphics routines [Ref. 10]. Turbo Pascal is a registered trademark of Borland International and TurboHALO is a trademark of Media Cybernetics, Inc.

and IMSI. The key improvement of SON OF SURF3D over SURF3-D that makes it useful for this application is that it is able to plot a three dimensional surface from a data file provided by the user. The data file used for this purpose must contain the following information in order

- Integer value for the number of y-rows
- Integer value for the number of x-columns
- Real value for the z-axis minimum
- Real value for the z-axis maximum
- Real value for the z-axis center (the intercept with the xy-plane)
- Real z values for each x,y point

Unfortunately, Don Gilbert of Dogstar Software has indicated that development of SON OF SURF3D for public release has stopped. However a copy may be obtained for a fee by writing to him at the following address:

DogStar Software  
PO Box 302  
Boomington, IN 47402  
Telephone (812) 333-5616

A graphics device and a printer are required for the graphics program. A math coprocessor is preferred but not absolutely necessary. SON OF SURF3D supports several graphics devices and printers with specific device driver files. The appropriate graphics driver device file must be stored in the directory C:\T\HALO\ as HALODEF.DEV. The printer device driver file must be renamed HALODEF.PRN and placed under the directory C:\T\HALO\ . The files SSURF.COM and HALORTP.EXE must be installed under the directory C:\T\HALO. All the required files are found in the HALO.ARC file on the disk supplied by Dogstar Software.

## 1. USE

Once installed, the program may be run by typing SSURF from within the C:\T\HALO directory. When ready, the program will display the menu depicted in Figure 51. The user may choose to plot any of the supplied pre-defined functions by pressing the appropriate letter such as C for the Cos Sqr function. Choosing any of the pre-defined functions in this way automatically places the cursor in the parameters section of the menu. Any or all the parameters may be then be altered prior to plotting. The user may choose to plot the program by pressing the function key F10 or he may choose another function by pressing Esc

3-D Functions: $Z=f(X,Y)$		
C) Cos Sqr		$z=\cos(\text{sqr}(x)+\text{sqr}(y))$
E) Error		$z=\text{erfi}(x,y)$
L) Ln Cos		$z=\ln(\cos(x))-\ln(\cos(y))$
Y) Your Formula		$z=\exp(-\text{sqr}(x)/2-\text{sqr}(y)/2)$
Parameters		
Plot radius	= 0.90	Z-axis Maximum=2.400
Hatch Increment	= 0.03	X-axis Maximum=3.000
Delta Increment	= 0.05	Y-axis Maximum=3.000
Hide Back Lines	= No	Z-axis zero =0.000
Hide Axes	= No	X-axis zero =0.000
Do X-hatching	= Yes	Y-axis zero =0.000
Do Y-hatching	= No	A rotation =3.000
Points only	= No	B rotation =-50.0
Virtual Screen	= No	C rotation =-70.0
Esc=Exit F2=Print F6=File F10=Draw Arrows=Rotate		

Figure 51. SSURF Main Menu

which will place the cursor back into the top part of the menu. Option Y) in the top part of the menu is the option of interest in that this option allows the user to specify a function or a complete pathname of a data file containing data as described above. Choosing this option does not place the cursor in the parameter section of the menu. Parameters may not be altered without first obtaining a plot upon selection of option Y). Therefore it is recommended that the user first select another option as described above, alter the parameters as desired, and press Esc to get back into the top portion of the menu before selecting option Y). In order to plot the three-dimensional surface of a data file, select option Y) and press return/enter. Then type in the complete pathname of the data file and press return/enter again. After a few seconds, the word "file" will appear behind the pathname indicating that the program is ready to plot the data. The data may then be plotted by pressing the function key F10. Flashing indices on the z-axis indicate that the plot is finished. The plot may be rotated at will by pressing the arrow keys. The user may print the plot by pressing the F2 function key. The Esc key will return the display back to the main menu and place the cursor in the parameters section.

The shape of the plot is largely dependent on the plotting parameters used to define it. Figure 52 depicts the parameters used for the plots displayed in this thesis.

Parameters		
Plot radius	= 0.70	Z-axis Maximum=1.000
Hatch Increment	= 0.05	X-axis Maximum=40.00
Delta Increment	= 0.05	Y-axis Maximum=40.00
Hide Back Lines	= Yes	Z-axis zero =-.500
Hide Axes	= Yes	X-axis zero =0.000
Do X-hatching	= Yes	Y-axis zero =0.000
Do Y-hatching	= Yes	A rotation =3.000
Points only	= No	B rotation =-70.00
Virtual Screen	= No	C rotation =-60.00

Figure 52. Sample parameter values for plots.

"Plot radius" refers to the size of the plot in the XY plane relative to the extent of the X and Y axes. Valid entries for "Plot radius: range from 0.01 to 1.00. "Hatch increment" refers to the spacing between the plotting lines. "Delta increment" refers to the increment used for interpolation between data points. Valid entries for both "Hatch increment" and "Delta increment" are 0.00 to 1.00.

The "Hide Back Lines" and the "Hide Axes" options may be used to keep the plot relatively clean. The user has the option of selecting either x hatching or y hatching or both. Choosing neither produces the same result as "Points only", which overrides the "X hatching" and "Y hatching" options. The "Virtual Screen" option supports the high-resolution capabilities of some printers. A device file named HALORVRI.DEV is required for this option. Valid entries for all these options are either "Yes" or "No".

"Z-axis maximum" defines the maximum value of the vertical scale, regardless of the maximum value of the function or data. "X-axis maximum" and "Y-axis maximum" define the maximum horizontal limits of the plot, regardless of

the extent of the data. SON OF SURF is capable of plotting as much as a 100 by 100 array of data centered at the intersection of the three axes. The valid entries for these options range from 0.01 to 100.00.

"Z-axis zero", "X-axis zero", and "Y-axis zero" define the origin of respective axis relative to the origin. Selecting something other than zero for any of these options physically moves the entire plot. The range of valid entries were not listed in the scanty documentation.

All plots may be rotated about the three axes at will, either by specifying the rotation in the parameters section of the menu or by using the arrow keys once a plot has been generated. "A rotation" appears to refer to rotation about the Z-axis, "B rotation" about the X-axis, and "C rotation" about the Y-axis. Although the range of valid entries for these rotations are  $-360.00$  to  $+360.00$ , all possible rotations can be specified within the range of  $-180.00$  to  $+180.00$ .

## APPENDIX B

### PROGRAM LISTINGS

#### A. SINGLE FOIL TR3 PROGRAM

```
PROGRAM TR3
C   MODIFICATION OF PROGRAM TRADs1, WHICH WAS WRITTEN BY
C   D. W. RULE NSWC, CODE MODIFIED SEPT. 1986 TO INCLUDE I_PERP
c   modified sept. 1987 to make w(i)= itot=ipar+iperp
c   instead of the ratio of iperp to ipar
C   MODIFIED BY WIL LONGSTAFF, NPGS, AUG. 1988
C   FOR THREE-DIMENSIONAL ANALYSIS
C
C   THIS PROGRAM ASSUMES A VACUUM TO MEDIUM TRANSITION
C
C   CALC. INTENSITY DIST. AS FUNC. OF ANGLE OF TRANSITION RAD.
C   ASSUMING GAUSSIAN BEAM SCATTERING ANGLE
C   G = LORENTZ FACTOR, S = RMS BEAM ANGLE IN RADIANS /SQRT(2)
C   T = ANGLE OF OBSERVATION IN RADIANS
C   INTEGER AC,BC,NNW,ROW,COL,XO,YO,COUNT,WC,LW,NC,NW,NI,NWW
C   INTEGER ENTRY,CHOICE,POLAR
C   REAL THETA(64),RAD2,RAD,SCALER,ZMIN,ZMAX,ZCEN,TMAX,AMAX,ANG
C   REAL W(600),X(600),Y(600),Z(600),TAU(500),INT(600),MAXY,MAXP,
+   c(4,600),dx(600),dy(600),cy(640),NMBR,PMAX,RMAX
C   CHARACTER ANS*1,ch*1,datfil*20,SFILE*15,DFILE*15
C   COMPLEX AI,EPS,RPAR,RPERP
C   DATA PI/3.141592654/,PSI/0.7853982/,S/0.001/,IFOIL/0/
C   DATA XN/0.618/,XK/5.47/,IPRINT/0/,INORM/1/,TWOFOIL/1.0/
C   DATA XO/32/,YO/32/,SCALER/620.258423/,ZMIN/0./,ZMAX/1.0/
C   DATA ZCEN/0.0/,ROW/64/,COL/64/,ANG/0.05/,RMAX/0.0/,XDUM/0./
C   DATA YMAX/0.0/,WMAX/0.0/,PMAX/0.0/,MAXY/0.0/,MAXP/0.0/
C   AI = (0.0,1.0)
C   WRITE(6,*) 'ENTER NAME OF 3-D GRAPHICS FILE.'
C   WRITE(6,*) 'EXAMPLE:  GRAPH.DAT'
C   WRITE(6,*) ' '
C   READ(6,17) SFILE
C   WRITE(6,*) 'ENTER NAME OF CORRESPONDING PARAMETER FILE.'
C   WRITE(6,*) 'EXAMPLE:  PRMTRS.DAT'
C   WRITE(6,*) ' '
C   READ(6,17) DFILE
17  FORMAT(A15)
C   OPEN(3,FILE='RADOUT.DAT',STATUS='UNKNOWN')
C   OPEN(4,FILE=DFILE,STATUS='UNKNOWN')
C   OPEN(5,FILE=SFILE,FORM='FORMATTED')
C   OPEN(8,FILE='SCRATCH',STATUS='UNKNOWN',ACCESS='DIRECT',
+   RECL=256)
C   REWIND 2
C   REWIND 3
123  WRITE(5,123) ROW,COL,ZMIN,ZMAX,ZCEN
C   FORMAT(2I3,3F8.4)
```

```

1   WRITE(6,*) 'WHAT IS THE DESIRED BEAM ENERGY IN MEV? '
    WRITE(6,*) 'PLEASE INCLUDE A DECIMAL PLACE.'
    WRITE(6,*) ' VALID ENTRIES ARE 5 MEV - 1000. MEV. '
    READ(6,*) ENERGY
    IF(ENERGY.LT.5.OR.ENERGY.GT.1000.) THEN
        GOTO 1
    ENDIF
    G = 1.0 + ENERGY/0.511
    TMAX=1./G
2   WRITE(6,*) 'The current values are:'
    WRITE(6,*) '1 RMS beam angle is ',s,' radians/sqrt(2).'
    WRITE(6,*) '2 IFOIL is ',ifoil,'.'
    WRITE(6,*) ' A value of one indicates that a scattering foil'
    WRITE(6,*) 'is present. A value of zero indicates that there'
    WRITE(6,*) 'is a target foil only.'
    WRITE(6,*) '3 The dielectric constant of the medium is'
    WRITE(6,*) ' ',XN,' + ',XK,'i.'
    WRITE(6,*) 'This program assumes a vacuum to medium transition.'
    WRITE(6,*) '4 Angular measurement is over',ANG,' radians.'
    IF (ABS(RMAX-0.) .LE. 1E-6) THEN
        WRITE(6,*) '5 Normalization is to the maximum total'
        WRITE(6,*) 'intensity for the energy entered for this run.'
        WRITE(6,*) 'The option is to normalize to the maximum total'
        WRITE(6,*) 'intensity for an energy of 100 MeV.'
        WRITE(6,*) 'In all cases, parallel intensity will be'
        WRITE(6,*) 'normalized to its own maximum value for the'
        WRITE(6,*) 'energy entered for this run.'
    ELSE
        WRITE(6,*) 'Normalization will be to 100 MeV.'
    ENDIF
    WRITE(6,*) ' '
    WRITE(6,*) '6 Accept current parameters.'
    WRITE(6,*) ' '
    WRITE(6,*) 'Enter the number without the decimal for the value'
    WRITE(6,*) 'you wish to change. Enter 6 for no changes.'
    WRITE(6,*) ' '
    READ(6,*) ENTRY
    IF (ABS(ENTRY-6) .LE. 1E-6) THEN
        GOTO 3
    ENDIF
    IF (ABS(ENTRY-1) .LE. 1E-6) THEN
        WRITE(6,*) 'PLEASE ENTER NEW VALUE FOR RMS BEAM ANGLE.'
        WRITE(6,*) ' '
        READ(6,*) S
        GOTO 2
    ENDIF
    IF (ABS(ENTRY-2) .LE. 1E-6) THEN
        WRITE(6,*) 'ENTER NEW VALUE FOR IFOIL.'
        WRITE(6,*) ' '
        READ(6,*) IFOIL
        GOTO 2
    ENDIF
    IF (ABS(ENTRY-3) .LE. 1E-6) THEN
        WRITE(6,*) 'Enter the real component: '
        WRITE(6,*) ' '
        READ(6,*) XN
        WRITE(6,*) 'Enter the imaginary component without the "i".'
        WRITE(6,*) ' '
        READ(6,*) XK

```

```

GOTO 2
ENDIF
IF (ABS(ENTRY-4).LE.1E-6) THEN
  WRITE(6,*)'Choose option.'
  WRITE(6,*)'1 Angle that is N*(1/Lorentz factor)'
  WRITE(6,*)'2 Enter angle in radians manually.'
  WRITE(6,*)' '
  READ(6,*) OPTION
  IF (ABS(OPTION-1).LE.1E-6) THEN
    WRITE(6,*)'Enter N, for N*(1/Lorentz factor)'
    WRITE(6,*)' '
    READ(6,*) NMBR
    ANG=NMBR/G
    SCALER=31./(SIN(ANG))
  C   WRITE(6,*)'SCALER IS ',SCALER
  ENDIF
  IF (ABS(OPTION-2).LE.1E-6) THEN
    WRITE(6,*)'Enter desired angle in radians.'
    WRITE(6,*)' '
    READ(6,*) ANG
    SCALER=31./(SIN(ANG))
  C   WRITE(6,*)'SCALER IS ',SCALER
  ENDIF
  GOTO 2
ENDIF
IF (ABS(ENTRY-5).LE.1E-6) THEN
  RMAX=881.412109
  GOTO 2
ENDIF
3  WRITE(4,*)'The parameters for ',SFILE,'were:'
  WRITE(4,*)' '
  WRITE(4,*)' ENERGY= ',ENERGY,' MeV'
  WRITE(4,*)' LORENTZ FACTOR= ',G
  WRITE(4,*)' RMS beam angle: ',s,' radians/sqrt(2).'
  WRITE(4,*)' IFOIL: ',ifoil
  WRITE(4,*)' '
  WRITE(4,*)' A value of one indicates that a scattering foil'
  WRITE(4,*)'was present. A value of zero indicates that there'
  WRITE(4,*)'was a target foil only.'
  WRITE(4,*)' '
  WRITE(4,*)' The dielectric constant of the medium was'
  WRITE(4,*)' ',XN,' + ',XK,'i.'
  WRITE(4,*)' '
  WRITE(4,*)' Angular measurement was over',ANG,' radians.'
  WRITE(6,*)'CHOOSE DESIRED POLARIZATION.'
  WRITE(6,*)'ENTER APPROPRIATE INTEGER FOR DESIRED POLARIZATION'
  WRITE(6,*)' '
  WRITE(6,*)'1 NO POLARIZATION--TOTAL INTENSITY'
  WRITE(6,*)'2 PARALLEL.'
  WRITE(6,*)'3 PERPENDICULAR.'
  WRITE(6,*)' '
  READ(6,*) POLAR
  IF (ABS(POLAR-1).LE.1E-6) THEN
    WRITE(4,*)'TOTAL POLARIZATION WAS SELECTED.'
  ENDIF
  IF (ABS(POLAR-2).LE.1E-6) THEN
    WRITE(4,*)'PARALLEL POLARIZATION ONLY.'
  ENDIF

```

```

IF (ABS (POLAR-3) .LE. 1E-6) THEN
  WRITE (4, *) 'PERPENDICULAR POLARIZATION ONLY.'
ENDIF
IF (ABS (IFOIL-1) .LE. 1E-6) THEN
  TWOFOIL=0.5
  WRITE (6, *) 'SCATTERING FOIL ASSUMED TO BE PRESENT'
ENDIF
IF (S*G .GE. 1.0) THEN
  WRITE (6, *) 'WARNING: S MUST BE LESS THAN 1/GAMMA FOR'
  WRITE (6, *) 'APPROXIMATIONS USED IN I_PERF.'
ENDIF
C ****TWOFOIL ADJUSTS ASYMMETRIC TERM IN IPAR; WHEN THERE IS A
C ****SCATTERING FOIL, SET IFOIL=1, THUS TWOFOIL=0.5
  B = SQRT (1. - (1./G)**2)
  S2= 2.0 * S**2
  S3=SQRT (PI*S2)
  CS=COS (PSI)
  SN2=1-CS**2
  EPS=XN**2 - XK**2 + 2.*AI*XN*XK
  RPAR= (EPS*CS-CSQRT (EPS-SN2)) / (EPS*CS+CSQRT (EPS-SN2))
  RPERP= (CS-CSQRT (EPS-SN2)) / (CS+CSQRT (EPS-SN2))
  RSQ=CABS (RPAR) **2
  RRL=REAL (RPAR)
DO 20 I=1, 64
  write (6, *) 'record= ', i
  DO 10 J=1, 64
    RAD2=REAL (( (I-XO) **2) + ((J-YO) **2) )
    RAD=SQRT (RAD2)
    THETA (J) =RAD/SCALER
    IF (J. LT. 32) THEN
      THETA (J) = (-THETA (J) )
    ENDIF
    IF (I. GT. 32. AND. J. GT. 32) THEN
      THETA (J) = (-THETA (J) )
    ENDIF
    X (J) =THETA (J)
    IF (ABS (I-1) .LT. 1E-6) THEN
      X1=X (1)
    ENDIF
    IF (ABS (I-64) .LT. 1E-6. AND. ABS (J-64) .LT. 1E-6) THEN
      X2=X (64)
    ENDIF
    T=THETA (J)
    F = T**2 / (1.0/G**2 + T**2) **2
    IF (S. EQ. 0.) THEN
      D= (B**2/PI**2) * (RSQ*F + (T/ABS (T))) *RRL*SQRT (F)
    ENDIF
    IF (S. GT. 0.) CALL DIST (T, G, B, S, S2, S3, TWOFOIL, RPAR, RPERP, DD, D)
    IF (IPRINT .EQ. 1) PRINT *, T, ' ', D, ' ', F
    Y (J) =D
  IF ( S .GT. 0.0) THEN
    Z (J) =DD
    TAU (J) = (DD-D) / (DD+D)
    TAU (J) =ABS (TAU (J) )
  
```

```

C*****W(I) IS ITOT = IPAR + IPERF
      W(J)=D+DD
      ENDIF
      IF ( S .EQ. 0.0) THEN
          TAU(J)=1.0
          Z(J)=0.0
          W(J)=D
      ENDIF
          IF (Y(J) .GE. YMAX) THEN
              YMAX=Y(J)
          ENDIF
          IF (Z(J) .GE. PMAX) THEN
              PMAX=Z(J)
          ENDIF
          IF (W(J) .GE. WMAX) THEN
              WMAX=W(J)
              AMAX=ABS(THETA(J))
              MAXY=Y(J)
              MAXP=Z(J)
          ENDIF
      IF (ABS(POLAR-1) .LE. 1E-6) THEN
          INT(J)=W(J)
      ENDIF
      IF (ABS(POLAR-2) .LE. 1E-6) THEN
          INT(J)=Y(J)
      ENDIF
      IF (ABS(POLAR-3) .LE. 1E-6) THEN
          INT(J)=Z(J)
      ENDIF
10      CONTINUE
      WRITE(8,REC=1) (INT(COUNT),COUNT=1,64)
20      CONTINUE
          WRITE(3,300) ENERGY,S,XDUM,XDUM
          WRITE(3,300) X1,X2
          WRITE(3,300) YMAX,WMAX,XDUM
          WRITE(3,*) ROW,COL
          WRITE(4,*) 'MAXIMUM TOTAL INTENSITY WAS ',WMAX
          WRITE(4,*) 'MAX TOTAL INTENSITY OCCURED AT ',AMAX,' RADIANS'
          WRITE(4,*) 'MAX INTENSITY PREDICTED FOR ',TMAX,' RADIANS'
          WRITE(4,*) 'MAXIMUM PARALLEL INTENSITY WAS: ',YMAX
          WRITE(4,*) 'MAXIMUM PERPENDICULAR INTENSITY WAS: ',PMAX
          WRITE(4,*) 'PARALLEL INTENSITY AT MAXIMUM INTENSITY: ',MAXY
          WRITE(4,*) 'PLRF. INTENSITY AT MAXIMUM INTENSITY: ',MAXP
          WRITE(6,*) 'NORMALIZING THE INTENSITY VALUES TO 1.0'
          DO 250 NI=1,64
              READ(8,REC=NI) (INT(NW),NW=1,64)
              DO 200 NNW=1,64
                  IF (INORM.EQ.1) THEN
                      IF (ABS(POLAR-2) .LE. 1E-6) THEN
                          INT(NNW)=INT(NNW)/YMAX
                          GOTO 100
                      ENDIF
                      IF (ABS(RMAX-0.) .LE. 1.E-6) THEN
                          INT(NNW)=INT(NNW)/WMAX

```

```

        ELSE
          INT(NNW) = INT(NNW) / RMAX
        ENDIF
100    ENDIF
C     ****NORMALIZES IPAR to unity WITH MAX VALUE OF IPAR, YMAX
C     ****normalizes itot=w(i) to unity with wmax
C     ****normalizes iperp=dd with wmax also
      WRITE(3,300) X(NNW), Z(NNW), Y(NNW), W(NNW), TAU(NNW)
300    FORMAT(5 (E14.7,1X) )
200    CONTINUE
      WRITE(5,222) (INT(NWW), NWW=1, 64)
222    FORMAT(64F8.4)
250    CONTINUE
      CLOSE (2)
      CLOSE (3)
      CLOSE (4)
      CLOSE (5)
      CLOSE (8)
END
      SUBROUTINE DIST(T,G,B,S,S2,S3,TWFOIL,RPAR,RPERF,IPERF,IPAR)
C     T = ANGLE OF OBSERVATION IN RADIANS
C     G = LORENTZ FACTOR, GAMMA
C     S = RMS SCATTERING ANGLE OR BEAM ANGLE
C     D = RESULTING DISTRIBUTION OF INTENSITY
      COMPLEX BETA,Z,W,AI,D1Z,E1Z,RPERF,RPAR
      REAL IPERF, IPAR
      DATA PI /3.141592654/,MO/1/
      AI = (0.0,1.0)
      BETA = 1.0/G - AI * T
      Z = BETA/(1.414213562*S)
      IF( CABS(Z) .LT. 6.1644) THEN
C     IF MO = 1, W = ERFC(Z), IF MO = 0, W = ERF(Z)
          CALL CERF(MO,Z,W)
          W=W*CEXP(Z**2.)
      ELSE
          CALL LCERF(Z,W,IER)
C     ****LCERF RETURNS W=CEXP(Z**2) * ERF(Z) FOR ABS(Z) .GT. SQRT(38)
      ENDIF
      D1Z = (G - BETA/S**2.) * W
      E1Z = (G + BETA/S**2.) * W
      D1 = REAL(D1Z)
      E1 = REAL(E1Z)
      D2 = (B*S*G)**2. * ( (1./S3)**3. * S2*D1/2. + 1./(F1*S3**2.) )
      E2 = B**2. * ( (1./S3)**3. * S2*E1/2. - 1./(PI*S3**2.) )
      IPERF = (CABS(RPERF)**2.) * D2
      IPAR = (CABS(RPAR)**2.) * E2 +TWFOIL*B**2.*REAL(RPAR)*AIMAG(W)
      +
          / ( PI*SQRT(FI*S2) )
      RETURN
      END
      SUBROUTINE LCERF(U,W,IER)
C     ****U IS COMPLEX INPUT VALUE
C     ****W IS THE VALUE OF CEXP(-U**2)ERFC(U) OUTPUT
C     ****REQUIRES ABS( ARG(U) ) LESS THAN ARG=3*PI/4
C     ****IF CABS(U) LESS THAN SQRT(38) THIS ROUTINE IS NOT VALID

```

```

C ****IER RETURNS AS 999 IF CONDITION ON ARG(U) IS VIOLATED
C ****IER RETURNED AS -999 IF CABS(U) IS TOO SMALL
C ****IF THE SUBROUTINE CONDITIONS ARE VIOLATED RETURNS W=(IER, IER)
  COMPLEX U,W,US,USUM,UPROD
  DATA PI/3.141592654/,ARG/2.3562/,RTP1/1.7724538509055/
    IER=0
    X=REAL(U)
    Y=AIMAG(U)
    TARG=ATAN2(Y,X)
    IF (ABS(TARG) .GT. ARG) THEN
      W=(999,999)
      IER=999
      RETURN
    ENDIF
    IF ( CABS(U) .LT. 6.1644) THEN
      W=(-999.,-999.)
      IER=-999
      RETURN
    ENDIF
    US=2.0*U*U
    USUM=(1.0,0.0)
    UPROD=(1.0,0.0)
    DO 10 I=1,37
      UPROD=-UPROD*(2*I-1)/US
      USUM=USUM+UPROD
10    CONTINUE
    W=USUM/(U*RTP1)
    RETURN
  END
SUBROUTINE CERF (MO, A, W)
C *****
C FORTRAN SUBROUTINE FOR COMPLEX ERROR FUNCTION
C *****
C MO = MODE OF OPERATION
C A = ARGUMENT (COMPLEX NUMBER)
C W = FUNCTION (COMPLEX NUMBER)
C -----
  COMPLEX A, W
  DIMENSION AZ(2), QZ(2), SZ(2), EF(2)
  DIMENSION TS(2), SM(2), TM(2), QF(2), CD(18), CE(18)
  DATA CD(1)/0.000000000000000E00/,CD(2)/2.08605856013476E-2/
  DATA CD(3)/8.29806940495687E-2/,CD(4)/1.85421653326079E-1/
  DATA CD(5)/3.27963479382361E-1/,CD(6)/5.12675279912828E-1/
  DATA CD(7)/7.45412958045105E-1/,CD(8)/1.03695067418297E00/
  DATA CD(9)/1.40378061255437E00/,CD(10)/1.86891662214001E00/
  DATA CD(11)/2.46314830523929E00/,CD(12)/3.22719383737352E00/
  DATA CD(13)/4.21534348280013E00/,CD(14)/5.50178873151549E00/
  DATA CD(15)/7.19258966683102E00/,CD(16)/9.45170208076408E00/
  DATA CD(17)/1.25710718314784E+1/,CD(18)/1.72483537216334E+1/
  DATA CE(1)/8.15723083324096E-2/,CE(2)/1.59285285253437E-1/
  DATA CE(3)/1.48581625614499E-1/,CE(4)/1.33219670836245E-1/
  DATA CE(5)/1.15690392878957E-1/,CE(6)/9.78580959447535E-2/
  DATA CE(7)/8.05908834297624E-2/,CE(8)/6.40204538609872E-2/
  DATA CE(9)/4.81445242767885E-2/,CE(10)/3.33540658473295E-2/

```

```

DATA CE(11)/2.05548099470193E-2/,CE(12)/1.07847403887506E-2/
DATA CE(13)/4.55634892214219E-3/,CE(14)/1.43984458138925E-3/
DATA CE(15)/3.07056139834171E-4/,CE(16)/3.78156541168541E-5/
DATA CE(17)/2.05173509616121E-6/,CE(18)/2.63564823682747E-8/

```

C

```

-----
AZ(1)=REAL(A)
AZ(2)=AIMAG(A)
001 ZS=AZ(1)*AZ(1)+AZ(2)*AZ(2)
SZ(1)=AZ(1)*AZ(1)-AZ(2)*AZ(2)
SZ(2)=2.0*AZ(1)*AZ(2)
QZ(1)=+AZ(1)
QZ(2)=+AZ(2)
SN=+1.0
IF(AZ(1))002,003,003
002 QZ(1)=-AZ(1)
QZ(2)=-AZ(2)
SN=-1.0
003 IF(ZS-1.0)014,014,004
004 IF(ZS-38.0)005,006,006
005 IF(SZ(1)+0.064*SZ(2)*SZ(2))014,014,012

```

C

C

C

ASYMPTOTIC EXPANSION

```

006 SM(1)=0.0
SM(2)=0.0
QF(1)=+SZ(1)/(ZS*ZS)
QF(2)=-SZ(2)/(ZS*ZS)
QM=0.564189583547756*EXP(-SZ(1))
TS(1)=QM*COS(-SZ(2))
TS(2)=QM*SIN(-SZ(2))
TM(1)=+(TS(1)*QZ(1)+TS(2)*QZ(2))/ZS
TM(2)=- (TS(1)*QZ(2)-TS(2)*QZ(1))/ZS
PM=-0.5
GO TO 008
007 PM=PM+1.0
TS(1)=TM(1)*QF(1)-TM(2)*QF(2)
TS(2)=TM(1)*QF(2)+TM(2)*QF(1)
TM(1)=-PM*TS(1)
TM(2)=-PM*TS(2)
IF(ABS(SM(1))+ABS(TM(1)).NE.ABS(SM(1)))GO TO 008
IF(ABS(SM(2))+ABS(TM(2)).EQ.ABS(SM(2)))GO TO 009
008 SM(1)=SM(1)+TM(1)
SM(2)=SM(2)+TM(2)
IF(PM.LT.36.5)GO TO 007
009 IF(QZ(1).LT.0.01)GO TO 019
EF(1)=SM(1)
EF(2)=SM(2)
010 IF(MO.EQ.0)GO TO 011
W=CMLPX(EF(1),EF(2))
IF(SN.EQ.1.0)RETURN
W=CMLPX(2.0-EF(1),-EF(2))
RETURN
011 EF(1)=SN*(1.0-EF(1))
EF(2)=-SN*EF(2)

```

```
W=CMPLX (EF (1) , EF (2) )  
RETURN
```

```
C  
C          RATIONAL FUNCTION APPROXIMATION  
C
```

```
012 SM(1)=0.0  
SM(2)=0.0  
QM=C.564189583547756*EXP (-SZ (1) )  
TS (1)=QM*COS (-SZ (2) )  
TS (2)=QM*SIN (-SZ (2) )  
QF (1)=-TS (1) *QZ (1) -TS (2) *QZ (2)  
QF (2)=TS (1) *QZ (2) +TS (2) *QZ (1)  
DO 013 I=1, 18  
TS (1)=SZ (1) +CD (I)  
TS (2)=SZ (2)  
SS=TS (1) *TS (1) +TS (2) *TS (2)  
TM (1)=+CE (I) *TS (1) /SS  
TM (2)=-CE (I) *TS (2) /SS  
SM (1)=SM (1) +TM (1)  
SM (2)=SM (2) +TM (2)  
013 CONTINUE  
EF (1)=QF (1) *SM (1) -QF (2) *SM (2)  
EF (2)=QF (1) *SM (2) +QF (2) *SM (1)  
GO TO 010
```

```
C  
C          TAYLOR SERIES EXPANSION  
C
```

```
014 TM(1)=1.128379167095513*QZ (1)  
TM(2)=1.128379167095513*QZ (2)  
SM(1)=TM(1)  
SM(2)=TM(2)  
PM=0.0  
015 PM=PM+1.0  
DM=2.0*PM+1.0  
TS (1)=TM (1) *SZ (1) -TM (2) *SZ (2)  
TS (2)=TM (1) *SZ (2) +TM (2) *SZ (1)  
TM (1)=-TS (1) /PM  
TM (2)=-TS (2) /PM  
TS (1)=TM (1) /DM  
TS (2)=TM (2) /DM  
IF (ABS (SM (1) ) +ABS (TS (1) ) .NE. ABS (SM (1) )) GO TO 016  
IF (ABS (SM (2) ) +ABS (TS (2) ) .EQ. ABS (SM (2) )) GO TO 017  
016 SM(1)=SM(1)+TS(1)  
SM(2)=SM(2)+TS(2)  
GO TO 015  
017 IF (MO.NE.0) GO TO 018  
W=CMPLX (SN*SM (1) , SN*SM (2) )  
RETURN  
018 EF (1)=1.0-SN*SM (1)  
EF (2)=-SN*SM (2)  
W=CMPLX (EF (1) , EF (2) )  
RETURN
```

```
C  
C          MODIFIED ASYMPTOTIC EXPANSION
```

```

C
019 SN=-SN
GO TO 017

```

## B. TWO-FOIL INTERFEROMETER PROGRAM

```

PROGRAM COHER3
C REVISION OF TEM2, COHER1 BY D.W. RULE
C REVISED BY WIL LONGSTAFF, NPGS AUG, 1988
C PLOTS NORMALIZED TR DATA IN THREE DIMENSIONS
C INCLUDES CHANGES MADE BY D.W. RULE FOR COHERENT CONTRIBUTION
C OF A CLEAR FRONT FOIL
C**** D. W. RULE, NSWC MAR. 1987 REVISION OF TINTF
C**CALC. INTENSITY DIST. AS FUNC. OF ANGLE OF TRANSITION RAD.
C CALCS. UNPOLARIZED DIST. AND THE PARALLEL & PERP COMPS.
C ASSUMING GAUSSIAN BEAM SCATTERING ANGLE FOR
C WARTSKI'S INTERFEROMETER
C
C G = LORENTZ FACTOR, S=SX=PROJECTED RMS BEAM ANGLE IN
C RADIANS IN X-Z PLANE
C SY=PROJECTED RMS BEAM ANGLE IN Y-Z PLANE IN RADIANS
C T = ANGLE OF OBSERVATION IN RADIANS MEAS. WRT 45 DEGS.
C INCLUDES BANDWIDTH OF WAVELENGTHS WLMIN TO WLMAX
C CHARACTER DATFIL*50,CH*1,SFILE*15,DFILE*15
C COMPLEX EPS, AI, Q, EPSIN, EPCOS, ZF, RTQ, Z2, Z4, RPARF, RPERF
C COMPLEX RPARB, RPERB, EPSF, TCOEF, SDELTA, RPARFSQ
C INTEGER AC, BC, NNW, ROW, COL, XO, YO, COUNT, WC, LW, NC, NW, NI, NNW
C INTEGER POLAR, CHOICE, ENTRY, N, OPTION
C REAL THETA(64), RAD2, RAD, SCALER, ZMIN, ZMAX, ZCEN, INT(64)
C REAL X(64), TAU(64), IPERP(64), IPAR(64), W(64), IPF, IPR
C REAL IPPF, IPEB, IPRF, IFRB, KOEFF, C(4, 64), DX(64), DY(64)
C REAL TMAX, AMAX, ANG, MAXY, MAXF, NMBR, PMAX, THMX, RMAX, QMAX
C ***ENERGY = BEAM ENERGY IN MEV
C ***XNB, XKB ARE REAL AND IMAG OPTICAL CONSTANTS OF METALIC (B)ACK FO
C ***XNF, XKF ARE OPTICAL CONSTANTS OF TRANSPARENT (F)RONT FOIL
C ***XL IS SEPARATION OF INTERFEROMETER IN CM
C ***PSI IS ANGLE OF BEAM WRT NORMAL TO THE FOIL, PSI=FI/4
C DATA PI/3.141592654/, PSI/0.7853982/, THMX/0./, MAXY/0./, MAXF/0./
C DATA IFILE/3/, IPRINT/0/, INORM/1/, IFOIL/0/, SX/.000210/
C DATA SY/.000120/, XL/1.2/, DFOIL/.005/WLMIN/4500./, DELT/7.79E-4/
C DATA WLMAX/4500./, XNF/1.48/, XKF/0./, XNB/.618/, XKB/5.47/
C DATA KK/3/, FF1/1.0/, TWFOIL/1.0/, XO/32/, YO/32/, ROW/64/
C DATA COL/64/, SCALER/620.25841/, ZMIN/0.0/, ZMAX/1.0/, ZCEN/0./
C DATA RMAX/0.0/, QMAX/0.0/, PMAX/0.0/, INT/64*0.0/
C WRITE(6,*) ' ENTER NAME OF GRAPHICS DATA FILE.'
C WRITE(6,*) ' EXAMPLE: GRAPH.DAT'
C WRITE(6,*) ' '
C READ(6,7) SFILE
C WRITE(6,*) ' ENTER NAME OF CORRESPONDING PARAMETER FILE.'
C WRITE(6,*) ' EXAMPLE: PRMTRS.DAT'
C WRITE(6,*) ' '
C READ(6,7) DFILE
7 FORMAT(A15)
OPEN(2, FILE='SCRATCH', STATUS='UNKNOWN', ACCESS='DIRECT',
+ RECL=256)
OPEN(3, FILE='TOUT.DAT', STATUS='UNKNOWN')
OPEN(4, FILE=SFILE, FORM='FORMATTED')
OPEN(5, FILE=DFILE, STATUS='UNKNOWN')
WRITE(4, 123) ROW, COL, ZMIN, ZMAX, ZCEN
123 FORMAT(2I3, 3F8.4)

```

```

1  WRITE(6,*)'WHAT IS THE DESIRED BEAM ENERGY IN MEV? '
   WRITE(6,*)'PLEASE INCLUDE A DECIMAL PLACE.'
   WRITE(6,*)' '
   READ(6,*) ENERGY
   G=1.0 + ENERGY/0.511
   THMX=1./G
   ANG = 31./SCALER
   WRITE(6,*)'The current parameters are:'
   WRITE(6,*)' '
2  WRITE(6,*)'1 RMS beam angle in the X-Z plane is ',SX,'radians'
   WRITE(6,*)' RMS beam angle in the Y-Z plane is ',SY,'radians'
   WRITE(6,*)'2 IFOIL IS ',IFOIL,'. A value of 1 indicates'
   WRITE(6,*)'that a scattering foil is present. A value of'
   WRITE(6,*)'zero indicates absence of scattering foil.'
   WRITE(6,*)'3 The optical constants for the back metallic foil'
   WRITE(6,*)'are ',XNB,'+',XKB,'i.'
   WRITE(6,*)'4 The optical constants for the front clear foil'
   WRITE(6,*)'are ',XNF,'+',XKF,'i.'
   WRITE(6,*)'5 Angular measurement is over ',ANG,' radians.'
   IF(ABS(RMAX-0.).LE.1E-6) THEN
     WRITE(6,*)'6 Normalization is to the maximum total'
     WRITE(6,*)'intensity for the energy entered for this run.'
     WRITE(6,*)'The option to normalize to the maximum total'
     WRITE(6,*)'intensity for an energy of 100 MeV.'
     WRITE(6,*)'In all casis, parallel intensity will be'
     WRITE(6,*)'normalized to its own maximum value for the'
     WRITE(6,*)'energy entered for this run.'
   ELSE
     WRITE(6,*)'Normalization will be to 100 MeV.'
   ENDIF
   WRITE(6,*)'7 Minimum wavelength is ',WLMIN,' angstroms.'
   WRITE(6,*)' Maximum wavelength is ',WLMAX,' angstroms.'
   WRITE(6,*)'8 Foil thickness is ',DFOIL,' centimeters.'
   WRITE(6,*)'9 Distance between foils is ',XL,' centemeters.'
   WRITE(6,*)'10 ACCEPT CURRENT PARAMETERS'
   WRITE(6,*)' '
   READ(6,*) CHOICE
   IF(ABS(CHOICE-10).LE.1E-6) THEN
     GOTO 3
   ENDIF
   IF(ABS(CHOICE-1).LE.1E-6) THEN
     WRITE(6,*)'ENTER NEW VALUE FOR X-Z PLANE RMS BEAM ANGLE'
     WRITE(6,*)' '
     READ(6,*) SX
     WRITE(6,*)'ENTER NEW VALUE FOR Y-Z PLANE RMS BEAM ANGLE'
     WRITE(6,*)' '
     READ(6,*) SY
     GOTO 2
   ENDIF
   IF(ABS(CHOICE-2).LE.1E-6) THEN
     WRITE(6,*)'ENTER NEW VALUE FOR IFOIL.'
     WRITE(6,*)' '
     READ(6,*) IFOIL
     GOTO 2

```

```

ENDIF
IF (ABS(CHOICE-3).LE.1E-6) THEN
  WRITE(6,*) ' ENTER THE REAL VALUE FOR THE BACK FOIL CONSTANT.'
  WRITE(6,*) ' '
  READ(6,*) XNB
  WRITE(6,*) 'ENTER THE IMAGINARY VALUE FOR THE BACK FOIL'
  WRITE(6,*) 'CONSTANT. DO NOT INCLUDE THE i.'
  WRITE(6,*) ' '
  READ(6,*) XKB
  GOTO 2
ENDIF
IF (ABS(CHOICE-4).LE.1E-6) THEN
  WRITE(6,*) 'ENTER THE REAL VALUE FOR THE FRONT FOIL CONSTANT.'
  WRITE(6,*) ' '
  READ(6,*) XNF
  WRITE(6,*) 'ENTER THE IMAGINARY VALUE FOR THE FRONT FOIL'
  WRITE(6,*) 'CONSTANT. DO NOT INCLUDE THE i.'
  WRITE(6,*) ' '
  READ(6,*) XKF
  GOTO 2
ENDIF
IF (ABS(CHOICE-5).LE.1E-6) THEN
  WRITE(6,*) 'Choose option.'
  WRITE(6,*) '1 Angle that is N*(1/Lorentz factor)'
  WRITE(6,*) '2 Enter angle in radians manually.'
  WRITE(6,*) ' '
  READ(6,*) OPTION
  IF (ABS(OPTION-1).LE.1E-6) THEN
    WRITE(6,*) 'Enter N, for N*(1/Lorentz factor)'
    WRITE(6,*) ' '
    READ(6,*) NMBR
    ANG=NMBR/G
    SCALER=31./(SIN(ANG))
  ENDIF
  IF (ABS(OPTION-2).LE.1E-6) THEN
    WRITE(6,*) 'Enter desired angle in radians.'
    WRITE(6,*) ' '
    READ(6,*) ANG
    SCALER=31./(SIN(ANG))
  ENDIF
  GOTO 2
ENDIF
IF (ABS(CHOICE-6).LE.1E-6) THEN
  RMAX=881.412109
  GOTO 2
ENDIF
IF (ABS(CHOICE-7).LE.1E-6) THEN
  WRITE(6,*) 'ENTER NEW MINIMUM WAVELENGTH. '
  WRITE(6,*) ' '
  READ(6,*) WLMIN
  WRITE(6,*) 'ENTER NEW MAXIMUM WAVELENGTH. '
  WRITE(6,*) ' '
  READ(6,*) WLMAX
  GOTO 2
ENDIF

```

```

ENDIF
IF (ABS (CHOICE-8) .LE.1E-6) THEN
  WRITE (6,*) ' ENTER VALUE FOR FOIL THICKNESS IN CENTIMETERS.'
  WRITE (6,*) ' '
  READ (6,*) DFOIL
  GOTO 2
ENDIF
IF (ABS (CHOICE-9) .LE.1E-6) THEN
  WRITE (6,*) 'ENTER DISTANCE BETWEEN FOILS IN CENTIMETERS.'
  WRITE (6,*) ' '
  READ (6,*) XL
  GOTO 2
ENDIF
3 WRITE (5,*) 'The parameters for ',SFILE,' were:'
WRITE (5,*) ' '
WRITE (5,*) 'ENERGY= ',ENERGY,' MeV'
WRITE (5,*) 'LORENTZ FACTOR= ',G
WRITE (5,*) ' RMS beam angle in the X-Z plane:',SX
WRITE (5,*) ' RMS beam angle in the Y-Z plane:',SY
WRITE (5,*) 'IFOIL: ',IFOIL,' A VALUE OF 1 INDICATES'
WRITE (5,*) ' THAT A SCATTERING FOIL WAS PRESENT. A VALUE OF '
WRITE (5,*) 'ZERO INDICATES ABSENCE OF SCATTERING FOIL.'
WRITE (5,*) 'THE DIELECTRIC CONSTANTS FOR THE BACK METALIC FOIL:'
WRITE (5,*) ' ',XNB,'+',XKB,'i.'
WRITE (5,*) 'THE DIELECTRIC CONSTANTS FOR THE FRONT CLEAR FOIL:'
WRITE (5,*) ' ',XNF,'+',XKF,'i.'
WRITE (5,*) ' Angular measurement was over ',ANG,' radians.'
IF (ABS (RMAX-0.) .LE.1E-6) THEN
  WRITE (5,*) ' Normalization to energy selected.'
ELSE
  WRITE (5,*) 'Intensity was normalized to 100 MeV.'
ENDIF
WRITE (5,*) ' MINIMUM WAVELENGTH: ',WLMIN
WRITE (5,*) ' MAXIMUM WAVELENGTH: ',WLMAX
WRITE (5,*) 'Foil thickness: ',DFOIL,' centimeters.'
WRITE (5,*) ' Distance between foils: ',XL,' centimeters.'
WRITE (6,*) 'CHOOSE THE DESIRED POLARIZATION.'
WRITE (6,*) 'ENTER APPROPRIATE INTEGER FOR DESIRED POLARIZATION.'
WRITE (6,*) ' '
WRITE (6,*) '1 NO POLORIZATION--TOTAL INTENSITY.'
WRITE (6,*) '2 PARALLEL.'
WRITE (6,*) '3 PERPENDICULAR.'
WRITE (6,*) ' '
READ (6,*) POLAR
IF (ABS (POLAR-1) .LE.1E-6 ) THEN
  WRITE (5,*) 'TOTAL POLARIZATION WAS SELECTED'
ENDIF
IF (ABS (POLAR-2) .LE.1E-6) THEN
  WRITE (5,*) 'PARALLEL POLARIZATION ONLY'
ENDIF
IF (ABS (POLAR-3) .LE.1E-6) THEN
  WRITE (5,*) 'PERPENDICULAR POLARIZATION ONLY'
ENDIF
c****ffl is factor for incoh. addn. of single foil intensities

```

```

c****from clear foil ffl=1.5 for looking thru foil
C   CALCULATING THE PROGRAM CONSTANTS
      S=SX
      VDC = SQRT (1.0 - (1.0/G)**2.0 )
      AI=(0.0,1.0)
      IF (IFOIL .EQ. 1) THEN
        TWFOIL=0.5
      ENDIF
      BMIN=PI*XL/(2.0*VDC*WLMAX*1.0E-08)
      BMAX=BMIN * WLMAX /WLMIN
      IF ( WLMAX .EQ. WLMIN ) THEN
        BMAX=BMIN
      ENDIF
      S2=2.0*S**2
      S3=SQRT(PI*S2)
      DELB = BMAX- BMIN
      IF ( S .GT. 0.0 .AND. BMAX .EQ. BMIN) THEN
        DELB =1.0
        B=BMIN
        Q=1.0/S2-AI*2.0*B
        RTQ=CSQRT(Q)
        Z2=AI*RTQ/G
        Z4=Q/G
      END IF
      CALL REFLEC (PSI, XNF, XKF, RPARFS, RPERFS, RPARF, RPERF)
      CALL REFLEC (PSI, XNB, XKB, RPARBS, RPERBS, RPARB, RPERB)
C   ***RPARFS, RPERFS ARE PARALLEL & PERP. REFLECTIVITIES OF FRONT FOIL
C   ***WHICH IS TRANSPARENT, RPARBS AND RPERBS ARE FOR BACK METALIC FOIL
C   ***RPARF RPERF AND RPARB RPERB ARE THE CORRESPONDING REFLECTION COEFFS
      KOEFF = VDC**2.0*RPERBS*SY**2.0/PI**2.0
      IF (S .EQ. 0.0) THEN
        B=BMIN
      ENDIF
      DO 20 I=1, 64
        WRITE (6, *) 'RECORD= ', I
        DO 10 J=1, 64
          RAD2=REAL(((I-XO)**2) + ((J-YO)**2))
          RAD=SQRT(RAD2)
          THETA(J)=RAD/SCALER
          IF (J.LT.32) THEN
            THETA(J)=(-THETA(J))
          ENDIF
          X(J)=THETA(J)
          IF (ABS(I-1) .LT. 1E-6 .AND. ABS(J-1) .LT. 1E-6) THEN
            TMIN=X(1)
            TMAX=(-TMIN)
            WRITE (IFILE, 15) ENERGY, G, SX, SY, XL
            WRITE (IFILE, 15) TMIN, TMAX, DELT, WLMAX
            WRITE (IFILE, 15) XNF, XKF, XNB, XKB, WLMIN
            WRITE (IFILE, *) ROW, COL
            FORMAT (5 (E14.7, 1X))
          ENDIF
          T=THETA(J)
          IF (S .GT. 0.0) THEN

```

15

```

C   **CALC. SINGLE FOIL PATTERNS IPPF (PERP) & IPRF (PAR) FROM (F)RONT FOIL.
    CALL DIST(T,G,VDC,SX,SY,S2,S3,TWFOIL,RPARFS,RPERFS,
+RPARF,IPPF,IPRF)
C   ***CALC. SINGLE FOIL PATTERNS IPPB (PERP) & IPRB (PAR) FROM (B)ACK FOIL.
    TFL = 1.0
    CALL DIST(T,G,VDC,SX,SY,S2,S3,TFL,RPARBS,RPERBS,RPARB,
+IPPB,IPRB)
        IF (BMAX .GT. BMIN) THEN
            CALL BANDIN(KK,T,G,S,S2,BMIN,BMAX,DPAR,DPERF)
        ELSE
            CALL DIST2(T,G,S,Q,B,S2,RTQ,Z2,Z4,DPAR,DPERF)
        END IF
        IPAR(J) = 2.0*(ff1*IPRB-RPARBS*DPAR/(DELB *FI**2.0) )+2.*IPRF
        IPERP(J) = 2.0*(ff1*IPPB-KOEFF*DPERF/DELB ) +2.*IPPF
C   **NOTE FACTOR OF 1.5 IN IPAR & IPERP TO SIMULATE 1ST SURFACE
C   **CONTRIBUTION WHICH IS INCOHERENT
C   IPAR, IPERP, OR W IS INTENSITY/(UNIT FREQ., UNIT SOLID ANGLE)
C   ***IN UNITS OF (CHARGE**2)/(VEL OF LIGHT)
        ELSE
            FT=1.0/G**2 + T**2
            D3=(T/FT)**2
            IPAR(J)=4.0 * RPARBS/FI**2 * D3 *SIN(B*FT)**2
            IPERP(J)=4.0*KOEFF* ( SIN(B*FT) / FT )**2
        END IF
        W(J)=IPAR(J)+IPERP(J)
C   ***IF S=0.0, D IS CALCULATED FROM WARTSKI'S EXPRESSION
        IF (IPRINT .EQ. 1 ) PRINT *, T, ' ', D
        IF (ABS(POLAR-1) .LE. 1E-6 ) THEN
            INT(J)=W(J)
        ENDIF
        IF (ABS(POLAR-2) .LE. 1E-6) THEN
            INT(J)=IPAR(J)
        ENDIF
        IF (ABS(POLAR-3) .LE. 1E-6) THEN
            INT(J)=IPERP(J)
        ENDIF
10    CONTINUE
        WRITE(2,REC=1) (INT(COUNT),COUNT=1,64)
        CALL NORM(T,IPAR,IPERP,W,TAU,INORM,QMAX,PMAX,AMAX,MAXY,
+MAXF)
        DO 550 BC=1,64
            WRITE(IFILE,33) X(BC),IPERP(BC),IPAR(BC),W(BC),TAU(BC)
33          FORMAT(5(E14.7,1X))
550        CONTINUE
20    CONTINUE
        DO 41 AC=1,64
            READ(2,REC=AC) (INT(WC),WC=1,64)
C   ****NORM REPLACES w WITH IPAR + IPERP, I.E. THE UNPOLARIZED INT
            IF (INORM .EQ. 1) THEN
                DO 200 NW=1,64
                    IF (ABS(POLAR-2) .LE. 1E-6) THEN
                        INT(NW)=INT(NW)/QMAX
                    GOTO 200
                ENDIF
            ENDIF

```

```

                INT(NW) = INT(NW) / RMAX
200          CONTINUE
          ENDIF
          WRITE(4,29) (INT(NW),NW=1,64)
29          FORMAT(64F8.4)
C          WRITE(6,*) (INT(NW),NW=1,64)
41          CONTINUE
          WRITE(5,*) 'MAXIMUM TOTAL INTENSITY WAS ',RMAX
          WRITE(5,*) 'MAX TOTAL INTENSITY OCCURED AT ',AMAX,' RADIANS.'
          WRITE(5,*) 'MAX INTENSITY PREDICTED FOR ',THMX,' RADIANS.'
          WRITE(5,*) 'MAXIMUM PARALLEL INTENSITY WAS: ',QMAX
          WRITE(5,*) 'MAXIMUM PERPENDICULAR INTENSITY WAS: ',PMAX
          WRITE(5,*) 'PARALLEL INTENSITY AT MAXIMUM INTENSITY: ',MAXY
          WRITE(5,*) 'PERP INTENSITY AT MAXIMUM INTENSITY: ',MAXP
          STOP
          END
          SUBROUTINE DIST2(T,G,S,Q,B,S2,RTQ,Z2,Z4,DFAR,DPERP)
C          T=ANGLE OF OBSERVATION, THETA RADIANS
C          G= LORENTZ FACTOR
C          S= SX= RMS BEAM DIVERGENCE ANGLE PROJECTED IN THE X-Z PLANE
C          Q= COMPLEX FUNCTION OF S, INTERFEROMETER SPACING L, AND WAVELENGTH
C          DPAR AND DPERP ARE THE INTERFERENCE TERMS IN THE DISTRIBUTION
          COMPLEX Q,AI,WC,WD,ZC,ZD,Z1,Z2,Z3,Z4,ZIQC,ZIQD,ZEX,
+          ZD2,RTQ,EZEX,ZPERP
          DATA PI/3.141592654/,MO/1/
          AI=(0.0,1.0)
          Z1=-T/(S2*RTQ)
          ZC=-AI*(Z1+Z2)
          ZD=AI*(Z1-Z2)
          Z3=-AI*T/S2
          Z5=G-2.0*Z4
          ZIQC=Z3-Z4
          ZIQD=Z3+Z4
          ZEX=AI*2.0*B*(1.0/G**2+T**2)-4.0*(B*T)**2/Q
          EZEX=CEXP(ZEX)
          CALL WERFC(ZC,ZD,WC,WD)
          ZD2=0.5*SQRT(PI/S2)*EZEX*( (G/2. + ZIQD) * WD
+          + (G/2. - ZIQC) * WC - 2.*RTQ/SQRT(PI) )
          DPAR = REAL(ZD2)
          ZPERP=0.25*SQRT(PI/S2)*G**2*EZEX*
+          ( WD*(G-2.0*RTQ*ZD) + WC*(G-2.0*RTQ*ZC) + 4.0*RTQ/SQRT(PI) )
          DPERP = REAL(ZPERP)
          RETURN
          END
          SUBROUTINE WERFC(ZC,ZD,WC,WD)
          COMPLEX ZC,ZD,WC,WD,U,W
          MO=1
          IER=0
          DO 10 I=1,2
              IF(I.EQ.1) THEN
                  U=ZC
              ELSE
                  U=ZD
              ENDIF
          ENDIF

```

```

          IF ( CABS(U) .LT. 6.1644) THEN
            CALL CERF (MO,U,W)
C      ****CERF RETURNS W=ERFC(U) IF MO=1, SEE DAHLGREN MATHLIB TR84-143
            W=W*CEXP(U**2.)
          ELSE
C      ****LCERF RETURNS W=CEXP(U**2.)ERFC(U) FOR ABS(U) .GT. SQRT(38)
            CALL LCERF (U,W,IER)
            IF (IER .NE. 0) PRINT *, 'ARG(U) OUT OF BOUNDS ',
+          'IN CALL TO LCERF'
            ENDIF
            IF (I .EQ. 1) THEN
              WC=W
            ELSE
              WD=W
            ENDIF
10      CONTINUE
          RETURN
        END
        SUBROUTINE LCERF (U,W, IER)
C      ****U IS COMPLEX INPUT VALUE
C      ****W IS THE VALUE OF CEXP(U**2)ERFC(U) OUTPUT
C      ****REQUIRES ABS( ARG(U) ) LESS THAN ARG=3*PI/4
C      ****IF CABS(U) LESS THAN SQRT(38) THIS ROUTINE IS NOT VALID
C      ****IER RETURNS AS 999 IF CONDITION ON ARG(U) IS VIOLATED
C      ****IER RETURNED AS -999 IF CABS(U) IS TOO SMALL
C      ****IF THE SUBROUTINE CONDITIONS ARE VIOLATED RETURNS W=(IER, IER)
        COMPLEX U,W,US,USUM,UPROD
        DATA PI/3.141592654/,ARG/2.3562/,RTP1/1.7724538509055/
        IER=0
        X=REAL(U)
        Y=AIMAG(U)
        TARG=ATAN2(Y,X)
        IF (ABS(TARG) .GT. ARG) THEN
          W=(999,999)
          IER=999
          RETURN
        ENDIF
        IF ( CABS(U) .LT. 6.1644) THEN
          W=(-999.,-999.)
          IER=-999
          RETURN
        ENDIF
        US=2.0*U*U
        USUM=(1.0,0.0)
        UPROD=(1.0,0.0)
        DO 10 I=1,37
          UPROD=-UPROD*(2*I-1)/US
          USUM=USUM+UPROD
10      CONTINUE
        W=USUM/(U*RTP1)
        RETURN
      END
      SUBROUTINE REFLEC (PSI, XN, XK, RPARS, RPERS, RPAR, RPER)
        COMPLEX AI, EPS, RPAR, RPER

```

```

      AI=(0.0,1.0)
      CS=COS(PSI)
      SN2=1-CS**2.
      EPS=XN**2. - XK**2. + 2.*AI*XN*XK
      RPAR=(EPS*CS-CSQRT(EPS-SN2))/(EPS*CS+CSQRT(EPS-SN2))
      RPER=(CS-CSQRT(EPS-SN2))/(CS+CSQRT(EPS-SN2))
      RPARS=CABS(RPAR)**2.
      RPERS=CABS(RPER)**2.
      RETURN
      END
      SUBROUTINE DIST(T,G,B,SX,SY,S2,S3,TWFOIL,RPARS,RPERS,
+ RPAR,IPERF,IPAR)
      C      T = ANGLE OF OBSERVATION IN RADIANS
      C      G = LORENTZ FACTOR, GAMMA
      C      S=SX=RMS SCATTERING ANGLE OR BEAM ANGLE PROJECTED IN X-Z PLANE
      C      SY=RMS SCATTERING ANGLE OR BEAM ANGLE PROJECTED IN Y-Z PLANE
      C      IPERF AND IPAR ARE RESULTING DISTRIBUTION OF INTENSITIES
      C      B = VDC IN MAIN PROGRAM, VDC = V/C, I.E. VEL.
      C      + OVER SPEED OF LIGHT
      C      COMPLEX BETA,Z,W,AI,D1Z,E1Z,RPERF,RPAR
      C      REAL IPERF, IPAR
      C      DATA PI /3.141592654/,MO/1/
      C      AI = (0.0,1.0)
      C      S=SX
      C      BETA = 1.0/G - AI * T
      C      Z = BETA/(1.414213562*S)
      C      IF( CABS(Z) .LT. 6.1644) THEN
      C      IF MO = 1, W = ERF(Z), IF MO = 0, W = ERF(Z)
      C          CALL CERF(MO,Z,W)
      C          W=W*CEXP(Z**2.)
      C      ELSE
      C          CALL LCERF(Z,W,IER)
      C      ****LCERF ETURNS W=CEXP(Z**2) * ERF(Z) FOR ABS(Z) .GT. SQRT(38)
      C      ENDIF
      C      D1Z = (G - BETA/S**2.) * W
      C      E1Z = (G + BETA/S**2.) * W
      C      D1= REAL(D1Z)
      C      E1 = REAL(E1Z)
      C      D2 = (B*SY*G)**2. * ( (1./S3)**3. * S2*D1/2. +
+      1./(PI*S3**2.) )
      C      E2 = B**2. * ( (1./S3)**3. * S2*E1/2. - 1./(PI*S3**2.) )
      C      IPERF = RPERS * D2 /TWFOIL
      C      IPAR = RPARS * E2 / TWFOIL + B**2.*REAL(RPAR)*AIMAG(W)
      C      + / ( PI*SQRT(PI*S2) )
      C      ****IF SCATTERING FOIL IS PRESENT TWFOIL = 0.5 AND SYMMETRIC TERM
      C      ***IN IPERF AND IPAR IS DOUBLED
      C      RETURN
      C      END
      C      SUBROUTINE NORM(T,IPAR,IPERF,W,TAU,INORM,RMAX,QMAX,PMAX,AMAX,MAXY,
+ MAXP)
      C      REAL INT(64),IPAR(64),IPERF(64),W(64),TAU(64),PMAX
      C      REAL QMAX,AMAX,MAXY,MAXP,RMAX
      C      DO 100 NNW=1,64
      C          IF (IPERF(NNW) .EQ. 0.0) THEN

```

```

        TAU (NNW) = 1.0
    ELSE
        TAU (NNW) = (IPERP (NNW) - IPAR (NNW)) / (IFAR (NNW) + IPERP (NNW))
        TAU (NNW) = ABS (TAU (NNW))
    ENDIF
C     ****ADD IPAR & IPERP FOR UNPOLARIZED INTENSITY
        W (NNW) = IPAR (NNW) + IPERP (NNW)
        IF (IPAR (NNW) .GE. QMAX) THEN
            QMAX = IPAR (NNW)
        ENDIF
        IF (IPERP (NNW) .GE. PMAX) THEN
            PMAX = IPERP (NNW)
        ENDIF
        IF (W (NNW) .GE. RMAX) THEN
            RMAX = W (NNW)
            AMAX = T
            MAXY = IPAR (NNW)
            MAXP = IPERP (NNW)
        ENDIF
100    CONTINUE
        RETURN
    END
    SUBROUTINE BANDIN (KK, T, G, S, S2, BMIN, BMAX, DFAR, DPERF)
        EXTERNAL F
        DIMENSION P (5)
        DATA NN/3/, FGI2/0.0/
C     ***P (1) WILL CONTAIN VALUE OF DPERF IN F (B, P) CALLS, WHILE F ITSELF
C     ***IS VALUE OF DFAR
C     ***NN=NO. OF PTS. PER SUBINTERVAL FOR GAUSSIAN INTEGRATION
C     ***KK=NO. OF SUBINTERVALS IN BMIN TO BMAX, INTEG. RANGE
C     ***F IS NAME OF FUNCTION CALLED BY FGI : F=F (X, P)
        P (2) = T
        P (3) = G
        P (4) = S
        P (5) = S2
        DFAR = FGI (BMIN, BMAX, NN, KK, F, P, FGI2)
        DPERF = FGI2
        RETURN
    END
    FUNCTION FGI (A, B, NN, K, F, P, FGI2)
C     5.01.05 FGI - FORTRAN GAUSSIAN INTEGRATION ROUTINE
C     5.01.05 DECK DATES 4/7/75
C     5.01.05 TEST CASE 36
        DIMENSION V (165), V1 (90), W (165), W1 (90), SUM (32), P (5), SUM2 (32)
        DIMENSION V2 (75), W2 (75)
        EQUIVALENCE (V (1), V2 (1)), (V (76), V1 (1)),
+         (W (1), W2 (1)), (W (76), W1 (1))
        DATA V2/
+ -0.774596669, 0. , 0.774596669, -0.861136312, -0.339981044,
+ .339981044, .861136312, -.906179846, -.538469310, .0,
+ 0.538469310, 0.906179846, -0.932469514, -0.661209386, -0.238619186,
+ 0.238619186, 0.661209386, 0.932469514, -0.949107912, -0.741531186,
+ -0.405845151, 0. , 0.405845151, 0.741531186, 0.949107912,

```

+ -0.960289856, -0.796666477, -0.525532410, -0.183434642, 0.183434642,  
 + 0.525532410, 0.796666477, 0.960289856, -0.968160240, -0.836031107,  
 + -0.613371433, -0.324253423, 0. , 0.324253423, 0.613371433,  
 + 0.836031107, 0.968160240, -0.973906529, -0.865063367, -0.679409568,  
 + -0.433395394, -0.148874339, 0.148874339, 0.433395394, 0.679409568,  
 + 0.865063367, 0.973906529, -0.978228658, -0.887062600, -0.730152006,  
 + -0.519096129, -0.269543156, 0. , 0.269543156, 0.519096129,  
 + 0.730152001, 0.887062600, 0.978228658, -0.981560634, -0.904117256,  
 + -0.769902674, -0.587317954, -0.367831499, -0.125233409, 0.125233409,  
 + 0.367831499, 0.587317954, 0.769902674, 0.904117256, 0.981560634/

DATA V1/

+ -0.984183055, -0.917598300, -0.801578091, -0.642349339, -0.448492751,  
 + -0.230458316, 0. , 0.230458316, 0.448492751, 0.642349339,  
 + 0.801578091, 0.917598400, 0.984183055, -0.986283809, -0.928434860,  
 + -0.827201315, -0.687292905, -0.515248636, -0.319112369, -0.108054949,  
 + 0.108054949, 0.319112369, 0.515248636, 0.687292905, 0.827201315,  
 + 0.928434884, 0.986283809, -0.987992518, -0.937273392, -0.848206583,  
 + -0.724417731, -0.570972173, -0.394151347, -0.201194094, 0. ,  
 + 0.201194094, 0.394151347, 0.570972173, 0.724417731, 0.848206583,  
 + 0.937273392, 0.987992518, -0.989400935, -0.944575023, -0.865631202,  
 + -0.755404408, -0.617876244, -0.458016778, -0.281603551, -0.095012510,  
 + 0.095012500, 0.281603551, 0.458016778, 0.617876244, 0.755404408,  
 + 0.865631202, 0.944575023, 0.989400935, -0.997263862, -0.985611512,  
 + -0.964762256, -0.934906076, -0.896321156, -0.849367614, -0.794483796,  
 + -0.732182119, -0.663044267, -0.587715757, -0.506899909, -0.421351276,  
 + -0.331868602, -0.239287362, -0.144471962, -0.048307666, 0.048307666,  
 + 0.144471962, 0.239287362, 0.331868602, 0.421351276, 0.506899909,  
 + 0.587715757, 0.663044267, 0.732182119, 0.794483796, 0.849367614,  
 + 0.896321156, 0.934906076, 0.964762256, 0.985611512, 0.997263862/

DATA W2/

+ 0.555555556, 0.888888889, 0.555555556, 0.347854845, 0.652145155,  
 + 0.652145155, 0.347854845, 0.236926885, 0.478628670, 0.568888889,  
 + 0.478628670, 0.236926885, 0.171324492, 0.360761573, 0.467913935,  
 + 0.467913935, 0.360761573, 0.171324492, 0.129484966, 0.279705391,  
 + 0.381830051, 0.417959184, 0.381830051, 0.279705391, 0.129484966,  
 + 0.101228536, 0.222381034, 0.313706646, 0.362683783, 0.362683783,  
 + 0.313706646, 0.222381034, 0.101228536, 0.081274388, 0.180648161,  
 + 0.260610696, 0.312347077, 0.330239355, 0.312347077, 0.260610696,  
 + 0.180648161, 0.081274388, 0.066671344, 0.149451349, 0.219086363,  
 + 0.269266719, 0.295524225, 0.295524225, 0.269266719, 0.219086363,  
 + 0.149451349, 0.066671344, 0.055668567, 0.125580369, 0.186290211,  
 + 0.233193765, 0.262804545, 0.272925087, 0.262804545, 0.233193765,  
 + 0.186290211, 0.125580369, 0.055668567, 0.047175336, 0.106939326,  
 + 0.160078329, 0.203167427, 0.233492537, 0.249147046, 0.249147046,  
 + 0.233492537, 0.203167427, 0.160078329, 0.106939326, 0.047175336/

DATA W1/

+ 0.040484005, 0.092121500, 0.138873510, 0.178145981, 0.207816048,  
 + 0.226283180, 0.232551553, 0.226283180, 0.207816048, 0.178145981,  
 + 0.138873510, 0.092121500, 0.040484005, 0.035119460, 0.080158087,  
 + 0.121518571, 0.157203167, 0.185538397, 0.205198464, 0.215263853,  
 + 0.215263853, 0.205198464, 0.185538397, 0.157203167, 0.121518571,  
 + 0.080158087, 0.035119460, 0.030753242, 0.070366047, 0.107159220,  
 + 0.139570678, 0.166269206, 0.186161000, 0.198431485, 0.202578242,  
 + 0.198431485, 0.186161000, 0.166269206, 0.139570678, 0.107159220,

```

+ 0.070366047, 0.030753242, 0.027152459, 0.062253524, 0.095158512,
+ 0.124628971, 0.149595989, 0.169156519, 0.182603415, 0.189450610,
+ 0.189450610, 0.182603415, 0.169156519, 0.149595989, 0.124628971,
+ 0.095158512, 0.062253524, 0.027152459, 0.007018610, 0.016274395,
+ 0.025392065, 0.034273863, 0.042835898, 0.050998059, 0.058684093,
+ 0.065822223, 0.072345794, 0.078193896, 0.083311924, 0.087652093,
+ 0.091173879, 0.093844399, 0.095638720, 0.096540089, 0.096540089,
+ 0.095638720, 0.093844399, 0.091173879, 0.087652093, 0.083311924,
+ 0.078193896, 0.072345794, 0.065822223, 0.058684093, 0.050998059,
+ 0.042835898, 0.034273863, 0.025392065, 0.016274395, 0.007018610/
  N=MIN0 (MAX0 (NN, 3), 17)
  M=N
  IF (N.GE.17) M=32
  NADD = 0
  IF (N.LE.3) GO TO 40
  IN = N-1
  DO 30 I=3, IN
  NADD = NADD + I
30  CONTINUE
40  DO 5 I=1, M
  SUM(I)=0.0
  SUM2(I)=0.0
  5  CONTINUE
  H=(B-A)/FLOAT(K)
  H2=H/2.
  AA=A+H2
  DO 20 L=1, K
  DO 10 I=1, M
  II = NADD + I
  X = H2*V(II) + AA
  SUM(I)=SUM(I)+F(X, P)
  SUM2(I)=SUM2(I)+F(1)
10  CONTINUE
  AA=AA+H
20  CONTINUE
  SUMT=0.0
  SUMT2=0.0
  DO 25 I=1, M
  II = NADD + I
  SUMT = SUMT + W(II)*SUM(I)
  SUMT2=SUMT2+W(II)*SUM2(I)
25  CONTINUE
  FGI=H2*SUMT
  FGI2=H2*SUMT2
  RETURN
  END
FUNCTION F(B, P)
DIMENSION P(5)
COMPLEX Q, RTQ, Z2, Z4, AI
AI=(0.0, 1.0)
P(1)=0.
T=P(2)
G=P(3)
S=P(4)

```

```

S2=P(5)
Q=1.0/S2 -AI*2.0*B
RTQ=CSQRT(Q)
Z2=AI*RTQ/G
Z4=Q/G
CALL DIST2(T,G,S,Q,B,S2,RTQ,Z2,Z4,DPAR,DPERP)
F=DPAR
P(1)=DPERP
RETURN
end
SUBROUTINE CERF(MO,A,W)
C *****
C FORTRAN SUBROUTINE FOR COMPLEX ERROR FUNCTION
C *****
C MO = MODE OF OPERATION
C A = ARGUMENT (COMPLEX NUMBER)
C W = FUNCTION (COMPLEX NUMBER)
C -----
C COMPLEX A, W
C DIMENSION AZ(2), QZ(2), SZ(2), EF(2)
C DIMENSION TS(2), SM(2), TM(2), OF(2), CD(18), CE(18)
C DATA CD(1)/0.00000000000000E00/,CD(2)/2.08605856013476E-2/
C DATA CD(3)/8.29806940495687E-2/,CD(4)/1.85421653326079E-1/
C DATA CD(5)/3.27963479382361E-1/,CD(6)/5.12675279912828E-1/
C DATA CD(7)/7.45412958045105E-1/,CD(8)/1.03695067418297E00/
C DATA CD(9)/1.40378061255437E00/,CD(10)/1.86891662214001E00/
C DATA CD(11)/2.46314830523929E00/,CD(12)/3.22719383737352E00/
C DATA CD(13)/4.21534348280013E00/,CD(14)/5.50178873151549E00/
C DATA CD(15)/7.19258966683102E00/,CD(16)/9.45170208076408E00/
C DATA CD(17)/1.25710718314784E+1/,CD(18)/1.72483537216334E+1/
C DATA CE(1)/8.15723083324096E-2/,CE(2)/1.59285285253437E-1/
C DATA CE(3)/1.48581625614499E-1/,CE(4)/1.33219670836245E-1/
C DATA CE(5)/1.15690392878957E-1/,CE(6)/9.78580959447535E-2/
C DATA CE(7)/8.05908834297624E-2/,CE(8)/6.40204538609872E-2/
C DATA CE(9)/4.81445242767885E-2/,CE(10)/3.33540658473295E-2/
C DATA CE(11)/2.05548099470193E-2/,CE(12)/1.07847403887506E-2/
C DATA CE(13)/4.55634892214219E-3/,CE(14)/1.43984458138925E-3/
C DATA CE(15)/3.07056139834171E-4/,CE(16)/3.78156541168541E-5/
C DATA CE(17)/2.05173509616121E-6/,CE(18)/2.63564823682747E-8/
C -----
C AZ(1)=REAL(A)
C AZ(2)=AIMAG(A)
001 ZS=AZ(1)*AZ(1)+AZ(2)*AZ(2)
C SZ(1)=AZ(1)*AZ(1)-AZ(2)*AZ(2)
C SZ(2)=2.0*AZ(1)*AZ(2)
C QZ(1)=+AZ(1)
C QZ(2)=+AZ(2)
C SN=+1.0
C IF(AZ(1))002,003,003
002 QZ(1)=-AZ(1)
C QZ(2)=-AZ(2)
C SN=-1.0
003 IF(ZS-1.0)014,014,004
004 IF(ZS-38.0)005,006,006

```

```

005 IF (SZ(1)+0.064*SZ(2)*SZ(2))014,014,012
C
C          ASYMPOTIC EXPANSION
C
006 SM(1)=0.0
SM(2)=0.0
QF(1)=+SZ(1)/(ZS*ZS)
QF(2)=-SZ(2)/(ZS*ZS)
QM=0.564189583547756*EXP(-SZ(1))
TS(1)=QM*COS(-SZ(2))
TS(2)=QM*SIN(-SZ(2))
TM(1)=+(TS(1)*QZ(1)+TS(2)*QZ(2))/ZS
TM(2)=- (TS(1)*QZ(2)-TS(2)*QZ(1))/ZS
PM=-0.5
GO TO 008
007 PM=PM+1.0
TS(1)=TM(1)*QF(1)-TM(2)*QF(2)
TS(2)=TM(1)*QF(2)+TM(2)*QF(1)
TM(1)=-PM*TS(1)
TM(2)=-PM*TS(2)
IF (ABS(SM(1))+ABS(TM(1)).NE.ABS(SM(1)))GO TO 008
IF (ABS(SM(2))+ABS(TM(2)).EQ.ABS(SM(2)))GO TO 009
008 SM(1)=SM(1)+TM(1)
SM(2)=SM(2)+TM(2)
IF (PM.LT.36.5)GO TO 007
009 IF (QZ(1).LT.0.01) GO TO 019
EF(1)=SM(1)
EF(2)=SM(2)
010 IF (MO.EQ.0)GO TO 011
W=CMPLX(EF(1),EF(2))
IF (SN.EQ.1.0) RETURN
W=CMPLX(2.0-EF(1),-EF(2))
RETURN
011 EF(1)=SN*(1.0-EF(1))
EF(2)=-SN*EF(2)
W=CMPLX(EF(1),EF(2))
RETURN

```

```

C
C          RATIONAL FUNCTION APPROXIMATION
C

```

```

012 SM(1)=0.0
SM(2)=0.0
QM=0.564189583547756*EXP(-SZ(1))
TS(1)=QM*COS(-SZ(2))
TS(2)=QM*SIN(-SZ(2))
QF(1)=TS(1)*QZ(1)-TS(2)*QZ(2)
QF(2)=TS(1)*QZ(2)+TS(2)*QZ(1)
DO 013 I=1,18
TS(1)=SZ(1)+CD(I)
TS(2)=SZ(2)
SS=TS(1)*TS(1)+TS(2)*TS(2)
TM(1)=+CE(I)*TS(1)/SS
TM(2)=-CE(I)*TS(2)/SS
SM(1)=SM(1)+TM(1)

```

```

SM(2)=SM(2)+TM(2)
013 CONTINUE
EF(1)=QF(1)*SM(1)-QF(2)*SM(2)
EF(2)=QF(1)*SM(2)+QF(2)*SM(1)
GO TO 010

C
C           TAYLOR SERIES EXPANSION
C
014 TM(1)=1.128379167095513*QZ(1)
TM(2)=1.128379167095513*QZ(2)
SM(1)=TM(1)
SM(2)=TM(2)
PM=0.0
015 PM=PM+1.0
DM=2.0*PM+1.0
TS(1)=TM(1)*SZ(1)-TM(2)*SZ(2)
TS(2)=TM(1)*SZ(2)+TM(2)*SZ(1)
TM(1)=-TS(1)/PM
TM(2)=-TS(2)/PM
TS(1)=TM(1)/DM
TS(2)=TM(2)/DM
IF (ABS(SM(1))+ABS(TS(1)).NE.ABS(SM(1)))GO TO 016
IF (ABS(SM(2))+ABS(TS(2)).EQ.ABS(SM(2)))GO TO 017
016 SM(1)=SM(1)+TS(1)
SM(2)=SM(2)+TS(2)
GO TO 015
017 IF(MO.NE.0)GO TO 018
W=CMPLX(SN*SM(1),SN*SM(2))
RETURN
018 EF(1)=1.0-SN*SM(1)
EF(2)=-SN*SM(2)
W=CMPLX(EF(1),EF(2))
RETURN

C
C           MODIFIED ASYMPTOTIC EXPANSION
C
019 SN=-SN
GO TO 017
END
^Z

```

## INITIAL DISTRIBUTION LIST

1. Defense Technical Information Center 2  
Cameron Station  
Alexandria, Virginia 22304-6145
2. Library, Code 0142 2  
Naval Postgraduate School  
Monterey, California 93943-5002
3. Physics Library, Code 61 1  
Department of Physics  
Naval Postgraduate School  
Monterey, California 93943-5002
4. Professor X. K. Maruyama, Code 61Mp 6  
Department of Physics  
Naval Postgraduate School  
Monterey, California 93943-5002
5. Professor F. R. Buskirk, Code 61Bs 2  
Department of Physics  
Naval Postgraduate School  
Monterey, California 93943-5002
6. Dr. D. W. Rule, Code R41 1  
Naval Surface Weapons Center  
Silver Spring, Maryland 20903-5000
7. Dr. R. B. Fiorito, Code R41 1  
Naval Surface Weapons Center  
Silver Spring, Maryland 20903-5000
8. Dr. Rainier Pitthan 1  
Stanford Linear Accelerator Center  
P.O. Box 4349, Bin 96  
Stanford, California 94309
9. Cpt. A. R. Wajtowich 1  
Department of Physics  
West Point, New York 10996
10. Mr. Don Gilmore 1  
DogStar Software  
P.O. Box 302  
Bloomington, Indiana 47402

11. LT W. G. Longstaff  
P.O. Box 1236  
Norfolk, Virginia 23501-1236

2